Delft University of Technology

Water level and discharge measurements

Larrarte, Frédérique ; Lepot, Mathieu; Clemens, F.H.L.R.; Bertrand-Krajewski, Jean-Luc; Ivetic, Damjan; Prodanovic, Dusan; Stegeman, B.

Important note
To cite this publication, please use the final published version (if applicable).
Please check the document version above.

Chapter 3

Water level and discharge measurements

*Frédérique Larrarte[1,2], Mathieu Lepot[3,4], Francois
H. L. R. Clemens-Meyer[3,5,6], Jean-Luc Bertrand-Krajewski[7],
Damjan Ivetić[8], Dusan Prodanović[8] and Bram Stegeman[3]*

[1]*Université Gustave Eiffel, Department for Geotechnics, Environment, Natural hazards and
Earth sciences, Marne-la-Vallée, France*
[2]*Laboratoire d'Hydraulique Saint-Venant, Chatou, France*
[3]*Delft University of Technology, Department Water Management, Delft, The Netherlands*
[4]*Un Poids Une Mesure, Lyon, France*
[5]*Deltares, Unit Hydraulic Engineering, Department of Experimental Facility Support, Delft,
The Netherlands*
[6]*Norwegian University of Science & Technology, Faculty of Engineering, Dept. Civil &
Environmental Engineering, Trondheim, Norway*
[7]*University of Lyon, INSA Lyon, Laboratory DEEP, Villeurbanne, France*
[8]*University of Belgrade, Faculty of Civil Engineering, Department of Hydraulic and
Environmental Engineering, Belgrade, Serbia*

ABSTRACT

The knowledge of water levels and discharges in urban drainage and stormwater management (UDSM) systems is of key importance to understand their functioning and processes, to evaluate their performance, and to provide data for modelling. In this chapter, devoted mainly to underground combined and separate sewer pipe systems, various methods and technologies are described and discussed. After an introduction to important aspects to deal with when measuring discharges in sewer systems, the following parts are presented successively: (i) measurement of water level with rulers, and pressure, ultrasonic and radar sensors, (ii) measurement of flow velocity with ultrasonic, Doppler, velocity profiler, free surface, and electromagnetic sensors, (iii) direct measurement of discharge with

pre-calibrated devices, physical scale models, computational fluid dynamics modelling and use of pumping stations, and (iv) detection and/or measurement of infiltration into and exfiltration from sewers, with flow or pressure measurements, tracer experiments, distributed temperature sensing and geophysical methods.

Keywords: Discharge, in- and exfiltration, measuring principles, pumping stations, sensor, technology, tracers, velocity, water level.

SYMBOLS

(Some symbols are used for different parameters; it should be clear from the context what is meant in a specific case.)

a	numerical coefficient (–)
A_r	aspect ratio B/h (–)
b	numerical coefficient (–)
$\vec{B}$	magnetic induction field (T)
B_{fs}	width of the free surface (m)
c_{air}	celerity of sound in the air (typically ∼340 m/s)
c_{water}	celerity of sound in the water (typically ∼1480 m/s)
C	tracer concentration (kg/m³ or mol/m³)
C_{BG}	tracer background concentration (kg/m³ or mol/m³)
C_{in}	concentration of tracer injected (kg/m³)
C_{IND}	concentration of indicator tracer (kg/m³ or mol/m³)
C_{INJ}	concentration of tracer injected during a tracer experiment (kg/m³)
C_{MEAS}	concentration of tracer measured during a tracer experiment (kg/m³)
C_{REF}	concentration of reference tracer (kg/m³ or mol/m³)
d_i	distance between the Doppler sensor and the particle i (m)
D	diameter (m)
E	exfiltration fraction (–)
E_m	voltage output of an electromagnetic sensor (V)
f_D	difference between transmission and reception frequencies (Hz) of a Doppler sensor
f_R	frequency of reception of a Doppler sensor (Hz)
f_S	frequency of emission of a Doppler sensor (Hz)
Fr	Froude number (–)
g	gravity acceleration (m/s²)
h	water level (m)
h_0	vertical distance between a water level ultrasonic sensor and the pipe invert level (m)
h_{max}	maximum water height at a point during a measurement period (m)
h_s	vertical distance from top of an underwater acoustic level sensor to pipe invert (m)
H	characteristic dimension of a physical scale model (m)
i	index
I	electrical current (A)
$\vec{j}$	virtual current vector (A)
k	numerical coefficient to estimate U_m from $\hat{U}$ (–)
K	Manning-Strickler coefficient (m^{1/3}/s)
K_x	dispersion coefficient (m²/s)

L	length (m)
m	index for physical scale model
M_{in}	mass of tracer injected in the investigated reach (kg)
$M_{IND,in}$	mass of indicator tracer injected in the investigated reach (kg)
$M_{IND,out}$	mass of indicator tracer downstream of the investigated reach (kg)
M_{INJ}	mass of tracer injected during a tracer experiment (kg)
M_{MEAS}	mass of tracer measured during a tracer experiment (kg)
M_{out}	mass of tracer measured downstream of the investigated reach (kg)
$M_{REF,in}$	mass of reference tracer injected in the investigated reach (kg)
$M_{REF,out}$	mass of reference tracer downstream of the investigated reach (kg)
n	geometrical scale factor (–)
N	number of particles observed by a Doppler sensor (–)
p	index for full-scale structure
P	pressure (Pa)
P_{elec}	electrical power (W)
P_{hydr}	hydraulic power (W)
q_{IND}	dosing rate of indicator tracer (m^3/s)
q_{INJ}	tracer injection discharge (m^3/s)
q_{REF}	dosing rate of reference tracer (m^3/s)
Q	discharge (m^3/s)
Q_{MEAS}	discharge measured by a tracer experiment (m^3/s)
Re	Reynolds number (–)
s	pipe invert slope (m/m)
S_i	elementary surface (m^2)
S_m	wet section (m^2)
t	time (s)
T_E	end time of the tracer spike at the downstream measurement location
T_r	return travelling time (s)
T_S	start time of the tracer spike at the downstream measurement location
U	voltage (V)
$\hat{U}$	mean velocity measured by a sensor in a fraction of the wet section (m/s)
U'	flow velocity along the measuring line for ultrasonic travel time sensors (m/s)
$U_{e\text{-}x}$	estimated longitudinal velocity (m/s)
U_{fs}	water velocity at the free surface (m/s)
U_i	flow velocity across the elementary area S_i (m/s)
U_m	mean flow velocity across a wet section (m/s)
U_{max}	maximum flow velocity across a wet section (m/s)
U_{ri}	local radial velocity of a particle i (m/s)
$U_{s\text{-}x}$	estimated longitudinal velocity by a Doppler sensor for a particle i (m/s)
U_x	longitudinal component of the flow velocity (m/s)
U_y	transverse component of the flow velocity (m/s)
U_z	vertical component of the flow velocity (m/s)
V	water velocity (m/s)
$\vec{v}$	streamwise velocity field (m/s)
$V(x, y, z)$	water velocity at the given point of coordinates (x, y, z) (m/s)

V_{in}	volume of tracer injected (m^3)
V_r	flow velocity measured by a Doppler sensor in its sampling volume (m/s)
$w(z)$	weighting function (–)
$\vec{W}$	Bevir's weight vector (–)
We	Weber number (–)
x	longitudinal coordinate (m)
y	transverse coordinate (m)
z	vertical coordinate (m), related to water height
Z_L	lower limit of integration of an electromagnetic sensor (m)
Z_{surf}	height of an electromagnetic sensor (m)
Z_U	upper limit of integration of an electromagnetic sensor (m)
ΔH	total pump head (m)
ΔH_{static}	static pump head (m)
η_{elec}	electromotor efficiency (–)
η_{pump}	pump efficiency (–)
ρ	density of water (kg/m^3)
Δt	measurement time step in tracer experiments (s)
α	angle of measurement for ultrasonic travel time sensors (rad or °)
β_i	angle between the direction of the movement of the particle i and the Doppler sensor (rad or °)
δ	depth of sediment (m)
λ	friction coefficient (–)
ν	kinematic viscosity of water (m^2/s)
θ	angle of emission of a Doppler sensor (rad or °)
θ_w	opening angle of the emission cone of a Doppler sensor (rad or °)
σ	surface tension of water (N/m)
τ	control volume of an electromagnetic sensor (m^3)
ξ	local head loss coefficient (–)

3.1 INTRODUCTION

Several types of data can be recorded to better understand and manage urban drainage and stormwater management (UDSM) systems. However, discharge is probably the most common one, especially to operate facilities and evaluate pollutants loads (Joannis, 2001). Therefore, methods to measure discharges are widely used in sewer systems. The discharge can barely be measured with a single sensor and its calculation is mostly based on combining data from two measurements. It can be estimated by:

(a) Measuring a volume (m^3) and measuring a duration (s): this method is limited to small channels and low flows as the key challenge is to be able to capture all the volume flowing through the channel (Figure 3.1). Obviously, this method cannot be used for continuous monitoring, and is hard to implement in urban drainage systems. In addition, such a volumetric method is invasive, with possible risks for the operators (see Section 7.2).

(b) Combining two measurements: typically, a water level measurement to calculate the wet section (m^2) and a velocity measurement (m/s).

(c) Using water level measurement(s) and a relation between the water level and the discharge.

(d) Electromagnetic induction measurement.

Figure 3.1 Implementation of a device to capture all the volume flowing through a weir. *Source*: Université Gustave Eiffel.

Even if the measuring device delivers results as discharge values, some calculation is always carried out, sometimes implicitly, using the readings of the sensor(s) (often two or more) to estimate the discharge. The following sections of this chapter are devoted to the (b) and (c) estimations listed above. Two cases are distinguished:

- Open channels, where the flow is driven by gravity, in Sections 3.3.1 to 3.4.5.
- Pressurized pipes, in Section 3.4.6.

A free surface flow is presented in Figure 3.2 with solid walls, and water level h (m) from the invert to the free surface where the width is B_{fs} (m). The discharge calculation usually requires knowledge of:
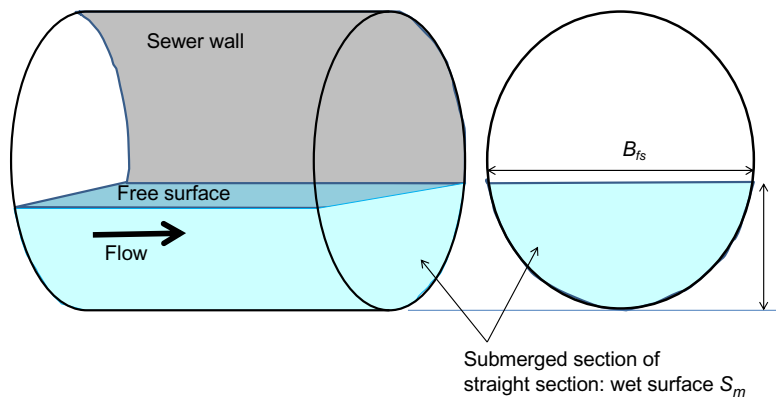

Figure 3.2 Definitions of main quantities for a free surface flow. *Source*: adapted from Larrarte *et al.* (2016a).

Damaged wall
Deposit
28 JUL 2011 6:26

Figure 3.3 A sewer section where sediment deposit and damaged wall hinder installation of sensors for discharge measurement. *Source*: Université Gustave Eiffel.

- Geometric quantities: cross section, slope, and roughness.
- Hydraulic quantities: water level (and, therefore, wet section or surface) and flow velocity.

The geometric quantities of the channel are usually considered as constant. However, this may not be true after important works, when sediment deposit occurs into the channel modifying the cross section

Water level (m), flow velocity (m/s) and flow rate (m³/s)
2.80
2.40
2.00
1.60
1.20
0.80
0.40
0.00
Rain event
Water level (m)
Flow velocity (m/s)
Flow rate (m³/s)
Dry weather
Dry weather
11 June
15 June
19 June
23 June
27 June
Date

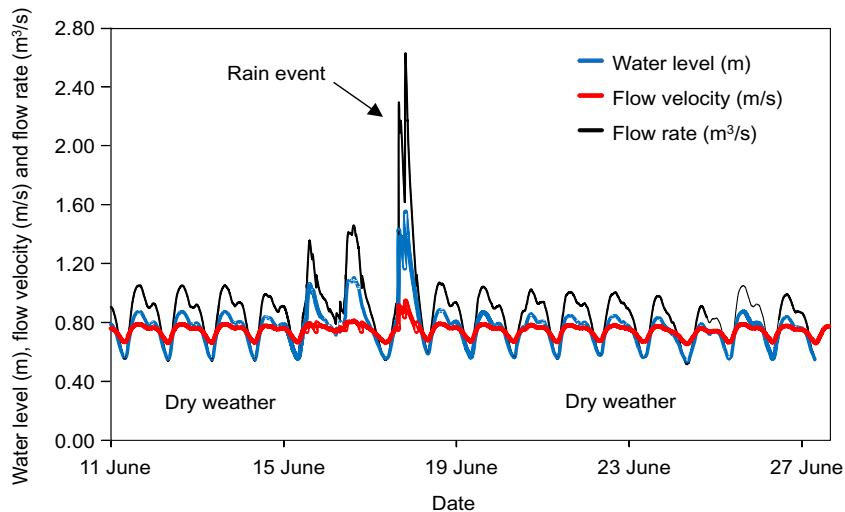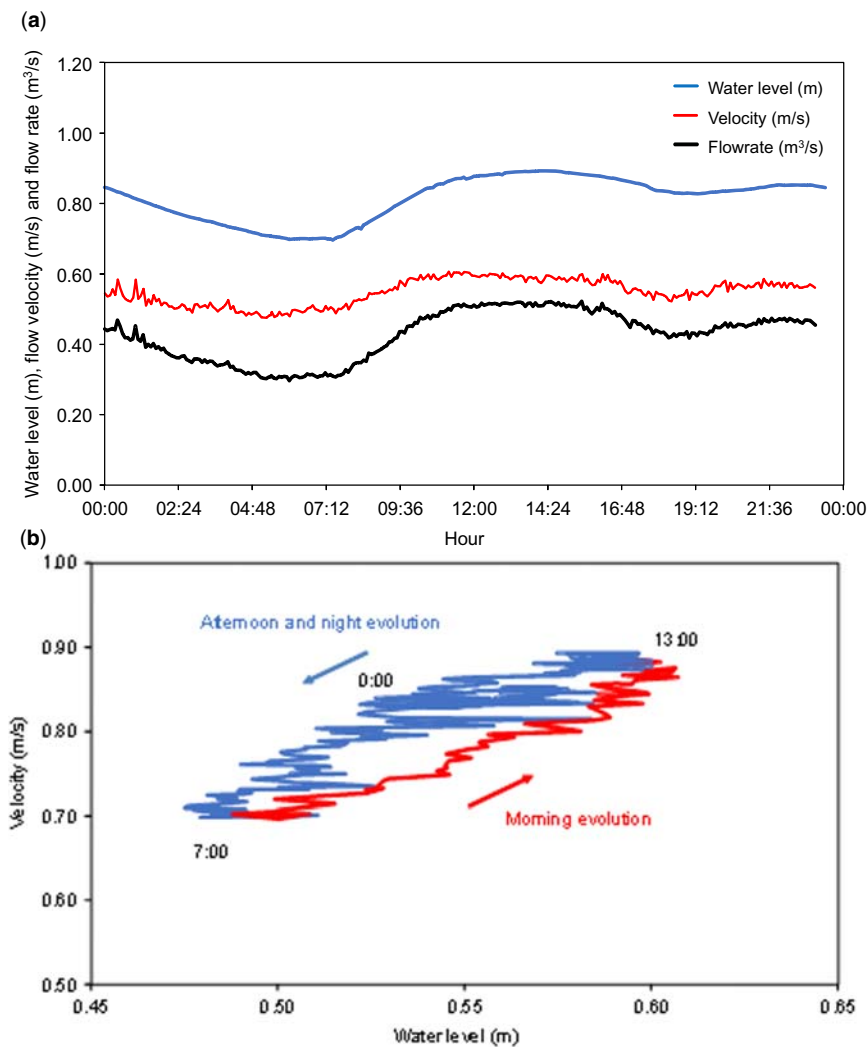

Figure 3.4 Typical flowrate patterns in a combined sewer in Nantes, France. *Source*: Université Gustave Eiffel.

Downloaded from http://iwaponline.com/ebooks/book/chapter-pdf/919169/9781789060119_0035.pdf
by TECHNISCHE UNIVERSITEIT DELFT user

(Figure 3.3), or when corrosion of the walls modifies the roughness (e.g. Stanić *et al.*, 2016). In addition, the hydraulic quantities change with time as shown in Figure 3.4 for a combined sewer pipe.

Figure 3.5(a) shows that water level and velocity do not vary with the same dynamics during a dry weather day. If the velocity is presented as a function of the water level (at the same time), the hysteresis becomes visible (Figure 3.5(b)).

Figure 3.6 shows a more complex example. During dry weather days from 22 to 31 December, the hysteresis is negligible but, during the rainy period (approx. 16–17 Dec.), an important downstream influence (backwater effect) occurs, causing the velocity to reduce when the water level rises.

Figures 3.5 Typical flowrate patterns in a combined sewer during dry weather conditions (a. time series, b. hysteresis). (a) temporal evolution of hydraulic parameters. (b) velocity as a function of water level: hysteresis. *Source*: Université Gustave Eiffel.
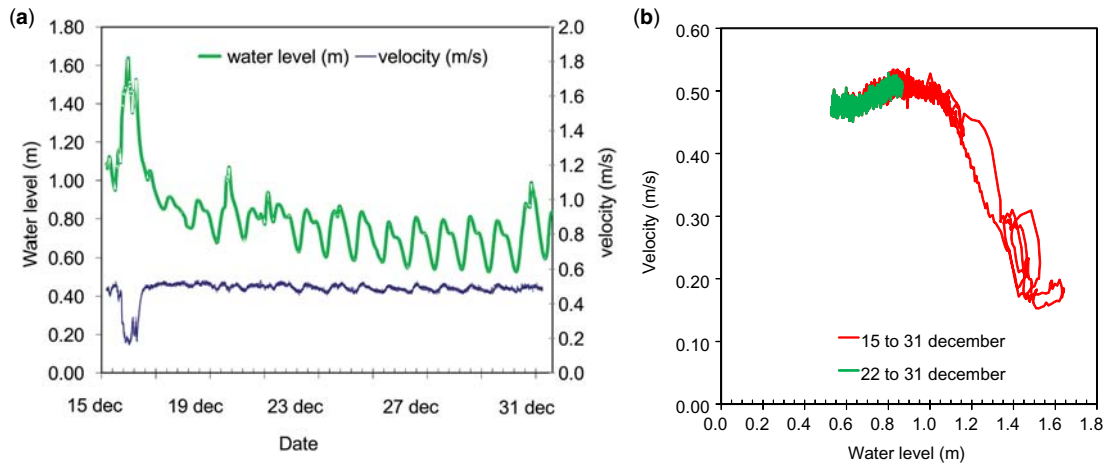
Figure 3.6 Flowrate patterns in a combined sewer with backwater effect (downstream influence). (a) temporal evolution of hydraulic parameters. (b) velocity as a function of water level: a hysteresis. *Source*: Université Gustave Eiffel.

In conclusion:

- When a univocal relation giving the velocity as a function of the water level exists (it happens either for artificially controlled sections (combined sewer overflows, weirs, Venturis, orifices, etc.) or for uniform steady flows, measuring solely the water level h is sufficient to estimate the discharge.
- When a univocal relation giving the velocity as a function of the water level does not exist, both the water level and the velocity have to be measured to estimate the discharge.

The first case is rare in sewer systems. Therefore, it is highly recommended to carefully select the measurement site before implementing any sensor (see Sections 6.2 and 6.3). Sewer operators may be good advisors as, by working daily in the network, they know areas affected by deposits, pipes with downstream influence, and other aspects that may affect measurements. Consulting maps of the network allows singularities such as confluences (Figure 3.7), bends, and changes in channel section or slope, that may have influence on the flow, to be located. Hydraulic simulations or short-term measuring campaigns may be useful to ensure the location is exempt of such effects. If no previous information exists, it is highly recommended to plan a measurement campaign to measure velocity and water level during several weeks with a few rain events to include diverse hydraulic conditions. Last but not least, the existence of a univocal relation has to be systematically validated before being used.

Another point needs to be highlighted. This book deals with metrology in urban drainage and stormwater management, the technologies presented are therefore those used in this context. It means that any part of the metrological chain implemented in sewer networks must be able to be operated in a corrosive and confined environment, sometimes complying with ATEX directives 1999/92/EC and 94/9/EC (applicable to explosive atmospheres including the electrical directives regarding Safety Extra-Low Voltage (SELV)). Additionally, of course, national/local sanitation regulations must be respected (see Section 7.2 for more information).

Figure 3.7 The water flowing from the left side channel influences the flow coming from the bottom. *Source*: Université Gustave Eiffel.

Key messages on sensors, measuring devices and sites

- KM 3.1: *Hydraulic context* – The hydraulic context of each site has to be taken into account at the early stage of the instrumentation process, especially velocity distribution and deposits
- KM 3.2: *Technologies* – For most data, there are various technologies available, with their respective pros and cons.
- KM 3.3: *Corrosion* – Sewer networks have a corrosive and confined atmosphere.
- KM 3.4: *Regulations* – National regulations must be respected.
- KM 3.5: *Staff* – Staff is a key element for professional metrology.

3.2 WATER LEVEL MEASUREMENT

The technologies commonly used for continuous monitoring of water level (Bertrand Krajewski *et al.*, 2000; Colin *et al.*, 2016) are presented in Sections 3.2.1 to 3.2.4. However, it is important to mention that in several cases direct measurement using a ruler may be necessary.

Water level measurement allows calculation of the wet section when the geometry of the section is known. The wet section is correct only if there are no deposits in the cross section. This point should be checked systematically. In the case where deposits are present, the sediment height has to be measured

as well, in order to calculate the real wet section. To the authors' knowledge, the only existing device able to continuously measure sediment height is a research prototype (Larrarte *et al.*, 2016b). When applying a free surface Venturi flume (e.g. a Diskin venturi device in Diskin, 1963), the risk of deposits in the measuring section is reduced thanks to the locally increased flow velocity and shear stress.

3.2.1 The simplest sensor: a ruler

A ruler can be considered as the simplest sensor because: (i) it does not require specific skills, (ii) there is no energy requirement and (iii) it is the cheapest one. However, this device has two main drawbacks: it is (i) costly in terms of staff costs and (ii) potentially dangerous since it requires direct access to the water in the sewer pipe. Of course, it cannot be used for continuous monitoring without image acquisition and image processing tools (e.g. Jeanbourquin *et al.*, 2011). When applied in flowing water, a ruler is an invasive measuring method (Figure 3.8): a 'bow wave' appears making the measuring result ambiguous. Even in motionless water, the reading accuracy cannot be better than 2–3 mm, which can be relatively inaccurate for small water depths.

3.2.2 Pressure sensor

The measuring principle of pressure sensors is based on the Bernoulli relation (Equation (3.1)): along a given stream line, the water height z (m) at the given point (x, y) is related to the pressure P (Pa) and to the velocity $V(x, y)$ (m/s), with conservation of the sum:

$$\frac{P}{\rho g} + z(x, y) + \frac{V(x, y)^2}{2g} \tag{3.1}$$

Several types of pressure sensors are available on the market. All of them require an atmospheric pressure compensation, a low velocity around the sensor and must be placed at the invert level. As an order of magnitude, a velocity of 1 m/s leads to an overestimation of the water level of 5 cm. For 2 m/s, the overestimation will be 20 cm (Equation (3.1)).

The first kind of sensor is named a bubbler (Figure 3.9(a)): it is a bubble generator, with the outlet at the invert level, that measures the required pressure to release a bubble. This pressure is equal to the hydraulic

Figure 3.8 Not so easy to read a ruler! Water level of 36 cm upstream, 35 cm downstream. *Source*: Université Gustave Eiffel.
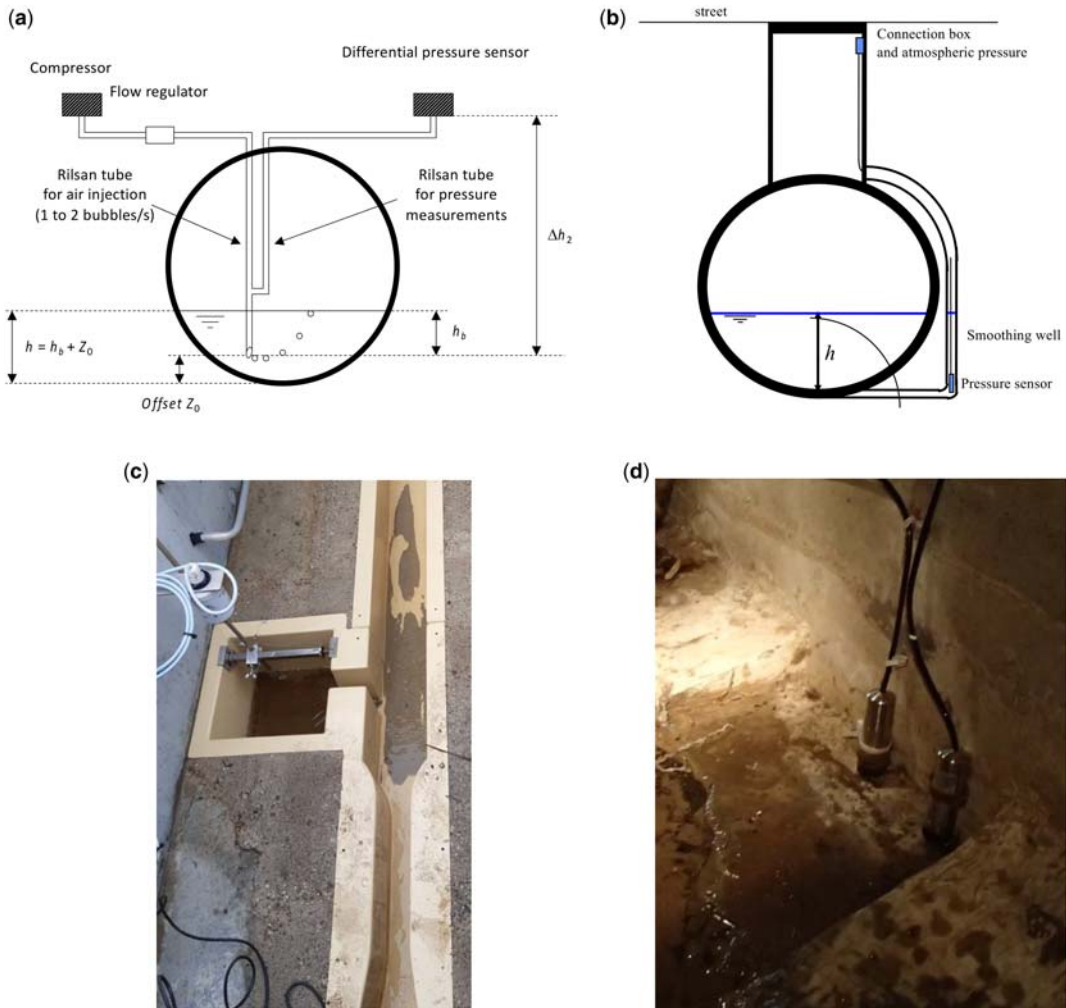
Figure 3.9 Pressure sensors: (a) installation of a bubbler, (b) installation of a piezometric sensor, (c) bubbler installed at the upstream end of a free surface Venturi channel, (d) piezometric sensor. *Sources*: (a) and (b) adapted from Bertrand Krajewski *et al.* (2000); (c) courtesy of Paul Verkroost (Efcon/A.V.M.) and (d) courtesy of Nicolas Walcker (INSA lyon).

head and can be converted into the water level (Equation (3.1)). This device is obviously sensitive to frost for its off-sewer part. These sensors require a gas source (e.g. bottle of nitrogen, atmosphere) and a compressor.

An alternative to the bubbler is the piezometric sensor (Figure 3.9(b)) that uses the piezoelectric properties of some materials. When the piezometric crystal is submitted to a pressure, electrical charges appear on the faces opposed to the constraint exerted on the sensor membrane. The intensity of the electrical signal is proportional to the pressure. Piezometric sensors are of particular interest in pipes

where dimensions are too small to install an ultrasonic sensor (which has a dead zone of typically a few tens of centimetres – see Section 3.2.3) or when the flow is or can be pressurized.

Pressure sensors are necessarily submerged and therefore sensitive to clogging and deposits.

3.2.3 Ultrasonic sensor

Ultrasonic sensors are widely used for long term monitoring stations. The water level is calculated through the measurement of the travel time of acoustic waves emitted by the sensor and reflected by the free surface, i.e. the wave travel from the sensor towards the free surface and back to the sensor.

For emerged situations (aerial sensor) the water level is calculated using Equation (3.2a):

$$h = h_0 - \frac{c_{air}\, T_r}{2} \tag{3.2a}$$

where c_{air} is the celerity of sound in the air (typically 340 m/s), T_r (s) is the return travelling time, and h_0 (m) is the vertical distance between the sensor membrane and the sewer invert level, as shown in Figure 3.10(a).
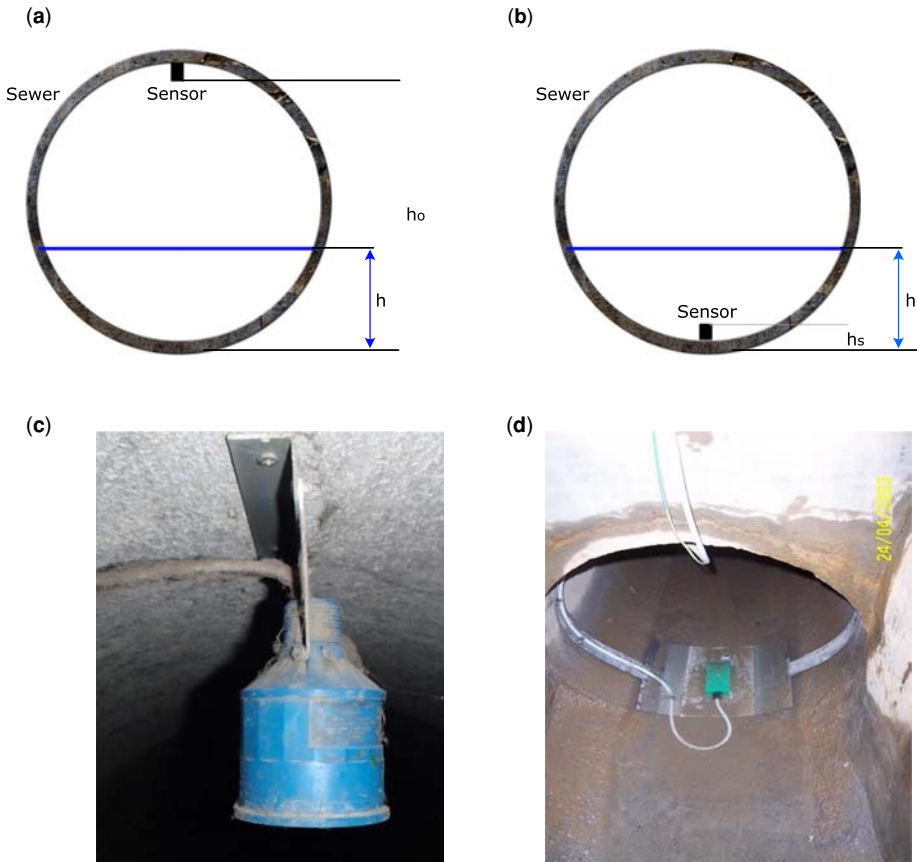

Figure 3.10 Ultrasonic sensors: installation principles at the crown (a) and invert (b) and photos of installation at the crown (c) and at the invert (d). *Sources*: (a) and (b) adapted from Bertrand Krajewski *et al.* (2000); (c) courtesy of Nicolas Walcker (INSA Lyon) and (d) courtesy of Paul Verkroost (Efcon/A.V.M.).

Aerial ultrasonic sensors present some advantages: they are small, cheap, not really prone to drift and require less maintenance than the submerged ones. Given the measurement principle, the results are unreliable when:

- Foam or floating debris is present at the free surface and in the measuring area.
- The composition, temperature, pressure and/or moisture of the atmosphere significantly influences the celerity of the sound.

While aerial sensors are the most widespread, there are also submerged ultrasonic sensors (Figure 3.10(b)). Equation (3.2a) then becomes Equation (3.2b):

$$h = h_s + \frac{c_{water}\, T_r}{2} \tag{3.2b}$$

where c_{water} is the celerity of sound in water (typically 1480 m/s), T_r (s) is the return travelling time, and h_s (m) is the vertical distance between the sensor membrane and the sewer invert level.

For aerial systems, the implicit assumption that the velocity of sound is known is often too strong due to variations in temperature, pressure and/or composition of the atmosphere. Additional measurement of these parameters, in particular temperature and air humidity, can partially correct those variations. However, this

Table 3.1 Advantages and disadvantages of various technologies for water level measurement.

Technology	Advantages	Disadvantages
Ruler	• Cheap • Almost always available • Non-sensitive to humidity	• No continuous measurements without image recording device • Not so easy to read
Bubbler	• Continuous measurements • Hydrostatic pressure measurement • Easy to install	• Requires regular maintenance as it is sensitive to fouling and clogging • Slow response time
Piezometric sensor	• Continuous measurements • No dead zone • Average investment cost • Low power consumption • Works also for pressurized flow • Easy to calibrate	• Contact with the water • Requires regular maintenance as it is sensitive to fouling • Drifts easily
Ultrasonic sensor	• Continuous measurements • Easy to install and maintain • No contact with the effluent • Low drift over time • Rather low cost	• Presence of a dead zone • Does not measure when the water level goes up to the sensor • Several disturbance factors (foams, floats, temperature gradients, haze, etc.)
Radar sensor	• Continuous measurements • Undisturbed by variations in temperature, mist, wind, foam and floatings • Easy to install and maintain • No contact with the effluent • Low drift over time • Low cost	• Slightly more expensive than the ultrasonic sensor • Energy consumption is higher than for the ultrasonic sensor • Does not measure when the water level goes up to the sensor

requires additional sensors (i.e. other additional potential problems and added uncertainties in the obtained measured values for the water level). The assumptions on the geometry (h_0 or h_S – Figure 3.10) need to be carefully checked. 'False' echoes may occur due to e.g. the shape of the manhole construction, or due to the presence of objects like spiderwebs. One main advantage with submerged systems is that the water temperature can be considered as constant along the distance h_s, the main disadvantage is that the sensor is very sensitive to clogging and deposits.

3.2.4 Radar sensor

Water level measurement with radar sensors is also based on a measurement of the travel time, but with electromagnetic waves instead of ultrasound waves. Radar waves do not need a support to propagate and they are not disturbed by variations in temperature, mists, wind, foams nor floating materials. Radar sensors are therefore preferred to ultrasound sensors if one of these constraints is present on the site. They are less subject to disturbances and produce non-ambiguous information if they cannot measure, which makes it easier to sort out false values in the case of loose free surface or dysfunction. With significant diminution of their costs during recent decades, radar sensors are being used more and more.

3.2.5 Summary

The main advantages and disadvantages of the above technologies most used in UDSM are summarized in Table 3.1.

3.3 VELOCITY MEASUREMENTS

As explained in the introduction of Section 3.2, when a univocal relation giving the velocity as a function of the water level does not exist, the velocity has to be measured in conjunction (space) and in synchronization (time) with the water level. In most cases, the geometry of the pipe or channel is known or can be assumed to be known. However, corrosion can generate a significant deviation from the initial cross section, in
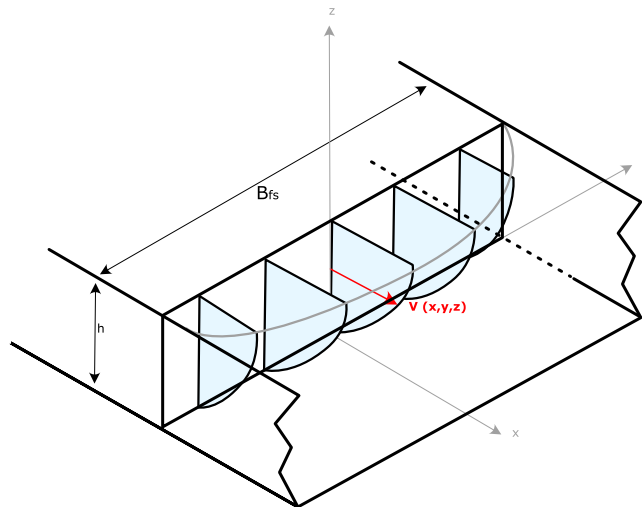

Figure 3.11 Streamwise velocity distribution in a wide channel section. *Source*: adapted from Larrarte *et al.* (2016a).
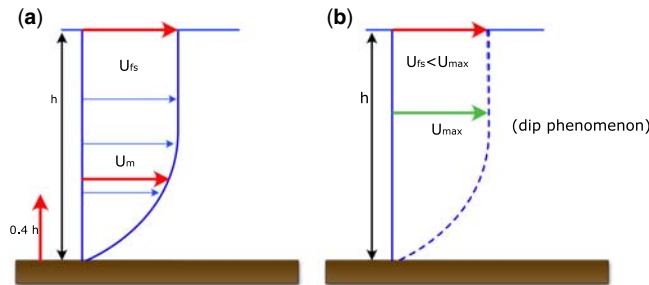
Figure 3.12 Vertical velocity profile in a channel central plane far from any singularities: large (a) and narrow (b) channels, i.e. respectively $A_r > 5$ and $A_r < 5$. *Source*: adapted from Larrarte *et al.* (2016a).

particular for concrete sewer pipes (see e.g. Clemens *et al.*, 2015 or Stanic, 2016). The presence of deposits is also a source of biases and difficulties in measurements.

Longitudinal velocities (Figure 3.11) increase from the invert level to the surface and from the walls towards the median plane of the flow. This schematization corresponds to the case of wide channels characterized by an aspect factor $A_r > 5$, with $A_r = B_{fs}/h$. In this case, the maximum velocity is observed at the free surface (Figure 3.12(a)). For narrower channels ($A_r < 5$), the velocity distribution shows a 'dip-phenomenon' effect: the maximum velocity is below the free surface (Figure 3.12(b)).

Circular or egg-shaped (ovoid) section pipes have an aspect ratio lower than 5 (Figure 3.13). Therefore, the maximum velocity is usually below the free surface (Figure 3.15), except for low filling rates. Consequently, their velocity profiles mismatch with the specifications of the international standard ISO 748 (ISO, 2007). The height of the measured average velocity may be different from the standard, as illustrated in Figure 3.14 for two combined egg-shaped sewers in Nantes, France (Larrarte, 2006): in the
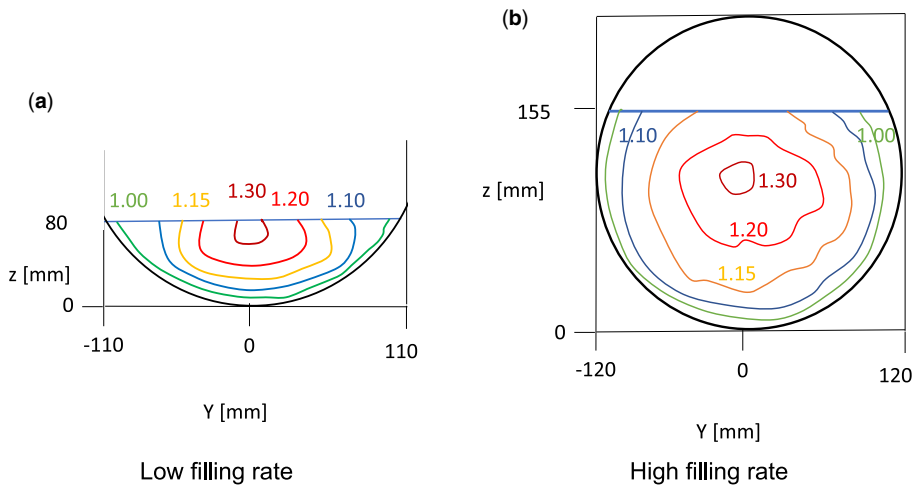

Figure 3.13 Velocity field (the isolines reflect the normalized values with respect to the mean velocity) in a circular section for low (a) and high (b) filling rates. *Source*: Experimental results adapted from Knight & Sterling (2000).
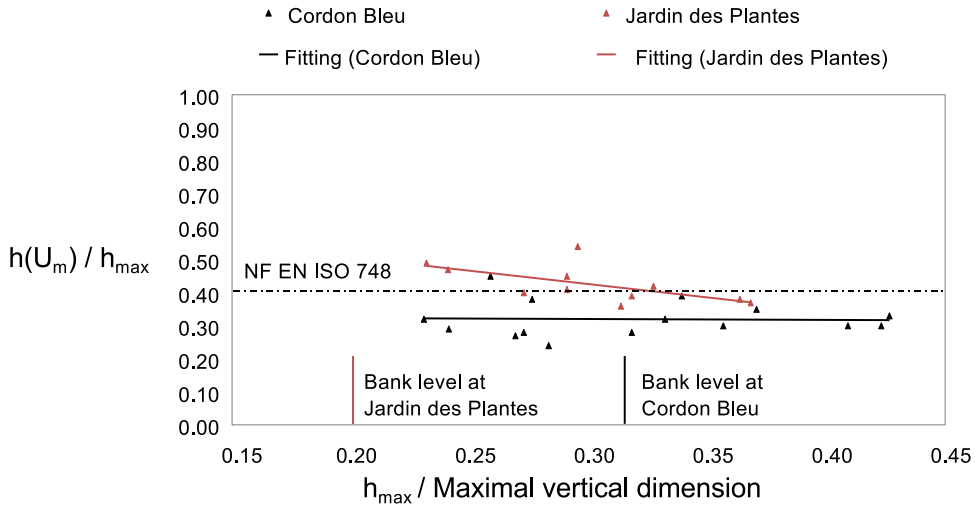
Figure 3.14 Vertical position of the average velocity for two combined egg-shaped channels in Nantes, France. *Source*: Larrarte (2006).

Jardin des Plantes sewer, the position of the mean velocity changes and moves towards the invert level with increasing filling rate, whereas it remains almost constant in the Cordon Bleu sewer.

Very large sewers are sometimes equipped with banks or sidewalks that increase the flow velocity for low discharges and thus reduce the risk of sedimentation. At low flow rates, the velocity field is distributed like in a single section (Figure 3.15(a)) with maximum velocity below the free surface and transverse and vertical velocity gradients. At higher flow rates, the section becomes compound and the velocity field is more heterogeneous: one observes in particular the presence of a local minimum velocity above the sidewalk (Figure 3.15(b)) and a very strong transversal velocity gradient in the vicinity of the vertical face of the bench. Such a velocity field cannot be expected to be stable and may vary over time, even when the flow rate remains stationary.
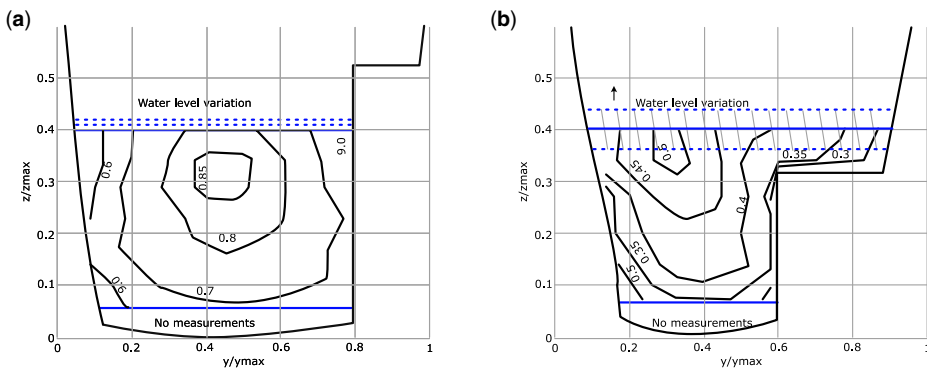

Figure 3.15 Velocity fields in a large combined sewer: low (a) and high (b) filling rates. *Source*: adapted from Larrarte (2006).

The mean velocity U_m (m/s) through a cross section is the flow divided by the wet section: it is the average of the longitudinal component (i.e. perpendicular to the section) of the velocities of all fluid particles which pass through the section at a given time. U_m can be approximated by sampling n points distributed across the section S_m (ISO, 2007):

$$U_m = \frac{1}{S_m} \sum U_i S_i \tag{3.3}$$

where U_i (m/s) is the local velocity at point i, perpendicular to the section, and S_i (m^2) is the surface element associated with this velocity (Figure 3.16).

An ideal velocity sensor should perform a complete sampling of the wet section to account for the entire velocity field. However, a real sensor usually does not deliver the true mean velocity U_m across the wet section but a mean velocity $\hat{U}$ representative of only a fraction of the wet section. This implies that a function f should be determined to estimate U_m from $\hat{U}$ (Equation (3.4)):

$$U_m = f(\hat{U}) \tag{3.4}$$

This function f is preferably reduced to a single numerical coefficient k over the whole range of velocities and filling rates (Equation (3.5)):

$$U_m = k\hat{U} \tag{3.5}$$

The two most used velocity sensors (transit time sensor and Doppler sensor) and some other emerging sensors or technologies are briefly described in the following sections.
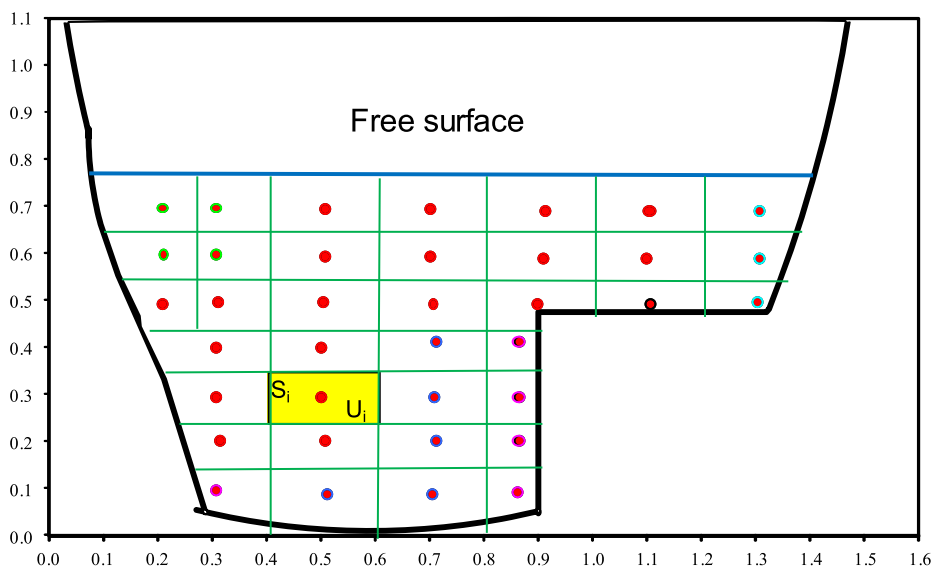

Figure 3.16 Example of discretization of a velocity field in surface elements S_i, each element being associated with a local velocity U_i. *Source*: Larrarte *et al.* (2016a).

> ⚠️ **Velocities**
>
> Sewer channels differ from rivers; the maximum velocity is below the free surface.
> The height of the mean velocity may change with the filling rate.

3.3.1 Ultrasonic travel time

The principle is based on the measurement of the travel time of ultrasonic waves between two sensors A and B (emitters and receivers), which are positioned at the same elevation, either on both sides of the pipe (Figure 3.17(a)) or on the same side (Figure 3.17(b)). The sensors are installed with an angle α specified by the manufacturer. L is the wave travel distance between A and B.

In practice, A and B are alternately transmitters and receivers. Let t_1 be the time taken by an acoustic signal emitted from A to reach B and vice versa t_2 from B to A. The transit time measurement considers the flow velocity by its projection U' along the line AB.

Considering, at the height z at which the sensors A and B are installed above the pipe invert (Figure 3.18), that the velocity component $U_x(z)$ parallel to the pipe axis is predominant compared to the respectively transverse and vertical components $U_y(z)$ and $U_z(z)$ ($U_z(z)$ is perpendicular to the plane of Figure 3.18 and is therefore not visible on the figure), the velocity $U'(z)$ measured along the line AB is converted into the longitudinal velocity $U_{e\text{-}x}(z)$ by application of the coefficient $1/\cos(\alpha)$. The mean velocity $\hat{U}(z)$ measured by the sensor along the line AB is given by Equation (3.6):

$$\hat{U}(z) = \frac{L}{2\cos(\alpha)}\left(\frac{t_2 - t_1}{t_1 t_2}\right) \tag{3.6}$$
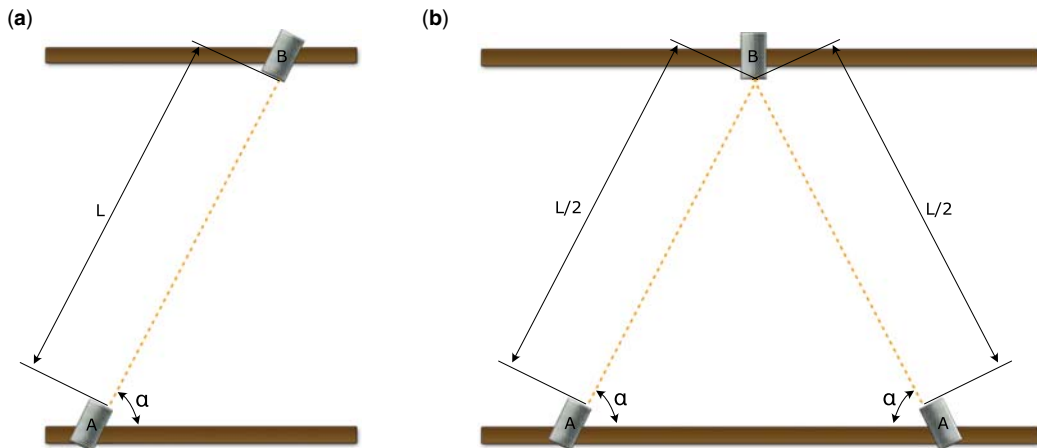

Figure 3.17 Schematic diagram of a transit time measurement system: sensors on both sides (a) or same side (b) of the channel. *Source*: adapted from Larrarte *et al.* (2016a).
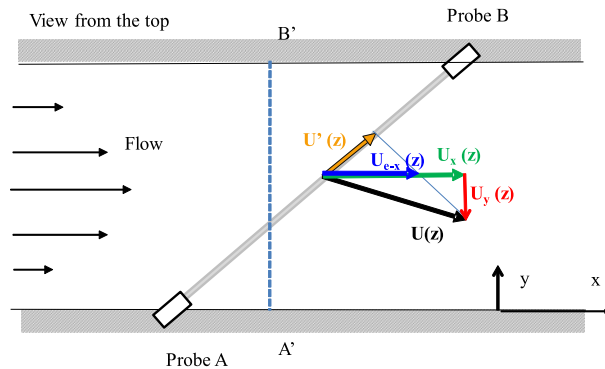
Figure 3.18 Influence of a strong transverse component of the velocity on the difference between the velocity U_{e-x} measured according to the probes A and B and the longitudinal velocity U_x. *Source*: adapted from Larrarte *et al.* (2016a).

$\hat{U}(z)$ is equal to the mean flow velocity $U_m(z)$ at the level z of the line AB (Equation (3.7)):

$$\hat{U}(z) \cong \frac{1}{L\cos(\alpha)} \int_0^L U'.dl = \frac{1}{L} \int_0^L U.dl = U_m(z) \tag{3.7}$$

Figure 3.18 shows that if the transverse component $U_y(z)$ of the velocity is significant, the measured longitudinal velocity $U_{e-x}(z)$ is very different from the real longitudinal velocity $U_x(z)$ (in green). The presence of non-negligible transverse velocity components is therefore a major source of error.

The line AB is called a path in the geometric sense of the term. This line allows homogeneous horizontal sampling of the transverse velocity profile (Figure 3.19(a)), but only at a given height. This measurement is representative of the flow at the height of the path. To obtain a better mean velocity estimate through the entire wet section, it is common to use several paths at different heights, by installing several couples of sensors (Figure 3.19(b)).
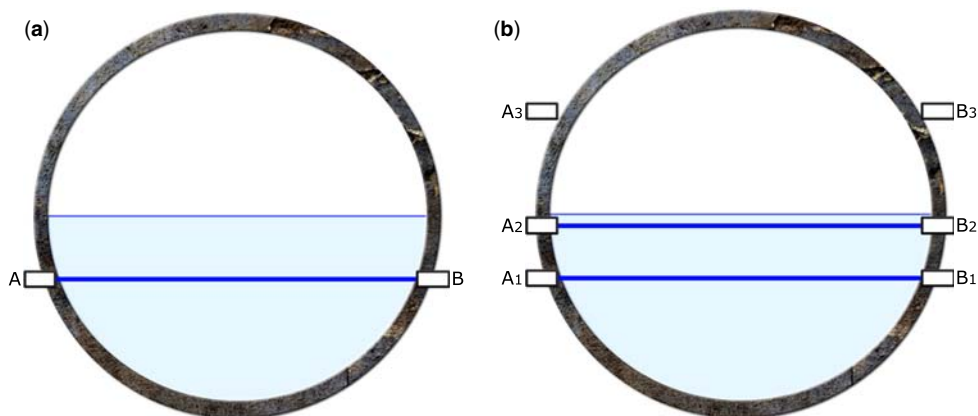

Figure 3.19 Scheme of installation of one couple (a) or several couples (b) of sensors. *Source*: adapted from Larrarte *et al.* (2016a).

The discharge is calculated by assigning a defined surface to each path and applying, where appropriate, corrective coefficients k_i to the velocities measured by the different paths (Equation (3.8)):

$$Q = \sum_{i=1}^{n} k_i \hat{U}_i S_i \tag{3.8}$$

where $\hat{U}_i$ and S_i are respectively the velocity measured by the i-th path and the corresponding wet surface. The coefficients k_i are different from 1 only for the lowest (near the pipe invert) and highest (close to the free surface) surface elements. The standard ISO 6416 (ISO, 2017) provides two methods for assigning surfaces to paths (not detailed here).

3.3.2 Acoustic Doppler flowmeter

An acoustic Doppler flowmeter (Figure 3.20) measures the velocity in a sampled volume by measuring the difference between the emitted (f_S) and received ($f_S + f_D$) frequencies (Hz) of acoustic waves. The frequency f_S is in the range 0.5 to 1 MHz. When acoustic waves encounter an acoustic impedance contrast (i.e. a density, e.g. particles or gas bubbles), the waves are reflected with a frequency f_R. The velocity V_R measured in the sample volume is directly proportional to the difference of frequencies $f_D = f_R - f_S$ (Equation (3.9)):

$$V_r = \frac{c_{water} f_D}{2 f_s} \tag{3.9}$$

where c_{water} (m/s) is the celerity of ultrasound in water, f_S (Hz) is the frequency of emission, and f_D (Hz) is the difference between the transmission and reception frequencies.

In theory, Doppler sensors can be placed anywhere in the flow (Figure 3.20). In practice, the location is of key importance to obtain accurate results. Indeed, the velocity V_r measured by the Doppler sensor is converted to the estimated mean velocity U_m according to hypotheses about the expected velocity field and profile (see below). The most common specifications correspond to a location of the sensor at the bottom of the pipe, in a central position (Figure 3.20(a), Figure 3.22). If the sensor is in a different
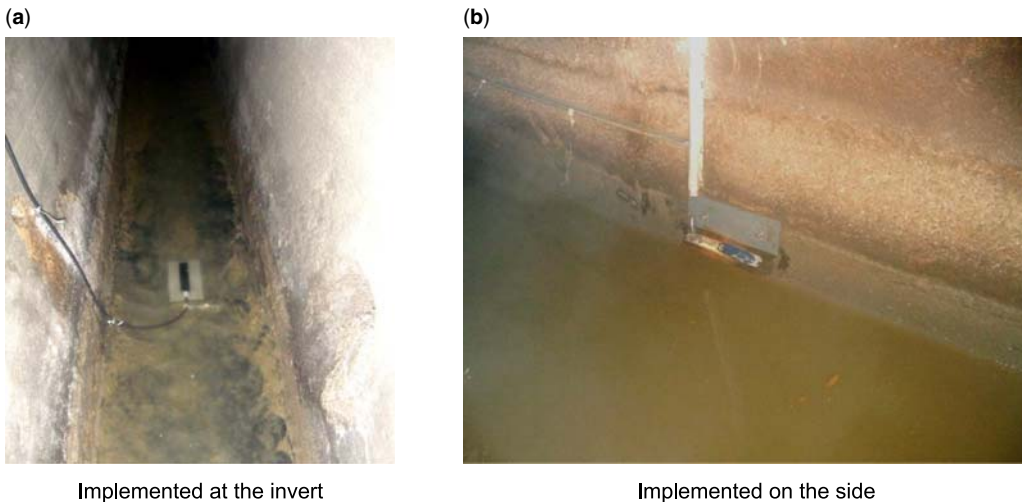
(a)   (b)

Implemented at the invert   Implemented on the side

Figure 3.20 Examples of acoustic Doppler sensor locations: on the invert (a) or on the side wall (b). *Source*: Université Gustave Eiffel.
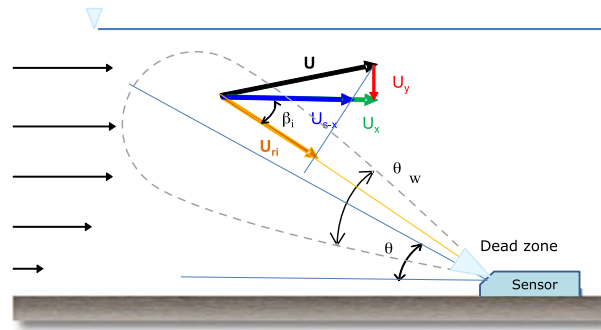
Figure 3.21 Principle of velocity measurement by a Doppler sensor. *Source*: adapted from Larrarte *et al.* (2016a).

location (e.g. on the wall, as shown on Figure 3.20(b)), an appropriate correction to estimate U_m from V_r is necessary to avoid biases which may be very significant (Lepot *et al.*, 2014). In addition, sensor locations with deposits or prone to clogging should be avoided.

For a given particle *i* within the flow (Figure 3.21), the velocity U_{s-x} along the flow axis is calculated from the velocity U_{ri} measured by the Doppler sensor by Equation (3.10):

$$U_{s-x} = \frac{U_{ri}}{\cos(\beta_i)} \tag{3.10}$$

where β_i is the angle between the direction of the movement of the particle *i* and the emission axis of acoustic waves.

For typical sensor location conditions (i.e. on the invert), the angle β_i is assumed to be equal to the angle θ_i, located in the vertical plane of symmetry of the sensor, which itself is assimilated to the emission angle θ of the sensor, even if strictly speaking this is only true for the particles located on the axis of the emission cone (Figure 3.21). The measurement volume explored by the Doppler sensor is a 3D cone as shown in Figure 3.22.
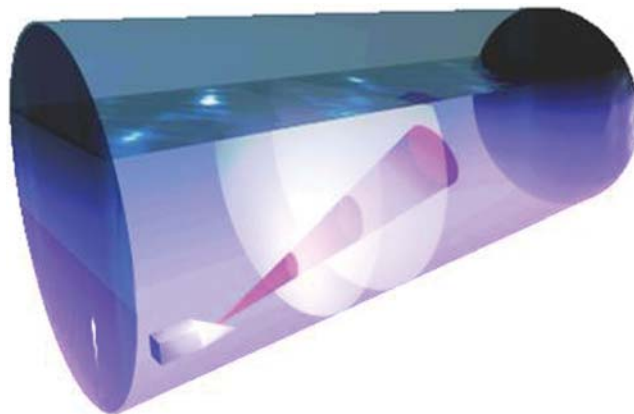

Figure 3.22 Scheme of the three-dimensional measurement cone (in pink) of a Doppler sensor and two sampled cross sections (in white). *Source*: courtesy Claude Joannis.

Table 3.2 Characteristics of three different Doppler sensors noted A, B and C (Larrarte *et al.*, 2008).

Sensor	Sensor A	Sensor B	Sensor C
Frequency (MHz)	1.0	0.5	1.0
Emission angle (degree)	15	31	14
Opening angle (degree)	17	10	24
Range (m)	>3.5	0.8	1.2

The international standard ISO 15769 (ISO, 2010) recommends some specifications for Doppler sensors:

- Emission angle θ.
- Opening angle θ_w of the ultrasonic beam.
- Range of the ultrasonic beam (i.e. the maximum distance along the measurement cone axis at which measurements are effective).
- Emission frequency f_S.
- Signal analysis.

As for ultrasonic travel time sensors (Figure 3.18), transverse or vertical velocity components tend to distort the measurement (Figure 3.21). Indeed, the true longitudinal velocity U_x (in green) may differ from the longitudinal velocity U_{s-x} estimated by the sensor (in blue) because the true velocity vector U (in black) at the location of the particle i is not necessarily parallel to the main axis of the pipe.

To estimate some specifications of Doppler sensors, Larrarte *et al.* (2008) developed a test bench and showed that these quantities vary considerably for different sensors (Table 3.2). During these tests, it was assumed that the maximum range is reached when the sensor is no longer able to read with an acceptable accuracy (i.e. less than 20%) the velocity of a controlled flow, located in a tube transparent to ultrasound, and immersed in a still water tank at a given distance from the Doppler sensor. It is therefore an arbitrary definition, which however partially reflects the actual *in situ* measurement capabilities and allows objective comparisons between different instruments.

The range is limited due to the attenuation of the received signals, whose intensity decreases when the distance to the sensor increases. This attenuation is a geometrical effect due to the distribution of the ultrasound energy on a spherical cap surface proportional to the square of the distance between the sensor transducer and the reflector (particle or bubble), along the return trip of the acoustic wave. Thus, the average velocity $\hat{U}$ given by the sensor is estimated from Equation (3.11):

$$\hat{U} = \frac{1}{\cos(\theta)} \frac{\sum_1^N \frac{U_{ri}}{d_i^4}}{\sum_1^N \frac{1}{d_i^4}} \tag{3.11}$$

where U_{ri} (m/s) is the local radial velocity of a reflector i, d_i (m) is the distance between the sensor and the reflector i, and N is the number of reflectors. When the term $1/d^4$ becomes too small, the corresponding signal becomes too weak with respect to noise, or, if it is not, the weight of the corresponding velocity becomes negligible.

Laboratory experiments have shown that wastewater, at usual suspended solids concentrations observed in sewers (below 1 g/L), does not attenuate ultrasound (Larrarte & Francois, 2012) and therefore has no influence on the range.
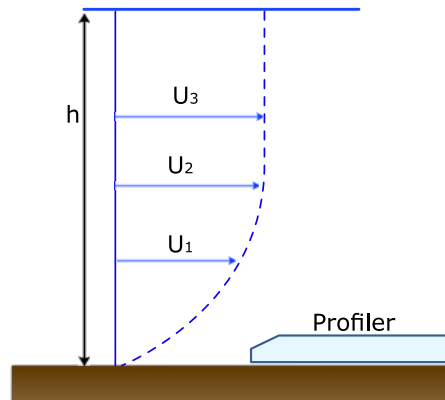
Figure 3.23 Principle of a Doppler profiler. *Source*: adapted from Larrarte *et al.* (2016a).

3.3.3 Velocity profilers

Aiming to correct the geometric attenuation effect affecting previously described standard Doppler sensors, new devices, named Doppler velocity profilers, have been available since the late 2000s (Figure 3.24 and Figure 3.25). They record both the scattered frequencies and the travel time of the emitted waves, which allows the determination of complete vertical velocity profiles, giving the velocities U_i, at different depths z_i (Figure 3.23). The discharge is then calculated using an area method (see Equation (3.3)), either assuming that the velocity is the same across the width of the wet section at each depth z_i or applying a weighting factor to account for slowing near the walls.

Figure 3.24 An ordinary Doppler sensor (left side, black sensor) and a Doppler profiler (right side, blue-grey sensor) during a comparison campaign. Note the tissues clogging on the connecting wires. *Source*: Université Gustave Eiffel.

Figure 3.25 The acoustic profiler used by Hemmerle *et al.* (2014) and Cedillo *et al.* (2016). *Source*: Hemmerle *et al.* (2014).

3.3.4 Free surface velocity measurements

Velocity measurement at the free surface is possible with sensors attached to the crown of the pipe (Figure 3.26), i.e. without contact with the effluent, except in case of exceptionally high flows. This technique offers decisive advantages in terms of maintenance, but the conversion of the velocity U_{fs} measured at the free surface to the mean velocity U_m through the wet section is more challenging (see introduction of Section 3.3.2). Proprietary (and often blind) data processing and algorithms provided by manufacturers for this conversion have to be carefully checked. Indeed, such a conversion is site specific and generic calculations cannot be assumed to be valid.
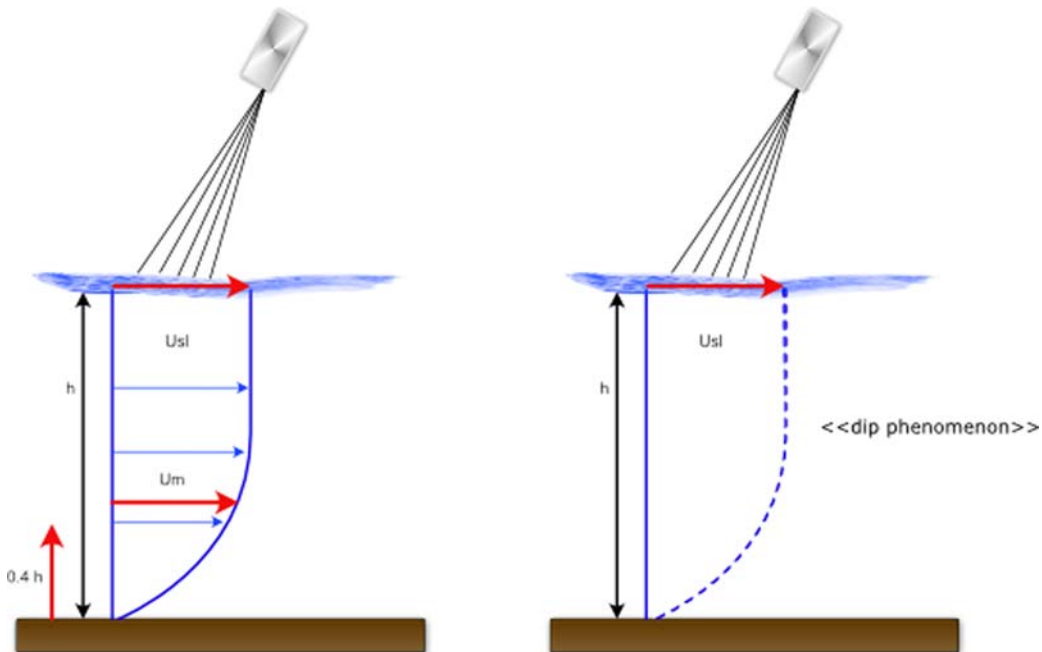

Figure 3.26 Measurement of free surface velocity U_{fs} and estimation of average velocity U_m. *Source*: adapted from Larrarte *et al.* (2016a).
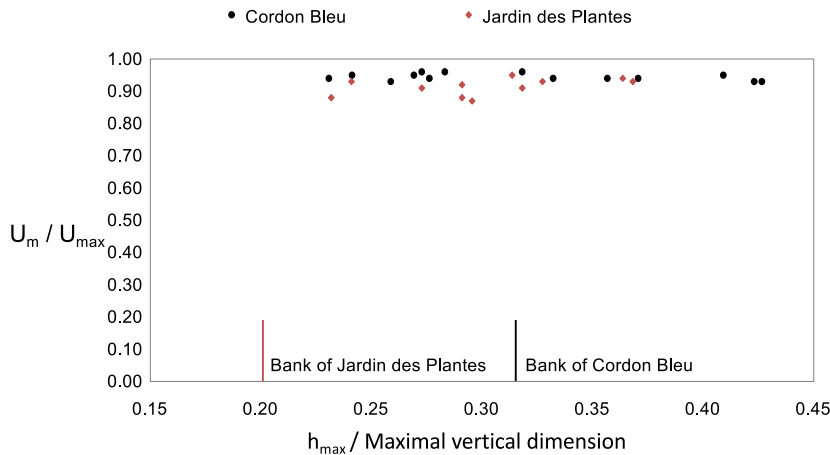
Figure 3.27 Evolution of the ratio of the average velocity U_m with the maximum velocity U_{max} for various filling rates for two egg-shaped sewers in Nantes, France. *Source*: adapted from Larrarte (2006).

The ISO 748 standard (ISO, 2007) indicates that the numerical coefficients to convert the free surface velocity U_{sl}, assumed to be the maximum velocity U_{max} along the vertical profile, to the mean velocity U_m, assumed to be observed at 60% of the total depth (i.e. $0.4 \times h$ from the pipe invert), vary from 0.84 to 0.90 depending on the pipe roughness. However, in two egg-shaped sewers, Larrarte (2006) found that empirical values of these numerical coefficients were between 0.90 and 0.96 (Figure 3.27).

Velocity measurements at the free surface typically use radar waves, but video imaging techniques are also under development. These techniques are developing rapidly for both sewers and rivers (Nguyen *et al.*, 2009).

Ideas on ultrasonic sensors

- I 3.1: Ultrasonic transit time flowmeter to measure flow velocity.
- I 3.2: Ultrasonic Doppler flowmeter to measure the velocity of particles and bubbles, assuming they are the same as the water velocity.

3.3.5 Electromagnetic sensor

The operating principle of electromagnetic (EM) flow/velocity sensors is based on Faraday's law of induction. The motion of the conductive fluid through a transversal magnetic field generates a voltage (Shercliff, 1962). To allow for the stationary analysis of the electromagnetic induction phenomenon, some electric and magnetic properties of the environment are assumed (Michalski *et al.*, 2001). Originally, under these assumptions, Kolin (1936) has given the basic relationship for the EM theory (Equation (3.12)):

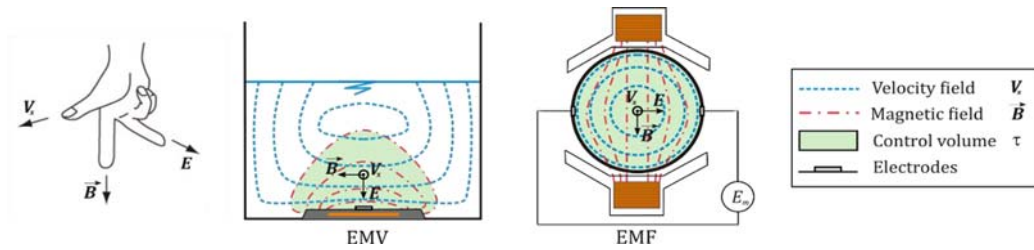$$\nabla^2 E = \text{div}(\vec{V} \times \vec{B}) \tag{3.12}$$

Figure 3.28 Right-hand rule governing Faraday's law of induction with cross-sectional illustrations of the EMV (bed mounted EM velocity meter) vs. the EMF (closed pipe EM flowmeter) sensors, and the reach of the respective control volumes. *Source*: Damjan Ivetić.

where $\vec{V}$ is the streamwise velocity field, $\vec{B}$ is the magnetic induction and $\text{div}(\vec{V} \times \vec{B})$ is treated as a charge distribution. The raw output signal is the voltage $E_m = E_m^1 - E_m^2$, induced between the electrodes of the EM sensor. The relations used in the electrical networks motivated an idea to describe how each part of the flow contributes to the voltage E_m (Equation (3.12)) through the weight function w (Shercliff, 1962) or, in a more rigorous formulation, through the weight vector $\vec{W}$ (Bevir, 1970):

$$E_m = -\int_0^\tau (\vec{V} \times \vec{B}) \cdot \vec{j} d\tau = \int_0^\tau \vec{V} \cdot (\vec{B} \times \vec{j}) d\tau = \int_0^\tau \vec{V} \cdot \vec{W} d\tau \tag{3.13}$$

where the cross product $\vec{B} \times \vec{j}$ defines Bevir's weight vector $\vec{W}$, τ is the control (sampling, or integrating) volume of the EM sensor (Figure 3.28) and $\vec{j}$ is the virtual current vector (i.e. the current density set up in the liquid by driving an imaginary unit current between a pair of electrodes). Since Faraday's law of induction is governed by the right-hand rule, the dominant contributor to the output E_m is the longitudinal component of the velocity vector, V_x, which is needed for flow measurement.

If the sampling volume τ envelops the whole cross section, such an EM device can be classified as a closed-pipe EM flowmeter (EMF). For EMFs, the output E_m is directly proportional to the average cross-sectional velocity $\bar{U}$. Conventional EMFs have high accuracy and precision and are common in pressurized flow application, where for axisymmetric flows, errors lower than 0.1% have been reported (Leeungculsatien & Lucas, 2013). In sewer systems, the EMF is mostly used downstream of pumping stations or on inclined reaches where aerated full-pipe conditions can be easily met, for diameters up to 0.6 m. Similar devices, but with lower accuracy, are available for application in pipes with varying flow depth, for diameters up to 0.8 m.

However, in sewers, the bed mounted EM velocity (EMV) sensors are more commonly used (Figures 3.29 and 3.30). In the bed mounted EMV application, τ is variable and depends on several factors: excitation current, coil design, conduit geometry, and water depth (for low depths). Since the excitation coil of the bed mounted EMV sensors is relatively small, the reach of the produced magnetic field is limited to the relative vicinity of the EMV (Figure 3.28). Consequently, the output voltage E_m is proportional to 'some' local velocity $\hat{U}$. The small control volume τ is considered as the biggest drawback of these sensors, as usually it is significantly smaller than in the case of the acoustic Doppler flowmeters. Therefore, additional care is necessary when considering the functional relationship needed to calculate $\bar{U}$ from the measured velocity $\hat{U}$ (Equation (3.13)). Laboratory tests as reported by Ivetić
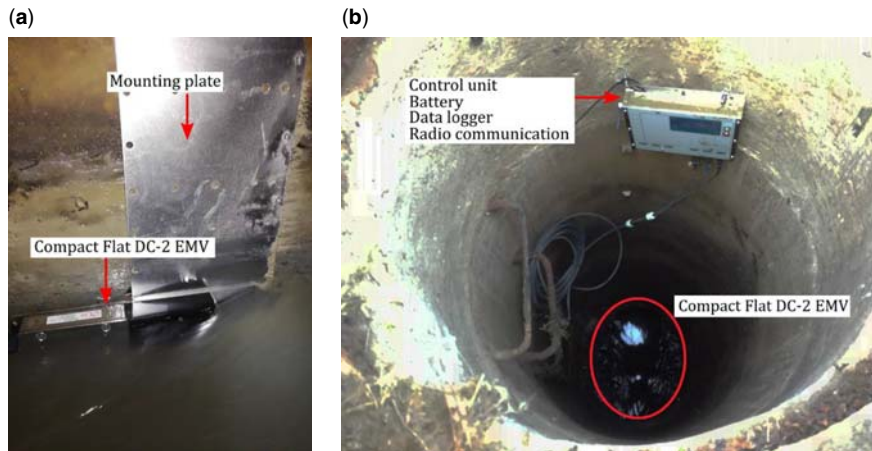
Figure 3.29 Application of the compact flat DC-2 EMV in the combined sewer system of Belgrade: (a) wall mounted; (b) bed mounted. *Source*: courtesy of Svet Instrumenata Ltd.

et al. (2018) imply that the constant coefficient k (Equation (3.5)) can be used to a certain extent, but it is deemed that in larger sewer pipes a function f (Equation (3.4)) is more suitable. If the variation of the longitudinal velocity distribution V_x is negligible across the width and length of the sensor control volume, a simplified mathematical model of the bed-mounted EMV operating principle can be used to define k and f (Ivetić *et al.*, 2019). The simplified model describes the EMV operating principle with
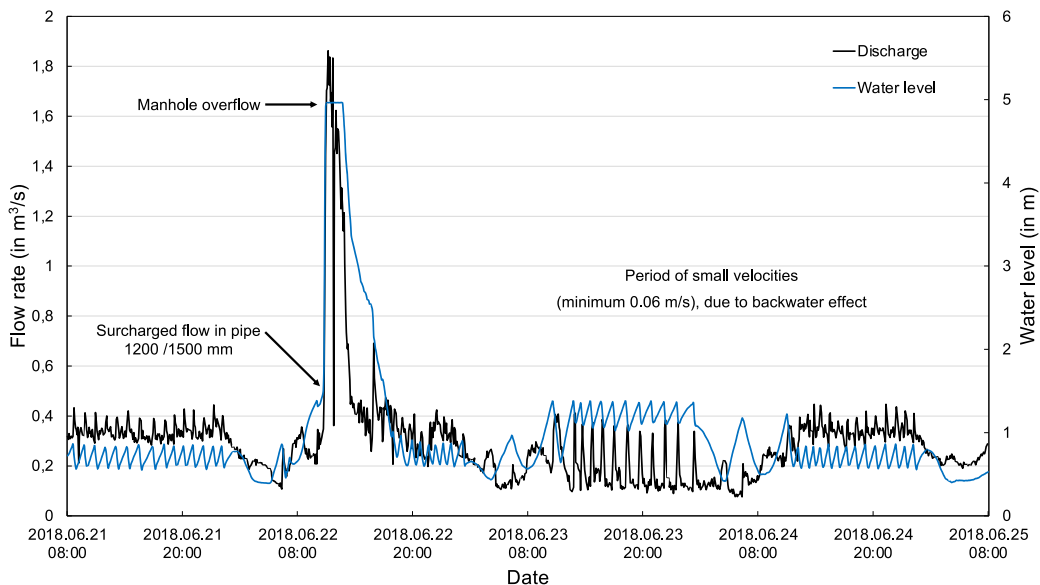

Figure 3.30 Flow rate and depth (pressure head) measured with compact flat DC-2 EMV, in the combined sewer collector of Belgrade. *Source*: adapted from Prodanović & Ivetić (2019).

only two technical parameters, one-dimensional weighting function $w(z)$ (Equation (3.14)) and the reach of the control volume noted as τ_{max}:

$$\hat{U} = \int_{Z_L}^{Z_U} w(z) \cdot V_x(z)dz \tag{3.14}$$

where z is the direction perpendicular to the sensor electrodes, and $Z_L = \max\{Z_{surf}, \delta\}$ and $Z_U = \min\{Z_{surf} + \tau_{max}, h\}$ define respectively the lower and upper limits of integration. If some porous sediment deposit of depth δ is present above the sensor body, the lower integration limit is shifted upwards. Similarly, if the water depth h is less than the sum of the sensor height Z_{surf} and reach of the control volume τ_{max}, the upper integration limit is shifted downwards.

Direct laboratory comparisons between EMVs and acoustic Doppler flowmeters (Aguilar *et al.*, 2016; Ivetić *et al.*, 2018) revealed that, although the control volume of the EMV is close to the probe, due to the operating principle, it is more precise and robust in the assessment of the average cross-sectional velocity $\bar{U}$. Also, the EMV can operate in full-bidirectional flows with velocities lower than a few centimetres per second, so they are convenient to use in flows influenced by backwater effects (Figure 3.30).

Potentially, the most interesting benefit of EMV use in urban drainage, experimentally examined in Ivetić *et al.* (2018), is the ability for velocity measurements in the case of sedimentation over the sensor housing (Figure 3.31). This is a common situation in sewers and even a small layer of sediment (or plastic bags, rags, toilet paper, etc.) may prevent the correct functioning of some other types of velocity sensors (mostly ultrasonic ones). However, if the sediment is porous and not affecting the EM properties of the device, EMVs continue to operate. For small sediment depths (i.e. a few millimetres), errors are negligible. For larger sediment depths δ, the output is biased. Preliminary laboratory results imply that a correction function model (CFM) can be experimentally determined for the particular sediment composition and EMV sensor model, to minimize the resulting bias. To apply the CFM at the measuring site, continuous sediment depth measurements are needed. The depth of the sediment above the EMV sensor is directly
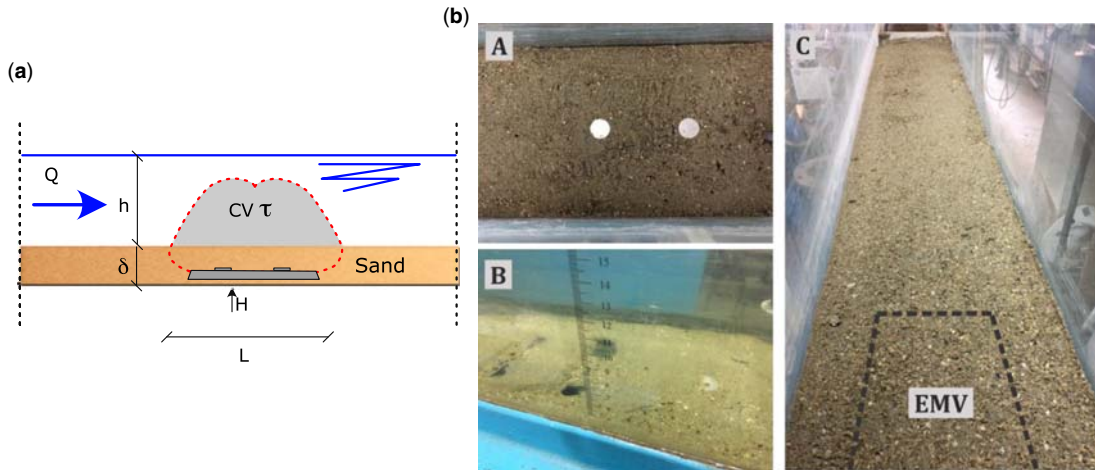

Figure 3.31 (a) schematic illustration of the EMV operation under sand sediment; (b) laboratory experiments: A) sand sediment depth of $\delta = 23$ mm, B) linearity loss with $\delta = 23$ mm due to dune formation, C) $\delta = 80$ mm. *Source*: adapted from Ivetić *et al.* (2018).

proportional to the slope and intercept values of the correction functions. It should be highlighted that in the case of sedimentation, the user should also compensate the water level measurements (reduced wet section area) for the presence of sediment.

On the other hand, failure mechanisms encountered with these devices are related to disruptions in the contact between the electrodes and the conductor (i.e. water). When the electrodes of the EM sensor are covered with an impervious material, such as cemented sediment or plastic bags, the current $\vec{j}$ path is disrupted or elongated and the resistance of the formed 'conductor' (water path between electrodes) is increased, resulting in a significant or complete loss of the output signal. Another failure mechanism is related to the hardness of water. If an insulating layer of limescale, resulting from the presence of calcium and magnesium carbonates, is formed on the electrodes of the EM sensor, again the resistance of the formed conductor (between electrodes) is dramatically increased, resulting in a decrease of the output voltage E_m. Highly aerated water can also present a problem, since air pockets can easily cover the electrodes and increase the uncertainty of the velocity measurements.

Ideas on EMV

- I 3.3: EMV meters can measure both pressure and velocity.
- I 3.4: EMV can operate under the porous sediment layer of few centimeters – but the output will be biased proportionally to the depth of the sediment layer.
- I 3.5: EMV measures the voltage difference generated by the motion of the conductive liquid through the sensor's magnetic field.

3.3.6 Manning-Strickler relation

The Manning-Strickler relation is just one of the most famous relations giving the flowrate without measuring the velocity. It is theoretically valid only for uniform permanent flows and it gives the mean velocity U_m as a function of the geometry of the site and the water level (Equation (3.15)):

$$U_m = K R_h^{\frac{2}{3}} s^{\frac{1}{2}} \tag{3.15}$$

where s (m/m) is the invert slope and K (m$^{1/3}$/s) is the Manning-Strickler coefficient that characterizes the roughness of the sewer walls. This coefficient should be validated on each site as shown by Jaumouillié *et al.* (2002). Although the Manning-Strickler relation is seemingly straightforward and easy to apply, it is not recommended for use because

- Backwater effects or hydraulic jumps can occur unnoticed and introduce unseen and significant systematic errors.
- The value of K cannot be assumed to be a constant but has rather to be named the Manning-Strickler variable quantity as it varies with the water depth (Bertrand Krajewski *et al.*, 2000).
- A fully developed velocity profile is implicitly assumed to be present, which is hard to guarantee or to check in practice.

Table 3.3 Advantages and disadvantages of various technologies for velocity measurements.

Technology	Advantages	Disadvantages
Transit time	• Accurate measurement • Less sensitive to fouling than Doppler sensors • Approved in ATEX zones • Continuous measurements • Can operate in mixed flow regimes (pressurized and free surface flows)	• Requires important civil engineering work • The sensors are fixed and cannot be removed • Delicate installation for alignment of the sensors • Relatively expensive equipment • Few manufacturers • Not suitable for small diameters (<1 m) • Not suitable for use in the presence of air bubbles
Acoustic Doppler flowmeter	• Little civil engineering work and quick installation • Prices and large number of suppliers • Possibility to associate velocity and water level measurements on the same device • Possibility of temporary use and autonomous power supply • Continuous measurements	• Range poorly defined, can be poorly adapted to channels greater than 1.5 m wide • Sensitive to clogging and sediment deposits • May be poorly adapted to slow flows (velocity <0.1 m/s), and low water levels (<0.1 m) • Sensitive to air bubbles
Doppler velocity profiler	• Rather easy to install • Various suppliers • Continuous measurements	• May be not so cheap • Range may be poorly defined
Free surface velocity measurements (radar)	• Reduced maintenance • Suitable for all types of water where the free surface is disturbed • Large velocity range • Quick installation • Suitable for high flow velocities (up to 10 m/s) • Continuous measurements	• Large device: minimum 40 to 90 cm wide • Conversion of free surface velocity to mean velocity to be calibrated
Electromagnetic flowmeter (EMF)	• Very good performance in closed pressurized pipes • Low maintenance • Does not disturb the flow • Suitable for highly contaminated media • Continuous measurements	• Sensitive to air bubbles • Civil engineering work constraints • Significant investment • No measurement below 10% pipe filling rate • Not easy to apply for free surface flows (need to envelop the whole wet perimeter)
Electromagnetic velocity meter (EMV)	• Reduced maintenance • Does not disturb the flow • Suitable for all diameters • Suitable for highly contaminated media • Possibility to associate velocity and water level measurements on the same device • Possibility of temporary use and an autonomous power supply • Continuous measurements • Operation under porous sediment	• Insulation of electrodes by limescale or plastic bags • Small control volume • Sensitive to air bubbles
Manning-Strickler relation	• Basically, requires only a water level measurement	• Limited to uniform steady flows, inaccurate, site specific calibration needed

> ⚠️ **Manning-Strickler**
>
> The Manning-Strickler relation is usually not applicable as a reliable method to estimate discharges in sewers.

3.3.7 Summary

The main advantages and disadvantages of the technologies that are most commonly used to measure the flow velocity in urban sewers are summarized in Table 3.3.

3.4 DIRECT DISCHARGE MEASUREMENTS
3.4.1 Pre-calibrated devices

A wide range of pre-calibrated devices exist for open channel flow measurement. The principle is to have the water level rising due to a contraction of the section and then, using a calibrated relation $Q(h)$, to calculate the flowrate. There are many different devices such as rectangular broad-crested weirs (ISO, 2008), triangular profile weirs (ISO, 2020), trapezoidal broad-crested weirs (ISO, 1999), round-nose horizontal broad-crested weirs (ISO, 1990), flat-V weirs (ISO, 2012) and calibrated flumes such as Venturi flumes (ISO, 2013), each with a number of advantages and disadvantages of varying importance depending on the characteristics of the sites to be monitored.

One common problem with those devices is their sensitivity to clogging due to debris in the flow or due to biofouling, which is certainly the case in wastewater. One has to be aware that when implementing these so-called pre-calibrated devices, the $Q(h)$ relations given in the standards or textbooks are valid only for a set of defined conditions (temperature range, certain water level thresholds due to surface tension effects, minimum water level to apply the relation, requirements on upstream and downstream flow conditions). Unless incorporated during the design, such conditions are difficult to apply in a practice situation at reasonable costs. A further disadvantage is that the implementation of any weir, flume or Venturi in an existing system will cause a backwater effect not taken into account in the system design, with possible risk of upstream flooding. Therefore, it is suggested to avoid using such constructions for discharge measurements as much as possible, with the exception of existing weirs or construction taken into account in the original design. It is stressed that for such constructions an *in situ* calibration is mandatory when data with a known uncertainty are to be obtained. Section 3.4.2 illustrates a comparison between $Q(h)$ relations resulting from a physical scale model and a computational model.

> ⚠️ **Pre-calibrated devices vs. conditions**
>
> Pre-calibrated devices are sensitive to clogging and sediment deposits.

3.4.2 *Q*(*h*) relation using laboratory physical scale models

An alternative to pre-calibrated devices consists of using existing structures in sewer systems as measuring devices, with case-by-case determined *Q*(*h*) relations. Such *Q*(*h*) relations can be determined by means of laboratory physical scale models, CFD (computational fluid dynamics) simulations or *in situ* measurements.

In complex geometries, like junctions, confluent channels or other locations with a strongly varying 3D velocity flow field (Figure 3.32), it is often not easy to identify a location for water level measurement that can be used as the input for a *Q*(*h*) relation. Although a CFD numerical model can be used to simulate the 3D velocity flow field, a laboratory physical scale model can be chosen as an alternative.

There are some reports in which the results of the comparison of CFD and physical models are reported. For example, van Daal-Rombouts (2017) and Dufresne *et al.* (2018) conclude that 'fair' agreement is found, with deviation in velocities up to 20–30% and water levels that are in good agreement between the CFD model and physical model. Both approaches have their strong and weak points. Especially in multi-phase problems (sediments, air entrainment), CFD models sometimes may show flows that are difficult to recognize yet represent 'unphysical' results. In such cases, an independent verification is needed, e.g. by means of a physical scale model. On the other hand, physical models are normally built to some geometric scale. A geometrical scale between 5 and 10 is generally accepted to result in manageable models while not suffering too much from scale effects. In a sense, physical scale models and CFD are used as complementary means. By using the results of a physical scale model to validate a CFD model, the latter can be used to answer 'what if' questions in a design process or scale up to the prototype scale to eliminate the scale effects of the physical scale model. For application of either CFD or a physical scale model, specialist knowledge and professional means are needed. With respect to CFD modelling, the calculation effort can be considerable, thus limiting the number of simulations that can be made within a reasonable timeframe. On the other hand, in a physical scale model, geometrical changes are not easily made and making a 'model run' requires time from specialized personnel. There is no general preference for either CFD or a physical scale model, both have strong and weak points. Making a choice is largely a matter of carefully considering the dominant processes involved. For example, when designing a pump sump, it is of importance to know the pre-rotation of the flow approaching the pump to avoid cavitation, further the occurrence of unstable vortices and air intake should be avoided. These

Figure 3.32 Example of a combined sewer overflow (CSO) laboratory physical scale model. *Source*: van Daal-Rombouts (2017).

phenomena are not considered to be correctly reproduced by CFD models. For this reason, application of physical scale models is recommended or even prescribed in some standards (see Hydraulic Institute, 2018; Verhaart *et al.*, 2016).

A key issue in the application of physical scale models is the choice of the geometrical scale while keeping in mind that the physical properties (viscosity, density) of the fluid used (virtually always water) cannot, or can to a limited extent only, be scaled. The viscosity is temperature dependent, so by varying the temperature the viscosity can be changed. As for surface tension, this parameter can be influenced by using a (preferably non-foaming) detergent, a reduction with a factor of $\sim$2 is feasible in this manner. Scaling effects can be reduced as much as possible. However, in many situations, it is impossible to apply geometric scaling and maintain a dynamic similarity between the full-scale structure and the physical scale model. In the case of a free surface flow, the scale is mostly chosen such that the Froude number *Fr* in both the physical scale model and full-scale structure are equal. This is the Froude similarity, i.e. the ratio between kinetic and potential energy is conserved as it is the dominant energy ratio in gravity driven flows. This poses some more or less severe restrictions on the range of water levels that can be tested effectively due to the non-scale-ability of surface tension and viscosity. In this respect the deviation between the physical scale model and the real structure for the Weber and Reynolds numbers (resp. *We* and *Re*) should be accounted for. In most practical situations in urban drainage, the flow is turbulent (i.e. $Re > 10^4$–10^6). As a rule of thumb, the Reynolds number in the physical scale model should not drop below $\sim 10^3$–10^4. With respect to the Weber number, there is no real consensus on the lower critical limit (opinions vary between 10 and 100). This implies, that when taking a geometrical scale *n*, the following limitations are to be respected (Equations (3.16)):

$$Fr_p = \frac{V_p}{\sqrt{gh_p}} = Fr_m = \frac{V_m}{\sqrt{gh_m}} \tag{3.16a}$$

$$Re_m = \frac{H_m V_m}{v} > 10^4 \tag{3.16b}$$

$$We_m = \frac{\rho V_m^2 L}{\sigma} > 10 - 100 \tag{3.16c}$$

where the indexes *p* and *m* refer respectively to the full-scale structure and the physical scale model, *V* (m/s) is the flow velocity, *g* (m/s^2) is the gravity acceleration, *h* (m) is the water level, *H* (m) is the characteristic dimension of the physical scale model, *v* (m^2/s) is the kinematic viscosity of water, ρ (kg/m^3) is the density of the water, *L* (m) is the characteristic length, and σ (N/m) is the surface tension.

The Weber number W_e (ratio between inertial forces and surface tension forces) is normally in the order of magnitude of 10^2–10^4. As with the Reynolds number, the Weber number cannot be assumed identical in the full-scale structure and scale model. Added surfactants can reduce the surface tension by approximately 30–50%, this may be utilized in a scale model when the Weber number becomes too small. When deciding on a geometrical scale *n*, this implies that:

- All geometrical measures scale with this factor *n*.
- When striving for Froude similarity, the velocity scales with $n^{0.5}$.
- The Reynolds number scales (in Froude similarity) with $n^{1.5}$.
- The Weber number scales with n^2.
- The discharge scales with $n^{2.5}$.

The impact of scaling is illustrated by an example taken from van Daal-Rombouts (2017) and van Daal-Rombouts *et al.* (2017). In this example, a scale model was used to find a *Q(h)* relation and a
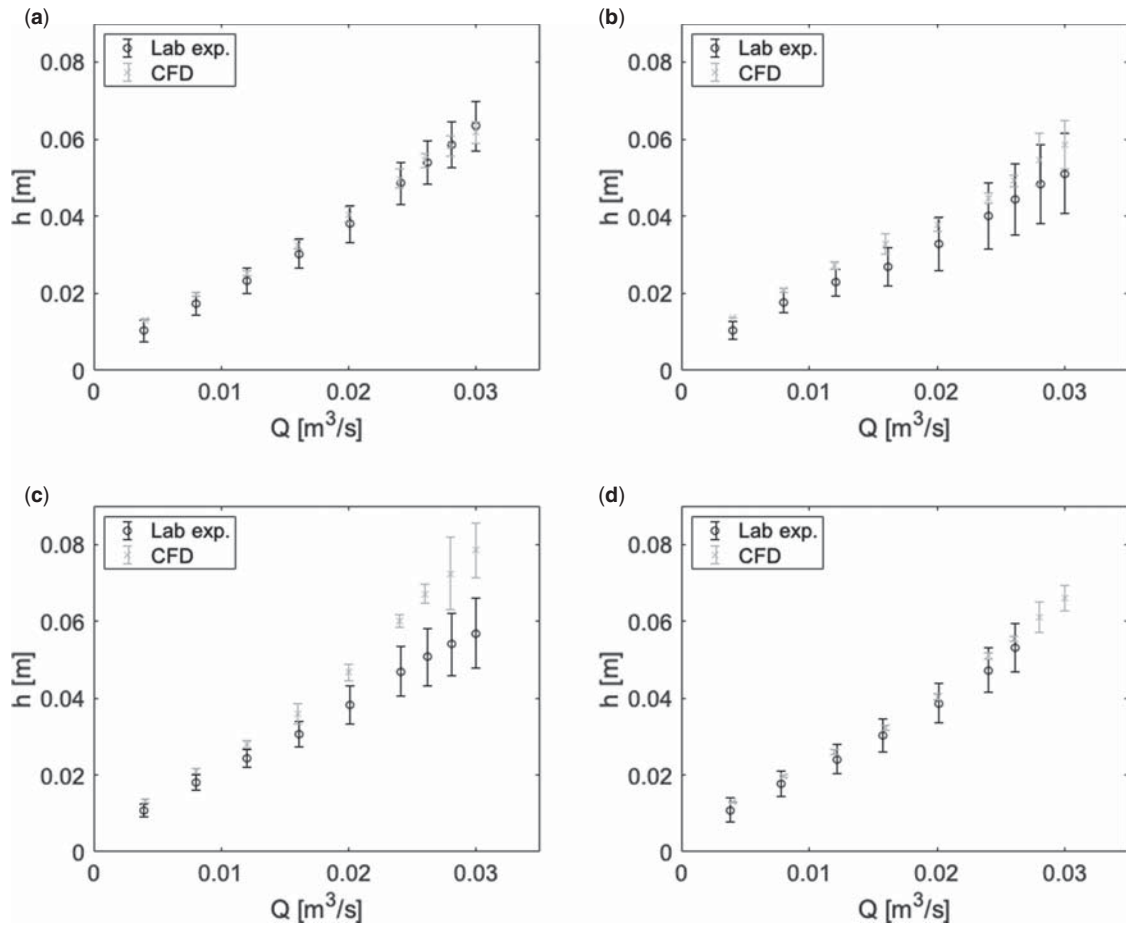
Figure 3.33 Results from physical scale model experiments and CFD modelling: (a), (b), (c) and (d) refer to four different locations along the length of the weir. As can be seen, there is a reasonable match between physical scale model and CFD model (after validation) apart from location (c) where significant deviations occur. *Source*: van Daal-Rombouts (2017).

suitable monitoring location for placing a water level sensor for a CSO construction as shown in Figure 3.32. In this case, $n = 8$. For the prototype a discharge of $\sim 5.5\,\text{m}^3/\text{s}$ was expected. The discharge in the scale model was reduced to a maximum of $\sim 0.03\,\text{m}^3/\text{s}$. Given the choice for the characteristic length scale, the Reynolds number in the prototype was $\sim 5 \times 10^4$ which is reduced by a factor of 81.5 to *ca.* 2000 in the physical scale model, which is just in the turbulent region. The Weber number, given the choice of the characteristic length in the order of magnitude of 100, is reduced by a factor of 64. As the Weber number reflects the ratio between inertial forces and surface tension forces, this indicates that in the full-scale structure the effect of surface tension (curvature of streamlines) is much less explicit than in the model. This directly translates back into a lower imitation of the range of discharges and water depths that can be explored in the physical scale model while assuming a classic $Q(h)$ relation in the form of $Q = ah^b$ in which the effect of surface tension is omitted. For all practical purposes, when measuring a water depth over the
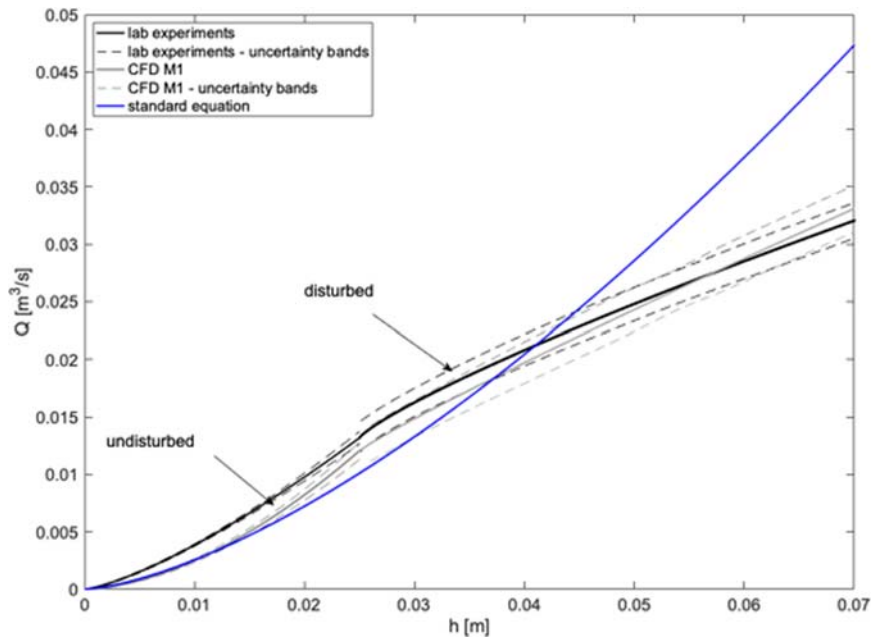
Figure 3.34 $Q(h)$ relations found for two locations as derived from physical scale and CFD models. 'Disturbed' refers to the situation in which backwater effects occurred. *Source*: van Daal-Rombouts (2017).

crest of a weir that is less than ∼6 mm, the usually applied $Q(h)$ relations (e.g. the Kindsvater & Carter (1957) formula) are, strictly speaking, not valid, nor in the full-scale structure, nor in the scale model.

A comparison between the results obtained from the physical scale model and results from a CFD simulation are shown in Figure 3.33.

In Figure 3.34 the resulting $Q(h)$ relations for two locations based on the physical scale model and the CFD model are shown. It can be observed that:

- The relations for the two locations are mutually different.
- There is no significant difference between physical scale and (validated) CFD models.
- The 'standard' equation shows significant deviations relative to the model-based relations.

The added value of the physical scale model in this case was found in the identification of suitable locations for the water level sensor and the validation of the CFD model. For a more in-depth treatise on hydraulic scale models and associated scale effects, the reader is referred to the literature, e.g. Ettema *et al*. (2000) and Heller (2011).

3.4.3 Chemical tracing

3.4.3.1 Principle

Tracer experiments offer a method to measure discharges, with a simple and single assumption: the mass of tracer is constant along the reach, i.e. the mass measured downstream is equal (Equation (3.17)) to the mass
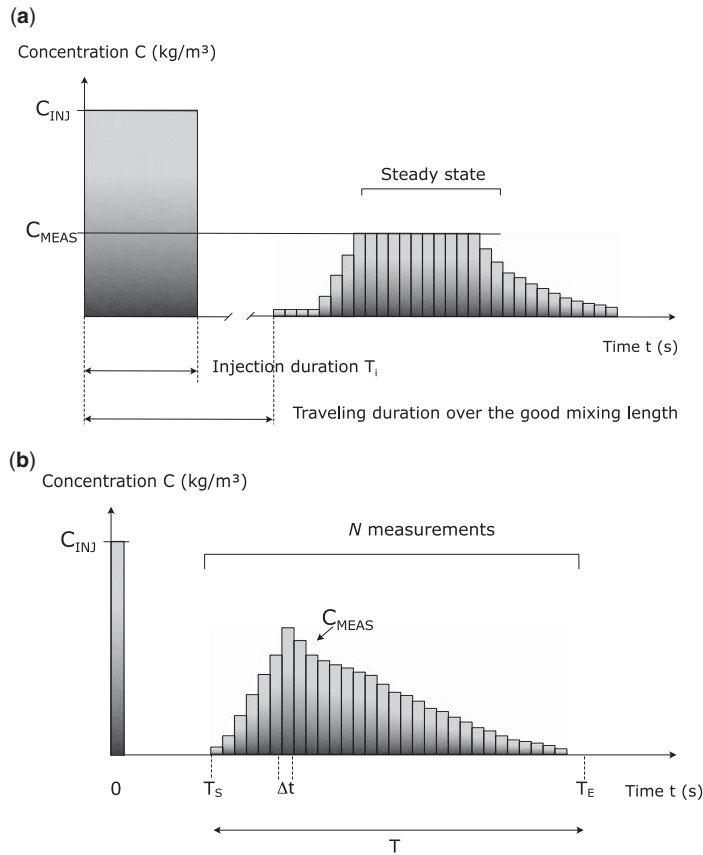
(a)

Concentration C (kg/m³)

(b)

Concentration C (kg/m³)

Figure 3.35 Injection and measured time series for both continuous (a) and spike (b) injections. *Source*: adapted from Bertrand Krajewski *et al.* (2000).

injected upstream:

$$M_{INJ} = M_{MEAS} \tag{3.17}$$

where M_{INJ} and M_{MEAS} are respectively the injected and measured masses of tracer (kg). There are two kinds of tracer experiments: continuous or spike injection (Figure 3.35).

The average discharge Q_{MEAS} (m³/s) along the reach can be calculated from Equations (3.18): Equation (3.18a) for continuous injection, Equation (3.18b) for spike injection.

$$Q_{MEAS} = q_{INJ} \times \frac{C_{INJ}}{C_{MEAS}} \tag{3.18a}$$

$$Q_{MEAS} = \frac{M_{INJ}}{\sum_{t=T_S}^{t=T_E} C_{MEAS} \times \Delta t} \tag{3.18b}$$

where q_{INJ} (m³/s) is the tracer injection discharge, C_{INJ} (kg/m³) is the concentration of the injected tracer, C_{MEAS} (kg/m³) is the tracer concentration measured downstream, T_S and T_E are respectively the start and end

Table 3.4 Available tracers and their pros and cons.

Tracers	Advantages	Disadvantages
Lithium	• –	• Not measurable continuously
Heavy water	• –	• Not measurable continuously
De-icing salts	• Low price • Availability • Measurable continuously with a conductivity meter	• Not constant background signal • Sometimes requires large volume for injection
Rhodamine B	• Measurable continuously with a fluorometer • Usually constant background signal	• Sensitive to TSS (total suspended solids)
Rhodamine WT	• Measurable continuously with a fluorometer • Usually constant background signal • Insensitive to TSS	• High price • Toxicity

times of the tracer spike at the downstream measurement location, and Δt (s) is the time step between two measurements.

For both methods, the estimation of Q_{MEAS} directly depends on the measurement of C_{MEAS}, which must absolutely be uniformly distributed across the measurement section. To ensure this uniform distribution, three conditions must be carefully checked along the reach: (i) there should be no active lateral house connection, (ii) the flow should not be split in two or more parts, and (iii) the length of the reach should be 75 times (respectively 150 times) longer than the largest hydraulic dimension of the wet section (water depth, width, etc.) if the injection is done in the middle (respectively on the side) of the flow. Several tracers can be used in urban drainage. Table 3.4 presents their pros and cons.

The continuous injection requires a larger quantity of tracer and more sophisticated hardware equipment, but the data processing is easier. On the contrary, spike injection experiments are easier to conduct, but require more elaborate data processing: to facilitate its application, the reader is invited to use the Excel® file and the Matlab® code available for download at https://doi.org/10.2166/9781789060102. For the tracer, de-icing salts are recommended for situations with a small discharge and short reach. When the injection volume becomes too large (a few tens of litres or more), Rhodamine WT is recommended.

3.4.3.2 A nine step operation protocol

This section gives a summary (Figure 3.36) of the spike injection method presented in detail in Lepot *et al*. (2014).

After the reach has been identified and appears to be suitable for such experiments (good mixing conditions), the first three steps deal with the preparation in the office or in the laboratory: (i) calibration of the measuring device (fluorometer for fluorescent tracer or conductivity sensor for de-icing salt), (ii) study of the injection device, i.e. study of the true volume injected by pipettes in the case where fluorescent tracer is used, and (iii) preparation of the solutions to be injected (de-icing salt at 180 g/L or dilution of commercial solution of fluorescent tracer).

The following steps can be done *in situ*. The fourth step consists of estimating the mass of tracer to inject, given the sewer reach and its hydraulic conditions. The basic equation of longitudinal dispersion (which describes the evolution of a tracer concentration C along a reach and over time) is required to understand
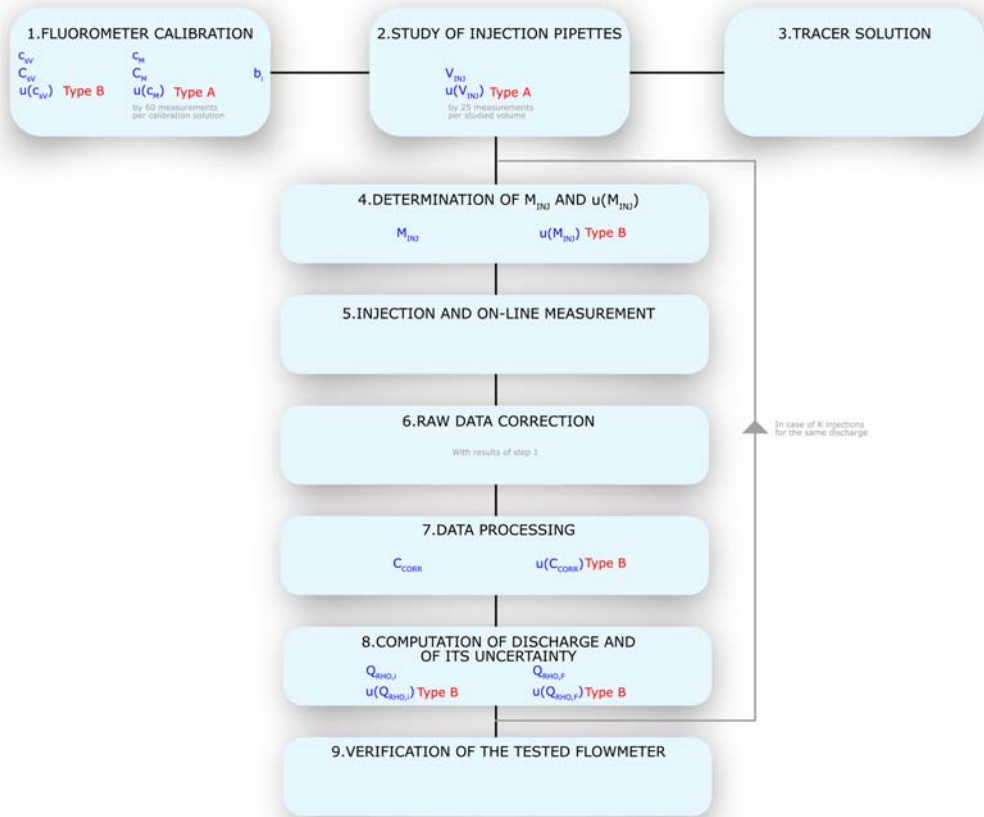
Figure 3.36 Sketch of the nine-step protocol, given here for Rhodamine WT. For details, please refer to Lepot *et al.* (2014). *Source*: adapted from Lepot *et al.* (2014).

this calculation (Equation (3.19)).

$$\frac{\partial C}{\partial t} + U_m \frac{\partial C}{\partial x} = K_X \frac{\partial^2 C}{\partial x^2} \tag{3.19}$$

where C is the tracer concentration (kg/m^3), x (m) is the distance from the upstream injection location, t (s) is the time, U_m (m/s) is the average flow velocity along the reach, and K_X (m^2/s) is the dispersion coefficient.

There are various possibilities to set the value of K_X (Rieckermann *et al.*, 2005). For most sewer reaches, straight and without back flow, the dispersion coefficient given in Equation (3.20) is recommended.

$$K_X = 6h\sqrt{ghs} \tag{3.20}$$

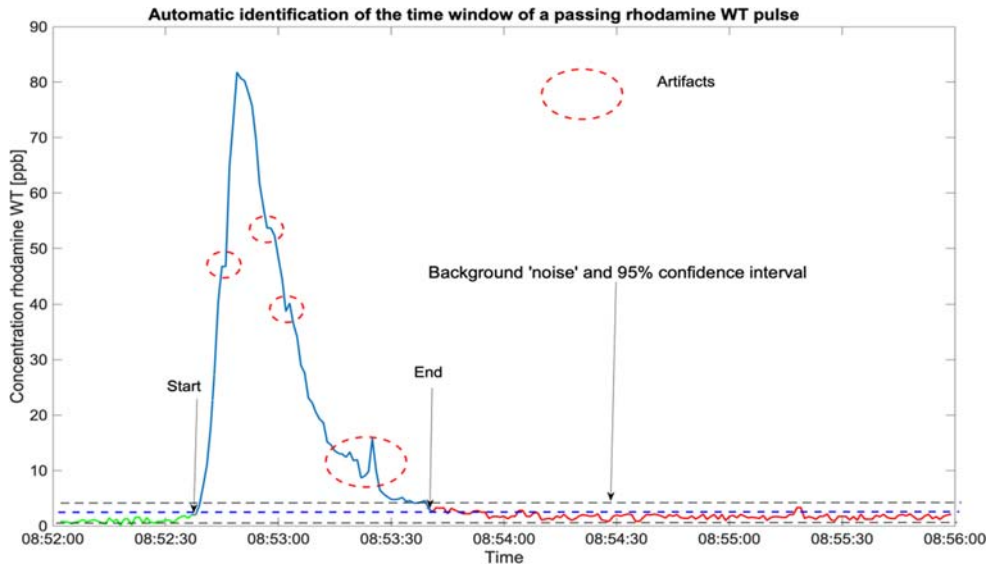where h (m) is the water level, and s (m/m) is the slope of the reach.

Figure 3.37 Data processing for the transit of a spike injection of Rhodamine WT. *Source*: adapted from Lepot *et al.* (2014).

Ideas on the M_{INJ} estimation

- I 3.6: *Sensors in place* – Since M_{INJ} should be only roughly estimated, data coming from even doubtful flowmeters could be used for this calculation (water level, velocity).
- I 3.7: *Water level* – Estimate the water level with a ruler.
- I 3.8: *Velocity* – By throwing floating materials (e.g. plant, balls), the free surface flow velocity U_{fs} can be estimated from their travel time along the reach. The mean flow velocity U_m can then be estimated by multiplying U_{fs} by a numerical coefficient approximately equal to 0.85 to account for the velocity profile (see Figure 3.12).

Equation (3.21) presents a possible analytical solution to the partial differential Equation (3.19):

$$C_{MEAS}(x, t) = \frac{M_{INJ}}{S_m \times \sqrt{4\pi K_X t}} e^{-\frac{(x-ut)^2}{4K_X t}} + C_{BG} \tag{3.21}$$

where S_m (m^2) is the average wet section along the reach. M_{INJ} should be chosen to ensure that the maximal value of C_{MEAS} at the measurement location is: (i) 3 to 4 times larger than the background concentration, C_{BG}, and (ii) within the linear range of the sensor calibration function. These maximal values are typically 2 g/L for salts and 80 ppb for Rhodamine WT.

Once M_{INJ} has been injected and C_{MEAS} is recorded (step 5), raw data need to be corrected (see Section 7.6 on sensor calibration) and processed (step 6, Figure 3.37). The data processing includes two steps: automatic identification of the start and end of the spike injection transit and removal of artefact and outlier values.

Once data have been cleaned, the discharge can be calculated (step 8, Equation (3.18b)). Its value might be used to check an existing flowmeter. Lepot *et al.* (2014) give all details to consider several injections and assess the uncertainties in all intermediate quantities and in the value of Q_{MEAS}.

⚠ No connection nor divergence along the reach

The tracer should be uniformly distributed across the downstream measuring section. Attention should be paid to the absence of or negligible inflows upstream of the measuring section, or to any divergence (e.g. bypass of the flow) downstream of the injection point as it engenders a loss of tracer resulting in an incorrect mass balance. In such cases, the locations of both injection and measuring points should be adapted to ensure appropriate conditions for the tracer experiment.

3.4.3.3 Examples of application

3.4.3.3.1 Rhodamine WT and de-icing salt tracings vs. flowmeter measurement of small discharges in a large sewer

Rhodamine WT and de-icing salt tracer experiments have been conducted at the inlet of a stormwater retention tank in Chassieu, France, in a large (diameter of 1.6 m) and steep (slope of 0.01 m/m) sewer. Results show that the flowmeter in place underestimates the flow and that Rhodamine WT and salt experiments deliver consistent results (Figure 3.38).

3.4.3.3.2 *Rhodamine WT tracing for two monitoring stations: large pipe, large discharges*

In a catchment of Greater Lyon, France, two measuring locations gave inconsistent discharge values: daily cumulated volumes in both locations were similar despite the fact that between the upstream and downstream locations, the population connected to the sewer system in the catchment increases by 20%. Rhodamine WT tracer experiments have been conducted for discharges varying from 250 to 550 L/s.

Figure 3.39 shows two important facts. The first being the difficulty in conducting tracer experiments immediately downstream of a pumping station: Figure 3.39(a): starts and stops of the pump generate mean values of the flow which are almost constant over pumping cycles due to the averaging by the *in situ* flowmeter, while the more instantaneous tracer experiment reveals that the flow varies significantly during pumping cycles. The second is the underestimation of the flow by the *in situ* flowmeter at the downstream location: all tracing experimental data are located above the expected ideal case (dashed red line) where the discharges given by the tracer experiments are supposed to be equal to the ones given by the flowmeter.
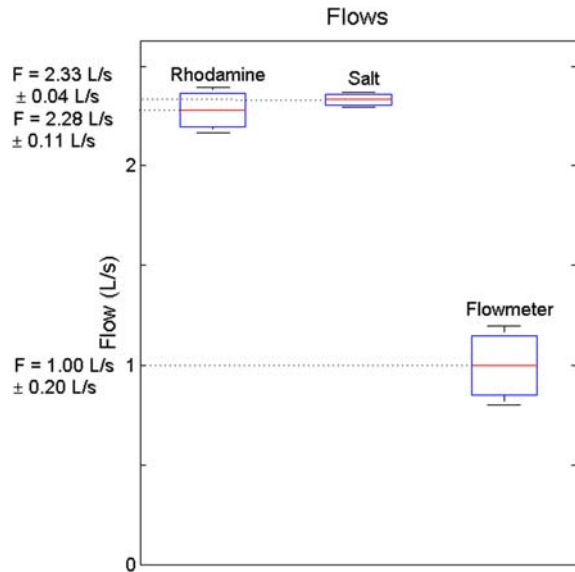
Figure 3.38 Comparative flow measurements with Rhodamine WT tracer experiment (left box plot), de-icing salt tracer experiment (central box plot) and in place flowmeter (right box plot) in the inlet sewer of a stormwater retention tank in Chassieu, France. *Source*: Lepot *et al.* (2014).
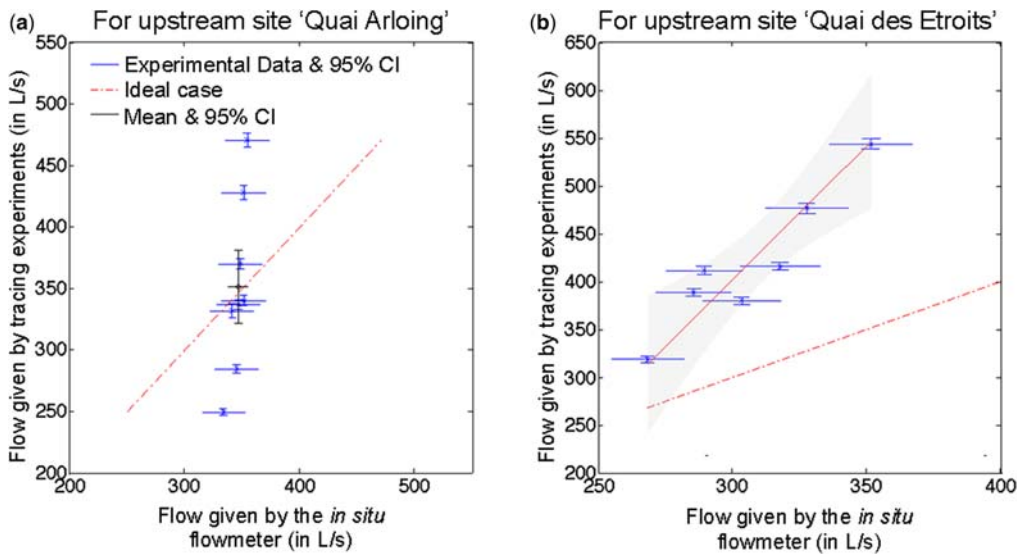

Figure 3.39 Flow measurements by Rhodamine WT tracer experiments and by in place flowmeters upstream (a) and downstream (b) of a pumping station in Greater Lyon, France. Blue horizontal bars represent the flow and its uncertainty given by the *in situ* flowmeter, and the blue vertical bars represent the corresponding flow and uncertainty given by tracer experiments carried out at the same moment. *Source*: adapted from Lepot *et al.* (2014).

> **Ideas on tips in the field**
>
> - I 3.9: *Control the flow* – Check if the flow can be increased, decreased or controlled in order to ensure stable conditions during the tracer experiments, or cover a wide range of hydraulic conditions as shown in the example of Figure 3.39.
> - I 3.10: *Repeat* – Given the low marginal cost of additional spike injections, it is often worth performing several injections to get more accurate results (repeated measurements) when staff and all equipment are on site.
> - I 3.11: *Be patient* – Be patient during two consecutive injections in the field, to ensure you can record the background signal between two peaks of tracer.
> - I 3.12: *Always check immediately* the recorded data (presence of values, clean peaks) in the field to ensure that the data can be processed later: do not wait to be back in the office to discover possible problems, errors, failures, etc.

3.4.4 Pumping stations

3.4.4.1 Introduction

Pumping stations play a key role in many urban drainage systems, especially in wastewater and combined systems in flat areas. The importance of monitoring pumping stations in urban drainage has been highlighted in some publications, e.g. Korving *et al.* (2006) or Kooij *et al.* (2015). Monitoring their performance is important for a range of reasons:

- Qualification/testing of newly built installations.
- In applications of Real Time Control, variation of pump discharge is often applied as one of the methods to adapt a system's behaviour.
- For asset management: decreasing performance can be detected, and corrective actions can be induced.
- Controlling energy consumption.
- Early warning of ageing processes.

The reasons mentioned necessitate permanent monitoring. However, this is not always applied due to financial reasons and/or a lack of interest. Next to a permanent monitoring set-up, monitoring campaigns with a short duration are applied as well, e.g. for commissioning tests or for troubleshooting reasons. Both applications require a different approach and will be briefly discussed hereafter.

The performance of a pumping station can only be judged by considering the influence of the pressure main (including appendages like (air)valves, check valves, Venturis, etc.). Further, the presence of siphons is known to be a source of malfunctioning due to the risk of the accumulation of air/gas pockets (Pothof & Clemens, 2010, 2011). In severe cases, this may even cause a reduction to a capacity of zero while a high energy consumption is sustained.

Most significant pumping stations that have been (re)constructed over the past few decades are equipped with at least the possibility of performing monitoring activities. This is mainly motivated by asset managerial considerations like the planning of maintenance or rehabilitation/replacement.
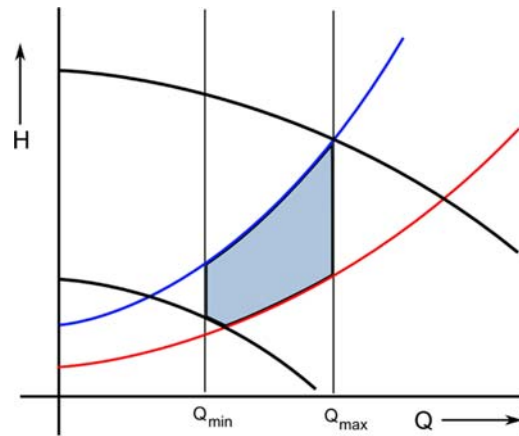
Figure 3.40 Characteristics of a variable speed pump. The black lines describe the pump characteristics, the blue and red lines indicate the characteristic of the pressure main. The blue line has a larger value for the static head and a higher friction. The shaded blue/grey area in the figure indicates the design window in which the system is supposed to operate under satisfactory conditions (among others, no occurrence of cavitation). *Source*: adapted from Tukker *et al.* (2016).

3.4.4.2 Theoretical considerations

A pump characteristic describes the relation between discharge and head, in conjunction with the hydraulic characteristics of the (system of) pressure main(s) to which the pump is connected. In particular, it defines the so-called operation area (Figure 3.40).

In the design phase, the area in which the pump is supposed to operate is defined (Figure 3.40). This area is chosen in such a manner that:

- Stable operation of the pump is guaranteed.
- The occurrence of cavitation is avoided as much as possible.
- The energy consumption is kept as low as possible.

The characteristic of the pressure main (Equation (3.22)) is defined by the static head difference in water head between pump sump and the level at which the water is discharged from the pressure main and the dynamic head that is defined by the friction losses in the system. The latter depends on the dimensions of the pipe, the number and type of bends, valves, etc.

$$\Delta H = \Delta H_{static} + \lambda \frac{LV^2}{2gD} + \sum \xi_i \frac{V^2}{2g} \tag{3.22}$$

where ΔH (m) is the total head, ΔH_{static} (m) is the static head, λ (−) is the friction coefficient, L (m) is the pipe length, D (m) is the pipe diameter, V (m/s) is the flow velocity, g (m/s^2) is the gravitational acceleration and ξ_i are local head loss coefficients.

Given the hydraulic characteristics of the pump and the pressure main, the pump must be supplied with enough power to operate in the desired work area. The power consumption is defined by Equation (3.23):

$$P_{elec} = \frac{P_{hydr}}{\eta_{pump} \times \eta_{elec}} = \frac{\rho g Q \Delta H}{\eta_{pump} \times \eta_{elec}} \tag{3.23}$$

where P_{elec} (W) is the electrical power, P_{hydr} (W) is the hydraulic power, η_{pump} (−) is the pump efficiency, η_{elec} (−) is the electromotor efficiency, ρ (kg/m^3) is the water density, Q (m^3/s) is the discharge, and ΔH (m) is the pump head.

The electrical power can be calculated directly from the power consumption and the voltage. Often, only the power consumption (Equation (3.24)) of the pump is registered because the voltage is assumed to be constant.

$$P_{elec} = UI \tag{3.24}$$

where U (V) is the voltage, and I (A) is the current.

For more information, Tukker *et al.* (2016) offer an in-depth treatise on design, operation and troubleshooting of (waste)water pumping stations.

It is known that, due to ageing, the characteristic of the pressure main changes over time. This is due to biofilm growth, sedimentation and/or the accumulation of gas/air bubbles in the system. In addition, the pump characteristic will also vary over time due to mechanical wear of bearings and propeller blades. These ageing processes result in an increased energy consumption and, in some extreme cases, in a total loss of capacity mainly caused by gas accumulation.

A routine activity when managing a pumping station is to regularly check for dynamic losses (last two terms in Equation (3.21)), especially when pressure difference and discharge are monitored for operational purposes. It provides a powerful and relatively cheap instrument to check on the performance of a pumping station/pressure main. The preferred situation is that a first reading is taken directly after putting the pumping station in operation and this reading is then used as a reference. Over time, an increase of the friction will occur, resulting in an increase in the power consumption (Equation (3.24)), as this is a slow process when caused by scaling of the pressure main or wear of the pump. Notwithstanding this, a regular check (e.g. once every month) is advised as the formation of biogas and/or the air entrainment in the pumping station may cause gas pockets that accumulate in the pressure mains and can cause a very significant increase in resistance and hence power consumption. Pothof *et al.* (2009) estimate that, due to the presence of air/gas pockets, a yearly excess amount of approx. 10,000 tons of CO_2 is emitted in the Netherlands by malfunctioning wastewater pumping stations.

In general, three main monitoring objectives can be distinguished:

- Check on the hydraulic characteristic of the pressure main.
- Check on the hydraulic characteristic of the pump.
- Pump performance.

3.4.4.3 Quantities to be measured

Obviously, one needs to simultaneously measure the head difference over the pressure main and the discharge for a first global view of the work point of the system. This can be done in a relatively simple manner when the pumping station has a built-in discharge sensor, which is the case in most large pumping stations.

When pump behaviour and energy consumption have to be known as well, one needs to measure:

- The discharge.
- The hydraulic head difference over the whole system.
- The hydraulic head difference over the pump.
- The energy consumption (electrical potential and electrical current, in the case of an electro-powered pump, which is the predominant type in practice).
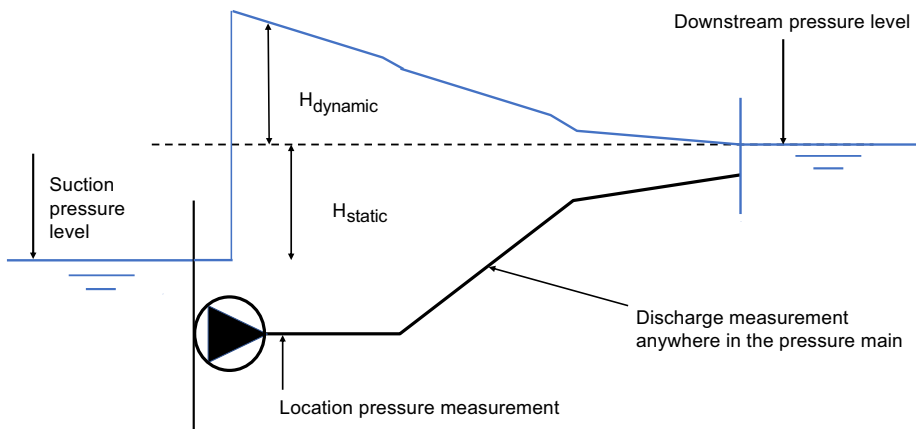- The rotation per minute (RPM) of the pump.

Figure 3.41 Generic scheme of a single pump/pressure main system. *Source*: Deltares.

It has to be emphasized that a stationary situation is assumed. One should therefore observe the monitoring data and choose a time window in which the system is stable. When it takes a long time (order of minutes or longer), depending on the size of the system and the presence of wind vessels to stabilize, this may hint at the presence of gas pockets in the system (see e.g. Lubbers, 2007).

When only interested in the hydraulic characteristic of the pressure main, only the following quantities need to be monitored (Figure 3.41):

- The discharge.
- The pressure directly downstream of the pump.

The downstream pressure level is normally known and to a good approximation stationary. If not, this water level needs to be monitored as well.

When doing so, the combination of discharge and total head is measured, allowing determination of the dynamic losses due to wall friction and local losses. If local losses need to be quantified individually, a pressure difference over the local part of the main (be it a bend, a valve or air vent) has to be measured.

When the pump characteristic needs to be measured (which, for practical reasons, is not recommended in an *in situ* set-up!), the following quantities need to be measured:

- The discharge.
- The suction pressure level.
- The pressure directly downstream of the pump.
- The downstream level only when not stationary.
- The rotations per minute (RPM) of the pump.
- The electrical potential and current.

When only interested in the behaviour at the working point, one measurement is sufficient. However, in most cases, then validating the pump characteristic has to be done over a wide range of discharges and total head. This can be tedious to achieve *in situ* as each measurement takes a minimum amount of time to obtain a stable situation, which puts demands on the availability of enough water to perform the test. Amongst other reasons, this is why the validation of a pump characteristic is preferably done in a

laboratory under known conditions, which also allows comparison of the pump characteristic with the original characteristic provided by the manufacturer.

3.4.4.4 Permanent monitoring set-up

In a permanent monitoring set-up, all quantities mentioned in Section 3.4.4.3 are measured simultaneously and allow generation of on-line information on the performance of the system, which can be used for planning maintenance or to detect defects at an early stage (see e.g. Kooij *et al.*, 2015). In such permanent monitoring set-ups, one is well advised to mount vibration sensors on the pump axis as well, as wear or damage on the propeller blades and/or bearing can be detected at a very early stage allowing for a quick response to avoid further damage.

In a permanent monitoring set-up, in most cases an electro-magnetic discharge sensor is used, as they are known to be robust, stable and offer good accuracy. These devices can only be implemented when this is foreseen during the design. Implementation in a later phase is often difficult/costly because of the demands put on the undisturbed length of pipe up and downstream of the device to ensure the correct flow conditions in the device (see e.g. ISO, 2003).

Figure 3.42 shows the specific energy consumption of a pumping station. The specific energy of a pumping station has been quantified for a range of discharges at $t = 0$, 4 and 8 weeks. The specific energy increases with time, which is an indication of either efficiency loss of the motor/pump system or an increase of the resistance of the pressure mains. As this is a two-pump system and the increase in energy consumption is present in single-pump and two-pump operation, the latter option is the most likely.
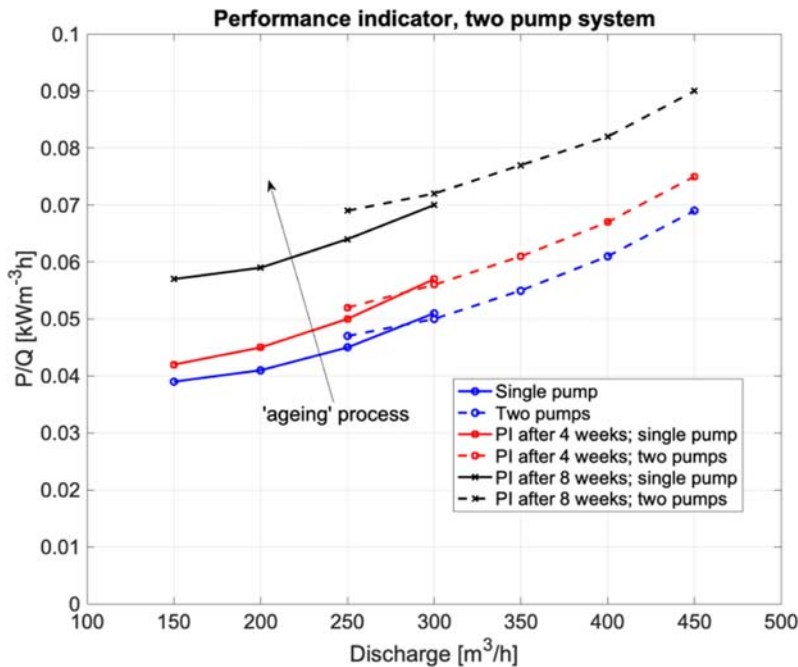

Figure 3.42 Evolution of the specific energy as a function of discharge for a dual-pump pumping station. The specific energy in this pumping station increases by a factor of almost 1.5 in the course of only 8 weeks. This may hint at the accumulation of gas pockets in the pressure main. The blue lines indicate the performance directly after cleaning at $t = 0$. *Source*: adapted from Tukker *et al.* (2016).

Figure 3.43 The cause of an increase in energy consumption became immediately clear when inspecting the pump. *Source*: courtesy Kees Kooij (Deltares).

3.4.4.5 Temporary measurements

Apart from pressure, discharge and power consumption, that can be used for defining a range of performance indicators (Figure 3.42) for daily operation and data for mid- and long-term asset management (Kooij *et al.*, 2015), the measurement of mechanical vibrations is often added as a monitoring quantity. An increase of vibrations, or changes in vibration patterns of pumps is often an indicator for either wear of the propeller and/or the bearings or the presence of some obstruction in the pump. Early registration can avoid damage and/or malfunctioning (Figure 3.43).

3.4.4.6 Incidental measurements

Many pumping stations are not equipped with permanent sensors for pressure and discharge and/or power consumption. Nevertheless, for asset managerial or legal reasons, the performance of these stations sometimes needs to be assessed. In cases where no built-in sensors are present, the main difficulty is found in getting access to locations for installing sensors. Especially, measuring discharge and pressure differences in a buried pressure main poses some challenges. As discussed in this chapter, several options for discharge measurement are available:

- Doppler acoustic (Sections 3.3.2 and 3.3.3).
- Travel time (Section 3.3.1).
- Tracer experiments (Section 3.4.3).

With respect to the latter, it has to be mentioned that depending on the choice of tracer this method can be expensive but has the advantage of offering a known and potential high degree of accuracy. Notwithstanding that this method is not often applied as it is difficult to establish during the monitoring activities, whether or not a stationary situation is obtained, tracers are mainly used to validate other discharge measuring methods.
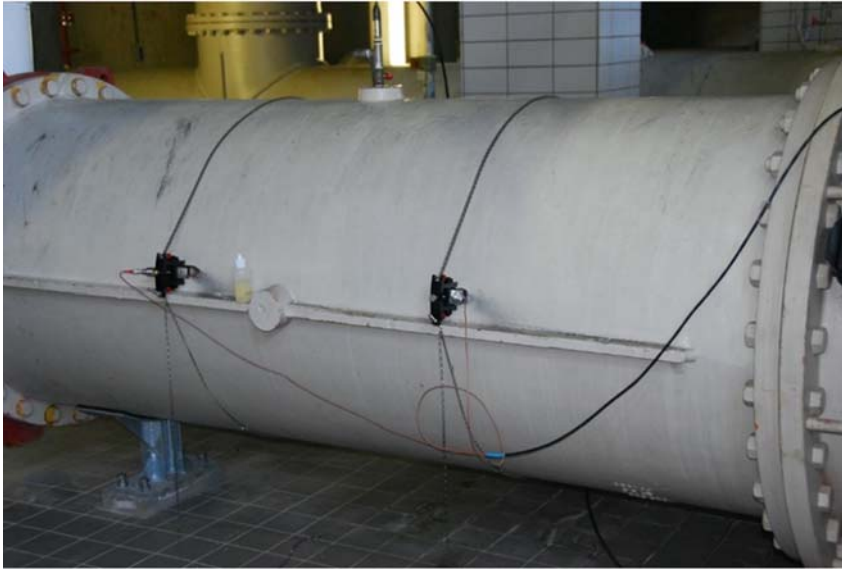
Figure 3.44 Clamp-on discharge measuring equipment installed. *Source*: courtesy Kees Kooij (Deltares).

Depending on the accessibility of the system and the availability of sufficient undisturbed length (see ISO, 2003), clamp-on acoustic sensors based on the travel time principle can be applied relatively easily.

An alternative to flowmeters (Figure 3.44) is to isolate the pump sump from the rest of the system and record the time it takes for the pump to pump out of the pump-sump a certain amount of water. This can only result in useable data when the following conditions are met:

- The change in water level during the experiment can be neglected compared to the total head, to limit the working point (Q, h) changing too much.
- A static situation is obtained. This may take up to a few minutes, especially when gas/air pockets are present in the system. One is well advised to interview the engineers who operate the station normally to find out the characteristics of the station.
- The exact geometry of the sump is known.

By measuring the water level as a function of time, the discharge can be estimated from the results. As in many cases the water level at the suction side of the pump is lowered during pumping, the static head difference needs to be monitored (note that this implies that there is, strictly speaking, never a stationary situation). However, if the change in static head is small compared to the total head during the measurement, this effect may be ignored along with the pressure directly after the pump. The situation at the discharging end of the pressure main defines whether or not one needs to monitor there as well. In cases where there is free outflow with no risk of backwater effects, there is no need to monitor the downstream end.

3.4.4.6.1 Measuring set-up for determining the hydraulic characteristic of the pressure main

In most cases, the pressure level at the downstream end of the main is known to a fairly good approximation and is determined by the local geometry of the construction. When striving for a stationary situation, there is

Figure 3.45 *In situ* constructed pressure measuring mount. *Source*: courtesy Kees Kooij (Deltares).

no real need for the two measurements to be perfectly synchronized with each other. The overall resistance factor can be determined from the stabilized signals obtained from the reading.

The construction of the measuring point for pressure requires some attention. Figure 3.45 shows an *in situ* constructed monitoring point. The most important issues to consider when constructing a measuring location for pressure in a pressure main are the following ones:

- Preferably mount the entrance at the side of the pipe, as the risk of clogging due to fat, etc. at the ceiling or bottom is substantial, as is the risk of gas or air bubbles disturbing the measurement at the ceiling of the pipe.
- Install a valve, this allows for mounting a compressor for cleaning out the pressure mount when it gets clogged.
- Avoid installing a pressure measuring point directly after a bend, a valve or any other appendage, as the pressure at such a location may show substantial variation in time due to locally disturbed pressure and velocity profiles and may prove to yield unusable results. As a rule of thumb, a distance longer than 5 times the pipe diameter is regarded as a minimum, although in many practical situations this is hard to achieve due to the existing design.

3.4.4.6.2 Measuring set-up for determining the hydraulic characteristic of the pump

In situ determination of the characteristics of a pump is normally only carried out for 'dry' installed set-ups (normally the bigger pumping stations). For most submersible pumps, the best option is to transport them to a test-stand in a laboratory or workshop. For *in situ* testing, the pump has to be operated at a range of values for discharge and hydraulic head. When the effect of mechanical settings (RPM) and efficiency has to be verified as well, power consumption has to be monitored. To effectuate a full *in situ* verification of the pump characteristic requires detailed planning, and the exact measuring set-up strongly depends on the local conditions, the engineering of pipes and appendages, and the type of pump. It is therefore not possible to go into further detail here.

3.4.5 Use of computational fluid dynamics

As the Hydrometry Charter (Banque Hydro, 1998) points out, hydrometry should not be a routine, but a profession open to technology, intelligence and questioning. It is the same state of mind that prompted many teams to develop computational fluid dynamics (CFD) skills and then studies to understand the hydraulics of sewers or to manage combined sewer overflows (Fach *et al.*, 2008, 2009; Jarman *et al.*, 2008) or to improve the implementation of sensors (Bonakdari, 2006; Bonakdari *et al.*, 2008; El Bahlouli and Larrarte, 2018; Larrarte *et al.*, 2004, 2010, 2017; Lipeme Kouyi, 2004; Lipeme Kouyi *et al.*, 2003, 2005; Vazquez *et al.*, 2005, 2006). Those numerical tools have also been used for flowmeter calibration by Hrabak *et al.* (1998).

In this context, Larrarte *et al.* (2004) have drafted a methodology for qualifying measurement sites in sewer systems. This approach has been refined within the framework of the MENTOR project (MEasurement sites conception method for sewer NeTwORks), funded by the French National Research Agency and showing how numerical modelling can contribute to measurements in sewer systems (MENTOR, 2016). In brief, CFD allows the simulation of flows at a potential measurement site described by its geometry, by the range of flows to be measured and by the range of variation of the different boundary conditions (other than the flow to be measured, and often confined to water levels). Two approaches can be defined. The first one is a generic approach for studying the sensitivity of the measured value and its associated error to measurement conditions. The second approach is a modelling of the combination "flows + sensors" specific to a given measurement site. A digital calibration can then be performed, i.e. a relationship between the measured quantities (height and velocity) and the flow rate that one wants to know. It is not easy to judge the quality of the results from a CFD simulation as the colourful pictures can look very convincing, while in reality the relation with the real world can be weak. It requires either the judgement of a very experienced hydraulic engineer and/or a well-documented validation of the CFD results. In very critical cases or when large investments are to be based on knowledge of the local hydraulics, the reader is well advised to ask for a validation the CFD results against measured data obtained e.g. from a physical scale model.

3.4.6 Summary

The main advantages and disadvantages of the methods that are most commonly used to measure discharges in sewer systems are summarized in Table 3.5.

3.5 INFILTRATION AND EXFILTRATION
3.5.1 Introduction

In- and exfiltration of water into and out of urban sewer systems is known to be an issue from many perspectives. These processes are unwanted as they negatively influence the system performance and increase the operational costs. In addition, local infiltration of groundwater may easily cause the occurrence of sinkholes in urban areas posing a risk of material damage and/or unsafe situations for the public. On the other hand, the on-purpose infiltration processes occurring in stormwater source control measures or sustainable urban drainage systems (SUDS) are essential for the performance of such infrastructures. In both cases, it is importance to estimate these quantities when managing UDSM systems.

This section focuses on underground sewer systems, infiltration measurements in SUDS are discussed in Chapter 4.

Table 3.5 Advantages and disadvantages of various methods for direct discharge measurements.

Method	Advantages	Disadvantages
Pre-calibrated devices	• Wide range of systems	• Require stable hydraulic conditions • Sensitive to clogging and sediment deposits
Physical scale model	• Allows real physical study at lower scale	• Requires the construction of the model • Similarity issues
Tracer experiments	• Measurement fully independent of the *in situ* sensors (water level, velocity) • Independent of hydraulic conditions	• Non-continuous measurements
Pumping station	• Already built, no need for additional sensors	• Effect of ageing on measured values • Requires *in situ* verification
CFD modelling	• Numerical method without measurement	• Requires expertise and computational power • Careful attention to hydraulics is mandatory

Leakage (in- or exfiltration) in underground sewer systems is notoriously tedious to detect/quantify. This especially holds true for exfiltration out of non-pressurized systems like gravity sewers. The main questions to be answered when monitoring in- and exfiltration are:

- Is there a leak?
- How much is leaking?
- Where is the leak located?

These questions can be answered at different spatial and time scales:

- At catchment scale (long term ∼ years).
- At pipe scale (short term ∼ days).
- At the pipe section scale (short term ∼ days).

3.5.2 Large scale measurement of infiltration

Infiltration of groundwater into gravity sewers poses a serious problem. In delta areas for example, the relative contribution of groundwater to the daily water volume treated in wastewater treatment plants (WWTPs) can mount up to 70% for ageing systems. In such a situation, it is of importance to find out which urban areas are responsible for this. A variety of relatively simple methods, known as triangle methods, have been proposed and applied to estimate the amount of parasitic water being collected and transported to the WWTP for treatment. All these methods follow more or less the approach outlined by Weiß *et al.* (2002).

The basic required input data are:

- The catchment.
- The daily amount of water discharged from the catchment for a given period of time (typically months to years).

- The amount of wastewater produced in the catchment as a daily average over a long period (typically months to years).
- Daily information on rainfall occurrence over the catchment.

From these data, a graph as shown in Figure 3.46 is produced.

The procedure is simple:

- Plot the days in order of ascending daily volume.
- Label each day with a precipitation larger than a certain threshold (e.g. 2–3 mm/day) as 'wet', and the other days as 'dry'.
- Determine the theoretical discharge of wastewater in the catchment (water supply data, possible groundwater extraction by industries).
- Construct a graph as shown in Figure 3.46.
- Determine the area labelled as 'parasitic water' in Figure 3.46. Note, the term 'parasitic water' is preferred over 'infiltrating water' as the excess volume may be caused by other mechanisms than infiltration alone (e.g. illegal discharges, leaking return valves, surface water pouring in via weirs that have a too low crest level etc.).

Obviously, this method cannot be considered very accurate, as many implicit assumptions are made. Nevertheless, it offers a relatively quick and cheap method to find out whether or not infiltration is a significant issue in a given catchment. Schilperoort (2004) and Schilperoort *et al.* (2007) report systematic deviations up to 50% when compared to results obtained with methods based on natural water isotopes. An elaborate description of the natural water isotope method can be found in e.g. De Bénédittis and Bertrand-Krajewski (2005).

Once a catchment is found to contribute significantly to infiltration, a certain refinement as to which locations are most likely to contribute to the infiltration can be made, using readily available data (in conjunction with GIS applications). In most cases, data on each conduit regarding dimensions, material, year of construction and geotechnical conditions are known.
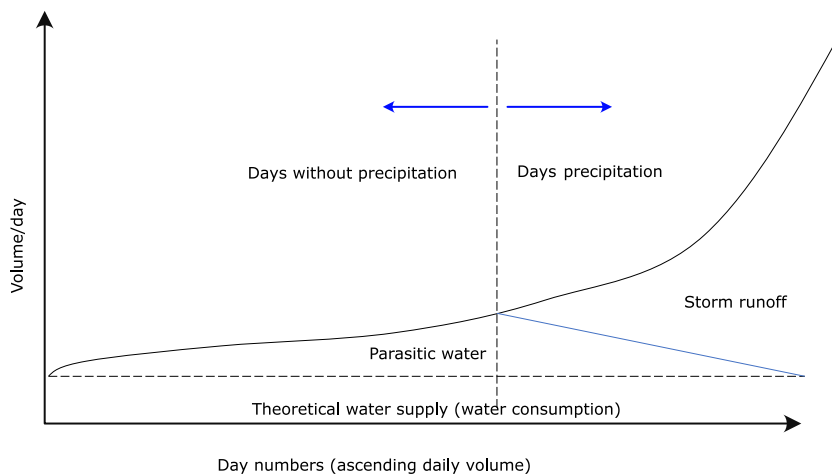

Figure 3.46 Scheme of the 'triangle method' as proposed by Weiß *et al.* (2002). *Source*: Francois Clemens-Meyer (Deltares/TU Delft/NTNU).

Figure 3.47 Clear example of infiltration of groundwater into a sewer pipe. *Source*: Deltares.

The first conduits to scrutinize are pipes situated below groundwater level, being of a minimum age (e.g. >30 years of operational service), known to have short pipe section lengths (this implies more joints), and being the suspected cause of reports on the occurrence of sinkholes and other citizen complaints. This selection of conduits may be subject to further investigation using more advanced technologies to detect leakage (e.g. closed circuit television (CCTV) inspections).

3.5.3 Detailed monitoring of in- or exfiltration

3.5.3.1 General

A first and obvious method to consider for detailed inspection of in- or exfiltration is CCTV inspection. This method, however, has some severe limitations:

- Quantification of the amount of leaking water is not possible.
- Exfiltration can only be detected indirectly (presence of displaced joints, cracks or root intrusion only hint at the possibility of exfiltration).
- Infiltration can be observed directly in a limited number of cases only, when occurring above water level and in a quantity that can be described as 'pouring' (Figure 3.47).
- CCTV inspection is known to suffer from serious quality flaws (Dirksen *et al.*, 2013).

CCTV can provide a first view of the overall status of the assets but is not a guarantee of obtaining high-quality information on where leakages occur or on their quantity. A range of alternative methods have thus been developed to detect and quantify in- and exfiltration from underground urban water systems. In the course of time, many technologies have been developed and applied in practice with various levels of success.

It is not intended to supply here a comprehensive and detailed overview of all technologies. A brief description along with some literature entries is given. It has to be stressed that, as not all technologies presented here have been subjected to rigorous scientific scrutiny yet, not all claims on the quality of information obtained can be taken to be correct.

3.5.3.1.1 Listening stick

The easiest method to use is the listening stick. This stick has an earpiece and is used to listen to the sound generated by leaks on e.g. pipe fittings (e.g. Glisic, 2014). An obvious drawback of this method is the fact that a human is used as an 'organic sensor', which is known to suffer from subjectivity and sometimes even bias (see e.g. Miller, 1956; Macmillan & Creelman, 2005). Apart from that, it is unlikely that all leakages can be detected in this manner as access to underground systems to apply the method is a serious obstacle.

3.5.3.1.2 Smoke testing

A relatively old but simple method is the smoke test. Smoke is injected into the sewer at a manhole. If there is a crack or a leak above the waterline the smoke is likely to show up at the surface (Figure 3.48).

3.5.3.1.3 Dye testing

Another simple method is the dye tracer test. A dye (e.g. Rhodamine WT) is injected into the sewer and the dilution of the dye is measured (Gokhale & Graham, 2004).

3.5.3.1.4 Flow monitoring

The simplest flow monitoring method is manual survey. During night-time, manholes are inspected in the presence of a significant flow (Gokhale & Graham, 2004). Alternatively, this flow could also be measured with two or more flowmeters to estimate the difference. These are however prone to unreliable results under specific circumstances (Smits *et al.*, 2008). Discharge measurements could however also be applied at a larger (e.g. network) scale to set up a water balance. To this end, discharge measurements from pumping stations could be compared to drinking water consumption, the water balance deficiency is a measure for in- or exfiltration (e.g. Korving *et al.*, 2012). Using this method one should be aware that not all water supplied into a household or an industrial process is discharged into the wastewater system, evaporation,
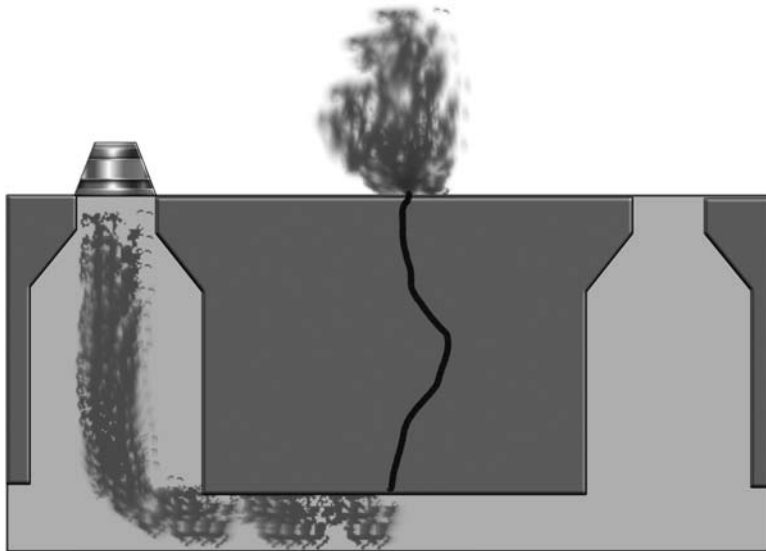

Figure 3.48 Principle of the smoke test method. *Source*: adapted from Gokhale & Graham (2004).

water being an ingredient of products made and garden watering cause a systematic deficiency. The same holds for water discharged into the wastewater systems that came from another source than the water supply system: private wells, companies having their own groundwater source. A comprehensive survey of water sources and water users in a given catchment is a mandatory action when considering flow monitoring as a means to detect in- or exfiltration.

3.5.3.1.5 Pressure test

For a pressure test, a (part of the) pipeline is isolated, and the internal pressure is set at a specific value. This pressure has to remain constant for a certain period (e.g. 30 minutes). During this period, the variation of the volume of water in the pipe is measured (EN, 2015). As an alternative, a prototype named the double packer consists of two inflatable discs to seal a pipe section of 80 cm. Freshwater is subsequently added to the interspace. Exfiltration is determined by monitoring the water volume in the interspace (Wolf, 2006).

3.5.3.1.6 Tracing methods

In the EU Project APUSS (Ellis & Bertrand-Krajewski, 2010), the QUEST (Rieckermann *et al.*, 2005) and QUEST-C (QUantification of Exfiltration from Sewers using artificial Tracers – with Continuous dosing) (Rieckermann *et al.*, 2007) methods have been developed. Artificial tracers are added to the wastewater flow to quantify exfiltration in a sewer reach by means of the quantification of the loss of tracer mass. The APUSS project has also developed various methods to quantify infiltration. One of these methods is the stable isotope method (Kracht *et al.*, 2007), which compares the isotopic compositions of the foul sewage and the infiltrating water.

3.5.3.1.7 Sampling and modelling

Sampling can also be used to trace leakage. Soil samples near the pipeline are collected to be analysed for parameters related to deterioration, e.g. contaminants or moisture content (Liu & Kleiner, 2013). Samples of wastewater and groundwater are analysed for drug remains to calibrate a groundwater flow model to estimate exfiltration (Fenz *et al.*, 2005). More recent research (Guérineau *et al.*, 2014) combined surface water quality modelling with analysis of surface water and sediment samples for *E. Coli* and wastewater micropollutants to estimate the amount of sewer exfiltration into a surface water canal.

3.5.3.1.8 Distributed temperature sensing

Distributed temperature sensing (DTS) is a technology developed in the 1980s (e.g. Dakin *et al.*, 1985) and introduced in hydrology and urban drainage in the past decade for, amongst other applications, detecting and locating infiltration (Hoes *et al.*, 2009; Panasiuk *et al.*, 2017; Schilperoort *et al.*, 2013). In this method, an in-sewer fibre optic cable is installed to conduct high-frequency temperature measurements over a long stretch of sewer pipes. This detects and locates temperature anomalies due to exchange of groundwater with wastewater. To detect and locate exfiltration and leakage from a pressure main, a fibre optic cable could be placed in the pipeline bed to monitor the temperature differences (Nikles *et al.*, 2004).

The measuring principle is based on the shift in wavelength of scattered laser light sent down a glass fibre. In Figure 3.49(a), a schematic representation of the measuring set-up is shown (Lopez-Higuera, 2002). A laser sends a light pulse through a directional coupler into a glass fibre. In the glass fibre, two types of scattering occur: Raman scattering (induced by molecular vibrations) and Brillouin scattering (bulk vibrations). The light is scattered back and recombined in the directional coupler for processing in an electro-optical device to quantify the shift(s) in wavelength. Figure 3.49(b) shows a typical result of the shifts occurring in the wavelength observed. The travelling time is measured as well and is used (Rayleigh scattering, assuming the speed of light to be known and constant) to identify the distance from
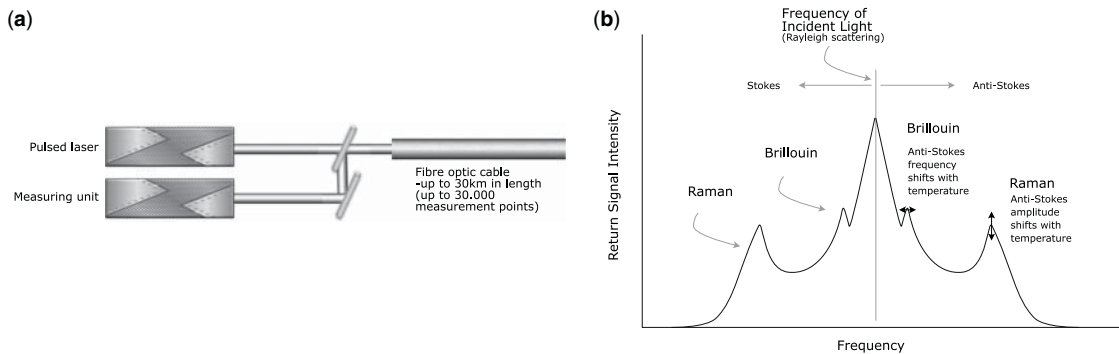
Figure 3.49 (a) DTS measuring principle, (b) Rayleigh, Stoke, anti-Stokes, Raman and Brillouin scattering. *Sources*: (a) adapted from https://roctest.com/wp-content/uploads/2017/01/SEN2-Manual1.0c.pdf, (b) adapted from https://www.bandweaver.com/technology/distributed-temperature-sensing/.

the light source where the scattering occurred. The Rayleigh backscatter has the same wavelength as the original signal and is used for distance determination. The Raman backscatter show a double shift in wavelength: (i) toward the red, with longer wavelength (named Stokes) and (ii) toward the blue, with shorter wavelength (named anti-Stokes). The ratio of the intensity peaks for the Stokes and anti-Stokes is a measurement of the temperature (for the underlying physical process details, the reader is referred to the literature, e.g. Lopez-Higuera, 2002). Brillouin scatter depends on bulk vibration, potentially the absolute difference between respectively Brillouin/Stokes-Rayleigh and Brillouin/anti-Stokes-Rayleigh can be used to detect pressure vibrations (sound) produced by small leakages in pressure mains (Sliwczynski & Krehlik, 2014).

A typical measuring result obtained from a DTS measuring campaign is shown in Figure 3.50.

When groundwater is infiltrating in a wastewater sewer and there is a temperature difference that is larger than the resolution of the measuring device (approximately 0.1 °C), the location of the infiltration can be determined. In modern systems, the uncertainty in location is in the order of 10 cm, and the uncertainty in the temperature is ∼0.1 °C, depending on duration of the measurement and the feasibility given the location. In general, a trade-off has to be made between time and space resolution, uncertainty level and the effect of water velocity. On a sense it resembles the situation when taking photo: one has to find a workable combination of shutter speed, aperture and the depth of focus/sharpness of the picture sought when targeting a moving object. In practice the main limiting factor is the amount of data generated (up to several Gbytes per day) when it comes to choosing these parameters.

Prior to any monitoring campaign, the DTS cable has to be calibrated after it has been installed in the system (Figure 3.51). By inserting the cable at a number of locations (preferably at accessible locations like manholes) in a bucket filled with melting ice, the offset (deviation between the reading obtained with the cable and the known temperature of the ice (0 °C) is known and is used as a systematic correction on the raw data in the data processing. In more recent equipment, there is the option of connecting Pt100 thermometers to enable end-to-end calibration of the cable. The reader is referred to Section 6.4.2 for practicalities regarding DTS.

3.5.3.1.9 Time domain reflectometry

Time domain reflectometry (TDR) as described by Cataldo *et al.* (2014) could be applied to detect and locate leakage. In this method, a sudden voltage increase propagates along a sensor or sensing element (e.g.
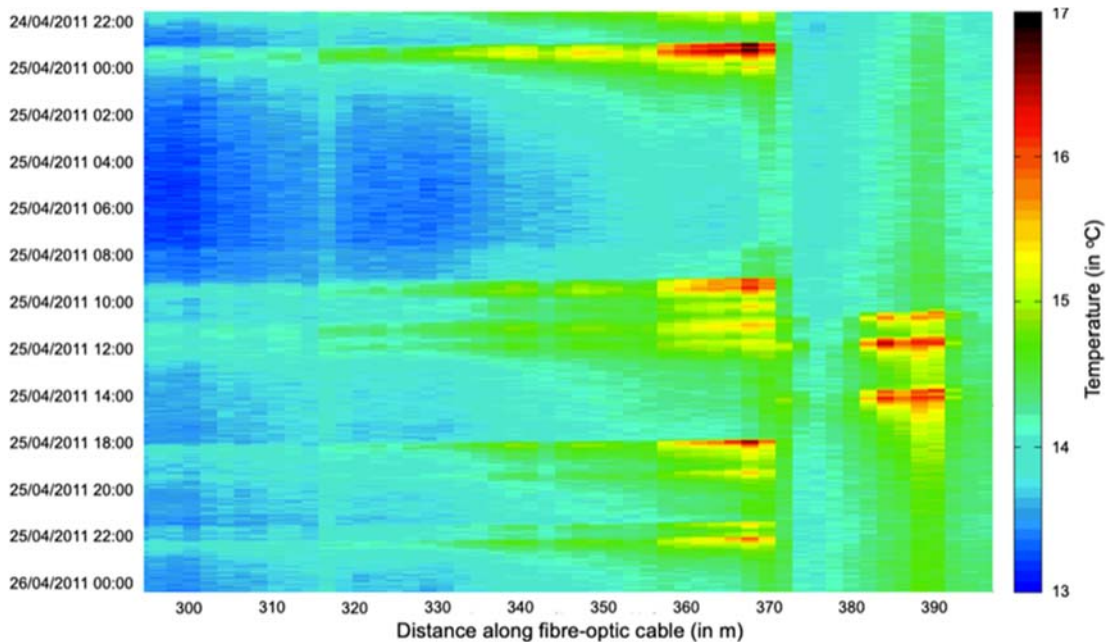
Figure 3.50 Example of a measuring result obtained with the DTS method in a storm sewer. At a distance of circa 367 m and 390 m, regular discharges of relatively warm water occur. This hints at a misconnection at those locations. *Source*: courtesy Rémy Schilperoort (Partners4UrbanWater).

two-wire transmission line) which could be installed at the pipe bedding. The variations of the electrical impedance, which is influenced by leakage, that are encountered along the way are monitored and schematized in a reflectogram.

3.5.3.1.10 Infrared thermography

Infrared thermography is a technique that can also be used to detect leaks and voids in the surrounding soil from the ground level (e.g. Wirahadikusumah *et al.*, 1998). This method detects temperature differences that occur as a result of the exchange between the pipeline and the surrounding soil. Lepot *et al.* (2017) demonstrated that infiltration through a crack can be detected using in-line infrared thermography.

3.5.3.1.11 Smartball

The Smartball is an acoustic concept. A ball equipped with acoustic sensors, an accelerometer, and a temperature and pressure sensor is inserted at an upstream part of the pipe system and flows downstream. The location of the ball and possible leaks are determined by analysing the emitted acoustic signal which is collected at the ground station (Liu & Kleiner, 2013).

3.5.3.1.12 SAHARA

Another acoustic concept is the SAHARA system. In this system, a sensor is mounted on an umbilical cable which is inserted at an upstream point of the pipe. The sensor, a hydrophone, is equipped with a small parachute which unfolds in the pipeline to let the sensor flow downstream (Figure 3.52). The

Figure 3.51 (a) DTS measuring computer, (b) Installation of a DTS cable. *Source*: courtesy Rémy Schilperoort (Partners4UrbanWater).

hydrophone can detect the sound which is generated by the leak. Subsequently, the location of the leak is recorded with a receiver at ground level (Rizzo, 2010).

3.5.3.1.13 Leak noise correlation

Leak noise correlators can also be used to detect and locate leakage. Hydrophones up and downstream of a possible leak can be used to listen to noise generated by the leak. Subsequently, the leak position is identified by the delay between the leak noise reaching each monitoring point (Davis *et al.*, 2013; Hao *et al.*, 2012).
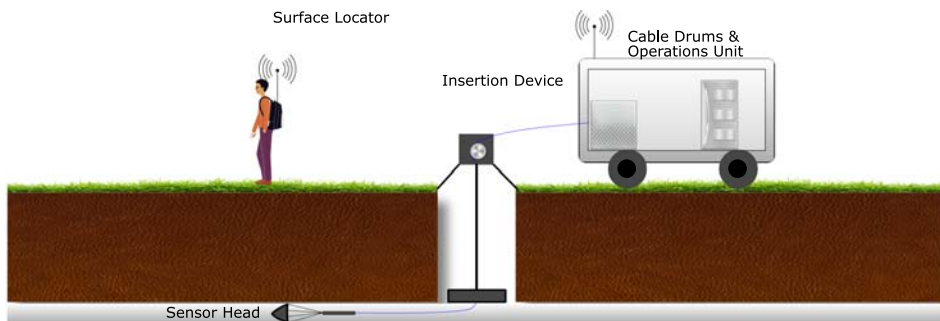
Figure 3.52 Principle of the SAHARA system. *Source*: adapted from Rizzo (2010).

3.5.3.1.14 Magnetic flux leakage

Electromagnetic methods are often used in pressurized systems. The magnetic flux leakage method uses large magnets to create a magnetic field around the pipe wall. This is applicable only to ferrous pipes. Defects are detected by measuring changes in the pipe magnetic permeability (Rizzo, 2010). A magnetic flux leakage unit is usually mounted on a pig (pipeline inspection gauges). These 'intelligent' pigs (Figure 3.53) are mainly used in oil pipelines, but there is an increasing interest in application in wastewater pressure mains (Driessen, 2016).

3.5.3.1.15 Ground penetrating radar

The ground penetrating radar (GPR) is also an electromagnetic method. GPR uses electromagnetic radiations in the microwave band. With a transmitter, microwaves are sent through materials of different dielectric constants to detect reflected signals from the subsurface. GPR can detect voids in and changes in soil saturation. Traditionally, GPR is used from the ground surface towards the soil, but in-pipe GPR systems also exist (Hao *et al.*, 2012; Liu & Kleiner, 2013).

3.5.3.1.16 Multi-sensor systems

Multi-sensor systems have also been developed over the years. In the PIRAT system (Kirkham *et al.*, 2000), CCTV is combined with sonar and laser profiling on a robot. Sonar is an acoustic technique that can be used to identify sediments and cracks below the water line. For inspection of cracks above the waterline, laser profiling can be used (Selvakumar *et al.*, 2014). In this technique a ring of light is projected on the sewer wall.

Another example of a multi-sensor system mounted on a pipe robot is SAM (Eiswirth *et al.*, 2000). This system uses, next to CCTV and a laser scanner, a microwave sensor (in-pipe GPR) and radioactive sensors (γ-g probe). These sensors are used to inspect the soil behind the pipe for changes in moisture content and voids. The γ-g probe acts as a source of gamma radiation. The backscatter of gamma rays, together with natural radiation, is recorded by the probe. The backscatter can be related to the density of the surrounding soil. Voids change the density and can therefore be detected (Heske, 2003). The rotatable microwave sensor records changes of the dielectric constant, which are different for dry and wet soils (Munser & Hartrumpf, 2003). Hydrochemical sensors (conductivity, pH and temperature) and an acoustic sensor (Herbst, 2002) are also installed on the robot to detect cracks and voids, based on impact echo. Sound waves are introduced in a concrete pipe wall with e.g. an automatic hammer.
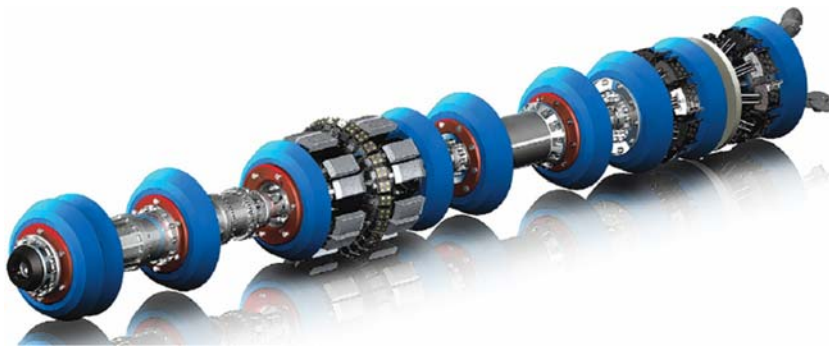

Figure 3.53 Example of an intelligent pipeline inspection gauge. *Source*: courtesy John Driessen (Sweco).

The waves reflected by internal flaws and external surfaces are subsequently recorded. A geo-electrical sensor is installed on a cable attached to the back of the robot to detect and locate leakages (Wolf, 2006). The latter is now commonly referred to as focused electro leak location (FELL) or electro-scanning.

Tracer-based and electrical conductivity-based methods are discussed in some length hereafter.

3.5.3.2 Electrical conductivity-based methods

Electrical methods rely on the fact that when leakage occurs, be it in- or exfiltration, this implies that the electrical resistance of the pipe wall is locally reduced. In this category, the following methods are reported:

- Focused electro leak location (FELL).
- Electrical resistivity tomography (ERT).

Heterogeneity of the underground in urban areas is a challenging environment, as multiple sources of noise may be present while being unnoticed. Mainly for this reason, no reliable generic information on detection limits, uncertainty or repeatability of these methods is known. No substantiated claims on uncertainty levels in measured in- or exfiltration discharges is available either.

3.5.3.2.1 Focused electro leak location (FELL)

The focused electro leak location (FELL) system has been developed in Germany within the interdisciplinary project SAM (Sewer Assessment with Multi-sensor Systems) to detect and locate leakages (Eiswirth *et al.*, 2000). An electric potential is applied between an electrode in the pipe (the sensor), and an electrode on the surface (Figure 3.54). The sensor is located below the waterline and to complete the electrical circuit the surface electrode is often a metal stake (e.g. Wilmut *et al.*, 2005). The electrical resistance of the pipe wall is high, unless there is a defect in the pipe such as a defective joint or a crack. The resulting increase in current is registered and coupled to the location of the sensor.

The main part of the FELL method is the geo-electrical sensor. Gokhale and Graham (2004) describe a commercialized version of this technique, the FELL-41 system. Since then some alternative systems with
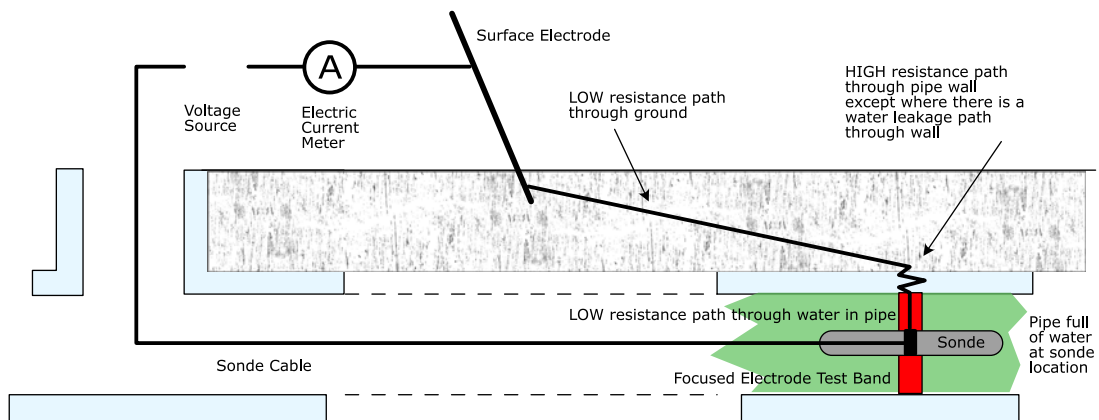

Figure 3.54 Principle of the focused electro leak location (FELL) method. *Source*: adapted from ASTM (2018).

the same measurement principle have also been developed. Next to the FELL-41 system, the MSI-1620 system is used by Tuccillo *et al.* (2011) as an alternative model.

Until now FELL has been applied in different studies to detect and locate leakage. Harris and Dobson (2006) compared FELL with joint pressure testing and CCTV. They concluded that FELL results coincide with joint pressure testing. However, the FELL results showed significantly more defective joints when compared to the CCTV, a result later confirmed by Tuccillo *et al.* (2011).

3.5.3.2.2 Electrical resistivity tomography (ERT)

Electrical resistivity tomography (ERT) is an active geo-electrical method that calculates the subsurface distribution of electrical resistivity from a large number of resistance measurements (Daily *et al.*, 2005). The subsurface resistivity is determined by applying a known electrical direct current between two electrodes. The ground resistivity is related to various geological parameters such as the mineral and fluid content, porosity, and degree of water saturation in the rock (Loke, 2020).

A range of electrode configurations is applied, also known as arrays. Different modes of deployment are available, e.g. vertical electrical sounding (VES) to determine the vertical variation in resistivity. Investigating the vertical and horizontal variation in resistivity along an investigation line is known as electrical resistivity tomography (ERT) (Figure 3.55). This 2D electrical survey assumes that resistivity does not change in the direction that is perpendicular to the survey line. To get more accurate results, a predefined grid of multiple survey lines could be combined to obtain a pseudo-3D plot (Reynolds, 2011).

Ramirez *et al.* (1996) used ERT with a combination of surface and subsurface electrodes to detect leakage from an underground tank in a test facility. The authors successfully monitored the movement of a released saline tracer from the tank in 2D, 3D and in time.

Jordana *et al.* (2001) applied ERT using surface electrodes to detect water leakages from a buried pipe in an experimental set-up and in a short pipeline buried in a farm field. Wood and Palmer (2000) investigated sewer exfiltration in Sydney with the mise-à-la-masse method in combination with ERT along a single line. They applied both methods at four different test-sites: two sewers located in open, overgrown areas allowing ease of access, and two sewers buried under roads. They concluded that in areas with large surface variations, such as might be associated with sewerage pipes laid under roads, the combination of the two methods to detect exfiltration may be ambiguous. Eiswirth *et al.* (1994) also used 2D ERT to investigate sewer exfiltration in a combination of flush experiments at a gravity sewer test-site in Rastatt, Germany. A 2D ERT profile was obtained before and after a flush experiment with a saline solution. Results of the study indicate they were able to detect exfiltration at multiple (12 out of 15) known defect locations.
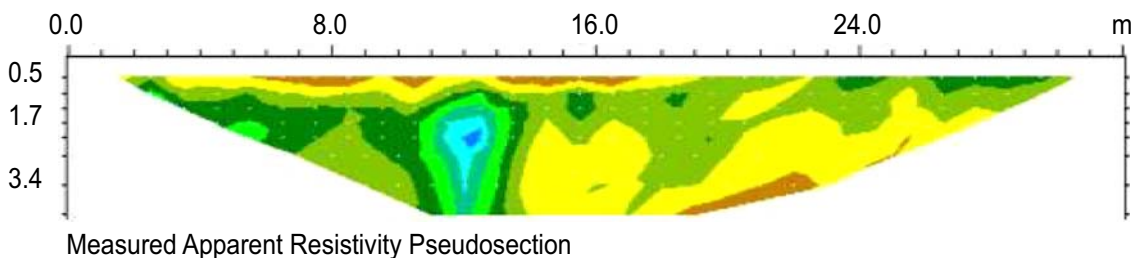

Measured Apparent Resistivity Pseudosection

Figure 3.55 Example of apparent resistivity pseudo section. *Source*: adapted from Loke (2020).

3.5.3.3 Tracer methods

The basic principle of exfiltration measurements with tracers is to dose a well-known amount of tracer injected into the sewer under investigation and to apply a mass balance in the investigation reach. Given the conservative behaviour of the substance, the tracer loss can directly be related to the leakage along the reach.

3.5.3.3.1 QUEST-C method

The QUEST-C method uses two different tracers, which are continuously dosed upstream and downstream of the reach under investigation. The underlying principle is that losses of the indicator tracer are mostly identified relative to a reference tracer which is not affected by exfiltration (Figure 3.56).

The straight-forward QUEST-C method assumes steady discharge in the sewer system during the experiment. Exfiltration is computed only from the two series of tracer concentration data. The dynamic approach of the QUEST-C uses the ratio of tracer loads. To this end, simultaneous discharge measurements at the sampling point are mandatory. The exfiltration fraction E can be estimated by Equation (3.25):

$$E = 1 - \frac{M_{REF,in}}{M_{IND,in}} \cdot \frac{M_{IND,out}}{M_{REF,out}} = \frac{\int c_{REF}(t) \cdot q_{REF}(t)dt}{\int c_{IND}(t) \cdot q_{IND}(t)dt} \cdot \frac{\int C_{IND}(t) \cdot Q(t)dt}{\int C_{REF}(t) \cdot Q(t)dt} \tag{3.25}$$

where c_{REF} and c_{IND} are the respective reference and indicator tracer concentrations of the dosing solutions, q_{IND} and q_{REF} are the respective dosing rates of the tracer solutions, C_{IND} and C_{REF} are the respective tracer concentrations in the sample, and Q is the discharge at the sampling point.

However, the computed exfiltration is systematically wrong if there is significant inflow/infiltration in the investigation reach.

In the APUSS project, the QUEST-C method was solely applied in field tests. This provides no full formal validation. Different tracer combinations were used: LiCl, NaBr (Prigiobbe & Giulianelli, 2011; Rieckermann *et al.*, 2007) and Rhodamine WT (Revitt *et al.*, 2006).

3.5.3.3.2 DEST method

Application of the DEST (detection of exfiltration from sewers using tracers) method implies a well-known mass of a single tracer is injected at an upstream point of the investigation reach. To complete the balance, downstream of the reach or system under investigation, the remaining tracer mass is determined. To this end, discharge is measured and combined with concentration measurements. By doing so, exfiltration can still be
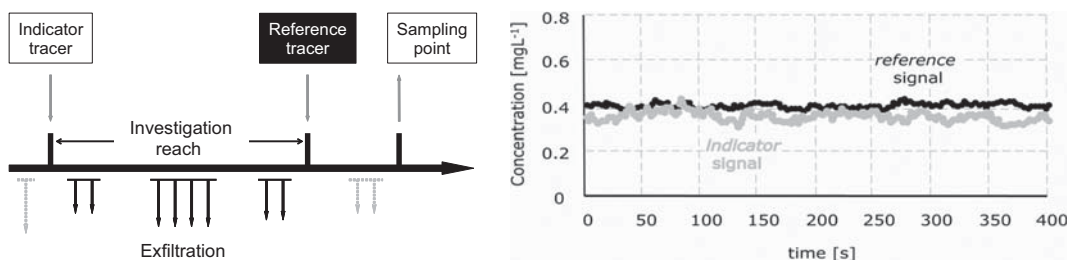

Figure 3.56 Concept scheme of the QUEST-C method. *Source*: adapted from Rieckermann *et al.* (2007).

detected if there is a significant inflow with a background tracer concentration in the sewer of interest. The exfiltration fraction E can be estimated by Equation (3.26):

$$E = \frac{M_{in} - M_{out}}{M_{in}} = 1 - \frac{\int Q(t)(C(t) - C_{BG}(t))dt}{V_{in}C_{in}} \tag{3.26}$$

where V_{in} is the dosed volume, C_{in} is the dosed tracer concentration, C is the tracer concentration in the sample, C_{BG} is the background concentration and Q is the discharge at the sampling point.

3.6 SUMMARY AND TRANSITION

This chapter introduced several sensors and methods to estimate or measure flows and validate recorded discharges data. Such measurements are conducted in many urban drainage systems in the world. They may look easy and well established, but they are often prone to error and biases that are not always obvious. Even when applying methods described in standards, one needs to be aware of the limitations posed by the conditions in field measurements on the applicability.

The combination of a water level and velocity measurement is likely the most used method in sewer pipes, but careful attention is mandatory in choosing and installing the devices. Section 6.3 of this book highlights some key points for such installations. Pre-calibrated devices are also well established. If these technologies are robust, they require detailed checks to set them up.

SUDS are slowly and surely becoming an alternative for stormwater management in urban catchment and/or remote places. Monitoring such decentralized systems poses different challenges: specific processes (evaporation, infiltration, low discharges) occur, and the constraints are slightly different (cost, number of sensors to set up, energy supply). The following chapter is devoted to those issues.

REFERENCES

Aguilar M. F., McDonald W. M. & Dymond R. L. (2016). Benchmarking laboratory observation uncertainty for in-pipe storm sewer discharge measurements. *Journal of Hydrology*, **534**, 73–86. doi: 10.1016/j.jhydrol.2015.12.052.

ASTM (2018). *ASTM F2550-13(2018) Standard Practice for Locating Leaks in Sewer Pipes by Measuring the Variation of Electric Current Flow Through the Pipe Wall*. ASTM International, West Conshohocken, PA (USA), 7 p. doi: 10.1520/F2550-13R18.

Banque Hydro (1998). *Hydrometry Quality Charter – Guide to Good Practices*. Ministry of Environment, Paris (France), 31 p. Available at https://library.wmo.int/doc_num.php?explnum_id=4709 (accessed 21 Nov. 2020).

Bertrand Krajewski J.-L., Laplace D., Joannis C. & Chebbo G. (2000). *Mesures en hydrologie urbaine et assainissement [Measurements in urban hydrology and sewer systems]*. Editions Technique et Documentation, Paris (France), 794 p. ISBN 978-2-7430-0380-4. (in French).

Bevir M. K. (1970). The theory of induced voltage electromagnetic flowmeters. *Journal of Fluid Mechanics*, **43**(3), 577–590. doi: 10.1017/S0022112070002586.

Bonakdari H. (2006). *Modélisation des écoulements en collecteur d'assainissement – Application à la conception de points de mesures [Modelling of flows in sewer pipes: application to the design of measurement points]*. PhD thesis, Université de Caen – Basse Normandie, Caen, France, 263 p. (in French).

Bonakdari H., Larrarte F., Joannis C. & Levacher D. (2008). Methodology for qualifying measurement sites within a drainage network: application to flow readings in a main drain. *Bulletin des Laboratoires des Ponts et Chaussées*, **272**, 9–19.

Cataldo A., Persico R., Leucci G., de Benedetto E., Cannazza G., Matera L. & de Giorgi L. (2014). Time domain reflectometry, ground penetrating radar and electrical resistivity tomography: A comparative analysis of

alternative approaches for leak detection in underground pipes. *NDT and E International*, **62**, 14–28. doi: 10.1016/j.ndteint.2013.10.007.

Cedillo S., Lepot M. & Clemens F. H. L. R. (2016). Potentiality of a velocity profiler to investigate sewers: results of laboratory experiments. *Proceedings of the 8th International Conference on Sewer Processes and Networks*, 31 Aug.–2 Sept., Rotterdam, The Netherlands, 42–43.

Clemens F. H. L. R., Stanic N., van der Schoot W., Langeveld J. G. & Lepot M. J. (2015). Uncertainties associated with laser profiling of concrete sewer pipes for the quantification of the interior geometry. *Structure and Infrastructure Engineering*, **11**(9), 1218–1239. doi: 10.1080/15732479.2014.945466.

Colin D., Herault C.-A. & Venandet N. (2016). *Guide pratique : mise en place de l'autosurveillance des réseaux d'assainissement [Practical guide: implementing self-monitoring of sewer systems]*. Agence de l'eau Rhin Meuse, Rozérieulles (France), 164 p. (in French). Available at http://cdi.eau-rhin-meuse.fr/Record.htm?idlist=4&record=19319019124911372919. (accessed 08 Dec. 2020).

Daily W., Ramirez A., Binley A. & LaBrecque D. (2005). Chapter 17 - Electrical resistance tomography - Theory and practice. In *Near-surface Geophysics (Investigations in Geophysics No. 13)*, D. K. Butler (ed.), Society of Exploration Geophysicists, Tulsa, OK (USA), pp. 525–550. ISBN 978-156080-130-6. doi: 10.1190/1.9781560801719.ch17.

Dakin J. P., Pratt D. J., Bibby G. W. & Ross J. N. (1985). Distributed optical fibre Raman temperature sensor using a semiconductor light source and detector. *Electronics Letters*, **21**(13), 569–570. doi: 10.1049/el:19850402.

Davis P., Sullivan E., Marlow D. & Marney D. (2013). A selection framework for infrastructure condition monitoring technologies in water and wastewater networks. *Expert Systems with Applications*, **40**(6), 1947–1958. doi: 10.1016/j.eswa.2012.10.004.

De Bénédittis J. & Bertrand-Krajewski J.-L. (2005). Measurement of infiltration rates in urban sewer systems by use of oxygen isotopes. *Water Science and Technology*, **52**(3), 229–237. doi: 10.2166/wst.2005.0080.

Dirksen J., Clemens F. H. L. R., Korving H., Cherqui F., Le Gauffre P., Ertl T., Plihal H., Mueller K. & Snaterse C. T. M. (2013). The consistency of visual sewer inspection data. *Structure and Infrastructure Engineering*, **9**(3), 214–228. doi: 10.1080/15732479.2010.541265.

Diskin M. H. (1963). Temporary flow measurement in sewers and drains. *Journal of the Hydraulics Division*, **89**(4), 141–159.

Driessen J. (2016). Onderzoek naar intelligente pigs voor persleidingen water [Research into intelligent pigs for water pressure pipes]. *Land+Water*, **5**, 34–35. (in Dutch).

Dufresne M., Vazquez J. & Bercovitz Y. (2018). Complementarities between physical modelling and computational fluid dynamics for an ecological continuity project. *Proceedings of 7th IAHR International Symposium on Hydraulic Structures*, 15–18 May, Aachen, Germany, 8 p. doi: 10.15142/T3V07R.

Eiswirth M., Heske C., Hötzl H., Schneider T. & Burn L. S. (2000). Pipe defect characterisation by multi-sensor systems. *Proceedings of the conference No-dig 2000*, 15–19 Oct., Perth, Australia, 12 p.

Eiswirth M., Lazar C. & Merkler G. P. (1994). Sewerage leakages as source of groundwater contamination. *Proceedings of the International Hydrogeological Symposium "Impact of Industrial Activities on Groundwater"*, 23–28 May, Constantza, Romania, 175–185.

El Bahlouli A. & Larrarte F. (2018). Proposal for improving discharge quantification in urban drainage. *Flow Measurement and Instrumentation*, **60**, 51–56. doi: 10.1016/j.flowmeasinst.2018.02.014.

Ellis J. B. & Bertrand-Krajewski J.-L. (eds) (2010). *Assessing Infiltration and Exfiltration on the Performance of Urban Sewer Systems (APUSS)*. IWA Publishing, London (UK), 180 p. ISBN 9781843391494.

EN (2015). *EN 1610:2015 Construction and testing of drains and sewers*. CEN – European Committee for Standardization, Brussels (Belgium), 38 p.

Ettema R., Arndt R., Roberts P. & Wahl T. (eds) (2000). *Hydraulic Modelling: Concepts and Practice*. ASCE, Reston, VA (USA), 390 p. ISBN 978-0784404157.

Fach S., Sitzenfrei R. & Rauch W. (2008). Assessing the relationship between water level and combined sewer overflow with computational fluid dynamics. *Proceedings of 11th International Conference on Urban Drainage*, 31 Aug.–5 Sept., Edinburg, Scotland, UK, 9 p.

Fach S., Sitzenfrei R. & Rauch W. (2009). Determining the spill flow discharge of combined sewer overflows using rating curves based on computational fluid dynamics instead of the standard weir equation. *Water Science and Technology*, **60**(12), 3035–3043. doi: 10.2166/wst.2009.752.

Fenz R., Blaschke A. P., Clara M., Kroiss H., Mascher D. & Zessner M. (2005). Quantification of sewer exfiltration using the anti-epileptic drug carbamazepine as marker species for wastewater. *Water Science and Technology*, **52**(9), 209–217. doi: 10.2166/wst.2005.0321.

Glisic B. (2014). Chapter 14 – Sensing solutions for assessing and monitoring pipeline systems. In *Sensor Technologies for Civil Infrastructures – Volume 2: Applications in Structural Health Monitoring*, M. L. Wang, J. P. Lynch & H. Sohn (eds.), Woodhead Publishing Limited, Cambridge (UK), pp. 422–460. ISBN 978-1-78242-242-6. doi: 10.1533/9781782422433.2.422.

Gokhale S. & Graham J. A. (2004). A new development in locating leaks in sanitary sewers. *Tunnelling and Underground Space Technology*, **19**(1), 85–96. doi: 10.1016/j.tust.2003.08.003.

Guérineau H., Dorner S., Carrière A., McQuaid N., Sauvé S., Aboulfadl K., Hajj-Mohamad M. & Prevost M. (2014). Source tracking of leaky sewers: A novel approach combining fecal indicators in water and sediments. *Water Research*, **58**, 50–61. doi: 10.1016/j.watres.2014.03.057.

Hao T., Rogers C. D. F., Metje N., Chapman D. N., Muggleton J. M., Foo K. Y., Wang P., Pennock S. R., Atkins P. R., Swingler S. G., Parker J., Costello S. B., Burrow M. P. N., Anspach J. H., Armitage R. J., Cohn A. G., Goddard K., Lewin P. L., Orlando G., Redfern M. A., Royal A. C. D. & Saul A. J. (2012). Condition assessment of the buried utility service infrastructure. *Tunnelling and Underground Space Technology*, **28**(1), 331–344. doi: 10.1016/j.tust.2011.10.011.

Harris R. J. & Dobson C. (2006). Sewer pipe infiltration assessment: Comparison of electro-scan, joint pressure testing and CCTV inspection. *Proceedings of the Pipeline Speciality Conference 2006*, July 30–Aug. 2, Chicago, USA. doi: 10.1061/40854(211)61.

Heller V. (2011). Scale effect in physical hydraulic engineering models. *Journal of Hydraulic Research*, **49**(3), 293–306. doi: 10.1080/00221686.2011.578914.

Hemmerle N., Randrianarimanana J.-J., Joannis C. & Larrarte F. (2014). Hydraulics and deposit evolution in sewers. *Proceedings of the 9th International Symposium on Ultrasonic Doppler Methods for Fluid Mechanics and Fluid Engineering*, 27–29 Aug., Strasbourg, France, 9–12.

Herbst J. (2002). Non-destructive testing of sewer pipes by an acoustical method. *Proceedings of the 19th IEEE Instrumentation and Measurement Technology Conference*, 21–23 May, Anchorage, USA, 849–853. doi: 10.1109/IMTC.2002.1006952.

Heske C. H. (2003). Hohlraumdetektion in der Umgebung erdverlegter Abwasserkanäle mit Hilfe einer γ-γ-Sonde [Detection of cavities in the environment of buried sewer pipes using a γ-γ-probe]. *Technisches Messen*, **70**(7–8), 377–385. doi: 10.1524/teme.70.7.377.22646.

Hoes O. A. C., Schilperoort R. P. S., Luxemburg W. M. J., Clemens F. H. L. R. & van de Giessen N. C. (2009). Locating illicit connections in storm water sewers using fiber-optic distributed temperature sensing. *Water Research*, **43**(20), 5187–5197. doi: 10.1016/j.watres.2009.08.020.

Hrabak D., Pryl K., Krejcik J. & Richardson J. (1998). Calibration of flowmeters using FLOW-3D software. *Proceedings of Novatech 1998*, 4–6 May, Lyon, France, vol. **2**, 139–144.

Hydraulic Institute (2018). *Rotodynamic Pumps for Pump Intake Design – ANSI/HI 9.8-2018*. Hydraulic Institute, Parsippany, NJ (USA), 132 p. ISBN 978-1-935762-71-3.

ISO (1990). *ISO 4374:1990 Liquid flow measurement in open channels. Round-nose horizontal broad-crested weirs*. ISO – International Organization for Standardization, Geneva (Switzerland), 18 p.

ISO (1999). *ISO 4362:1999 Hydrometric determinations. Flow measurement in open channels using structures. Trapezoidal broad-crested weirs*. ISO – International Organization for Standardization, Geneva (Switzerland), 31 p.

ISO (2003). *ISO 5167-1:2003 Measurement of fluid flow by means of pressure differential devices inserted in circular cross-section conduits running full – Part 1: General principles and requirements*. ISO – International Organization for Standardization, Geneva (Switzerland), 33 p.

ISO (2007). *ISO 748:2007 Hydrometry – Measurement of liquid flow in open channels using current-meters or floats*. ISO – International Organization for Standardization, Geneva (Switzerland), 46 p.

ISO (2008). *ISO 3846:2008 Hydrometry – Open channel flow measurement using rectangular broad-crested weirs*. ISO – International Organization for Standardization, Geneva (Switzerland), 28 p.

ISO (2010). *ISO 15769:2010 Hydrometry – Guidelines for the application of acoustic velocity meters using the Doppler and echo correlation methods*. ISO – International Organization for Standardization, Geneva (Switzerland), 61 p.

ISO (2012). *ISO 4377:2012 Hydrometric determinations – Flow measurement in open channels using structures - Flat-V weirs*. ISO – International Organization for Standardization, Geneva (Switzerland), 59 p.

ISO (2013). *ISO 4359:2013 Liquid flow measurement in open channels – Rectangular, trapezoidal and U-shaped flumes*. ISO – International Organization for Standardization, Geneva (Switzerland), 75 p.

ISO (2017). *ISO 6416:2017 Hydrometry – Measurement of discharge by the ultrasonic transit time (time of flight) method*. ISO – International Organization for Standardization, Geneva (Switzerland), 58 p.

ISO (2020). *ISO 4360:2020 Hydrometry – Open channel flow measurement using triangular profile weirs*. ISO – International Organization for Standardization, Geneva (Switzerland), 30 p.

Ivetić D. (2019). *Assessment of the Liquid Flow Rate in Complex Flow Conditions with Flat Electromagnetic Sensors*. PhD thesis, University of Belgrade – Faculty of Civil Engineering, Belgrade, Serbia (in Serbian).

Ivetić D., Prodanović D. & Stojadinović L. (2018). Bed-mounted electromagnetic meters: Implications for robust velocity measurement in urban drainage systems. *Journal of Hydrology*, **566**, 455–469. doi: 10.1016/j.jhydrol.2018.08.068.

Ivetić D., Prodanović D., Stojadinović L. & Pavlović D. (2019). Bed-mounted electromagnetic meters: Assessment of the (missing) technical parameters. *Flow Measurement and Instrumentation*, **68**, 101588. doi: 10.1016/j.flowmeasinst.2019.101588.

Jarman D. S., Faram M. G., Butler D., Tabor G., Stovin V. R., Burt D. & Throp E. (2008). Computational fluid dynamics as a tool for urban drainage system analysis: a review of applications and best practice. *Proceedings of the 11th International Conference on Urban Drainage*, 31 Aug.–5 Sept., Edinburg, Scotland, UK, 10 p.

Jaumouillié P., Larrarte F. & Milisic V. (2002). New devices for 2D sampling of velocities and pollutant concentrations in sewers. *Proceedings of the 3rd International Conference on Sewer Process and Networks*, 15–17 April, Paris, France, 171–178.

Jeanbourquin D., Sage D., Nguyen L., Schaeli B., Kayal S., Barry D. A. & Rossi L. (2011). Flow measurements in sewer based on image analysis: automatic flow velocity algorithm. *Water Science and Technology*, **64**(5), 1108–1114. doi: 10.2166/wst.2011.176.

Joannis C. (2001). La mesure de débits en assainissement [Discharge measurement in sewers]. *La Houille Blanche*, **5**, 58–62. doi: 10.1051/lhb/2001057. (in French).

Jordana J., Gasulla M. & Pallàs-Areny R. (2001). Electrical resistance tomography to detect leaks from buried pipes. *Measurement Science and Technology*, **12**(8), 1061–1068. doi: 10.1088/0957-0233/12/8/311.

Kindsvater C. E. & Carter R. W. C. (1957). Discharge characteristics of rectangular thin plate weirs. *Journal of the Hydraulics Division*, **83**(6), 1–36.

Kirkham R., Kearney P. D., Rogers K. J. & Mashford J. (2000). PIRAT – A system for quantitative sewer assessment. *The International Journal of Robotics Research*, **19**(11), 1033–1053. doi: 10.1177/02783640022067959.

Knight D. & Sterling M. (2000). Boundary shear in circular pipes running partially full. *Journal of Hydraulic Engineering*, **126**(4), 263–275. doi: 10.1061/(ASCE)0733-9429(2000)126:4(263).

Kolin A. (1936). An electromagnetic flowmeter – Principle of the method and its application to blood flow measurements. *Proceedings of the Society for Experimental Biology and Medicine*, **35**(1), 53–56. doi: 10.3181/00379727-35-8854P.

Kooij C., Mühle S., Clemens F. H. L. R., Pothof I. W. M. & Blokzijl F. H. (2015). Performance indicators for complex wastewater pumping stations and pressure mains. *Proceedings of the 1st International Conference on Industrial Networks and Intelligent Systems (INISCom)*, 2–4 March, Tokyo, Japan, 94–99. doi: 10.4108/icst.iniscom.2015.25838.

Korving J. L., Admiraal N., Veurink J. & van Bijnen M. (2012). Rioolvreemd water efficiënt opsporen en effectief aanpakken [Find and cure parasitic water]. *H twee O*, **45**(2), 35–37. (in Dutch).

Korving J. L., Clemens F. H. L. R. & van Noortwijk J. M. (2006). Statistical modeling of the serviceability of sewage pumps. *Journal of Hydraulic Engineering*, **132**(10), 1076–1085. doi: 10.1061/(ASCE)0733-9429(2006)132:10 (1076).

Kracht O., Gresch M. & Gujer W. (2007). A stable isotope approach for the quantification of sewer infiltration. *Environmental Science and Technology*, **41**(16), 5839–5845. doi: 10.1021/es062960c.

Larrarte F. (2006). *Contributions à la métrologie en réseau d'assainissement [Contributions to metrology in sewer systems].* Habilitation thesis (HDR), Université de Caen – Basse Normandie, Caen, France, 104 p. + annexes. (in French).

Larrarte F., Bardiaux J.-B., Battaglia P. & Joannis C. (2008). Acoustic Doppler flow-meters: a proposal to characterize their technical parameters. *Flow Measurement and Instrumentation*, **19**(5), 261–267. doi: 10.1016/j.flowmeasinst. 2008.01.001.

Larrarte F., Dufresne M., Mignot E., Lipeme Kouyi G., Rivière N., Vazquez J. & Joannis C. (2017). Débitmètrie et mécanique des fluides numérique : contribution à l'évaluation et à la réduction des incertitudes des mesures de vitesse moyenne [Flow measurement and computational fluid dynamics: contribution to the assessment and control of uncertainties on mean velocity measurement]. *La Houille Blanche*, **6**, 67–72. doi: 10. 1051/lhb/2017060. (in French).

Larrarte F. & Francois P. (2012). Attenuation of an ultrasonic beam by suspended particles and range of acoustic flow meters in sewer networks. *Water Science and Technology*, **65**(3), 478–483. doi: 10.2166/wst.2012.873.

Larrarte F., Jaumouillié P. & Joannis C. (2004). Computational fluid dynamics: an aid for designing the instrumentation of sewer sections. *Proceedings of Novatech 2004*, 6–10 June, Lyon, France, vol. **1**, 729–736.

Larrarte F., Joannis C. & Bonakdari H. (2010). Qualification and design of flow meter measurement sites within sewer networks. *Bulletin des Laboratoires des Ponts et Chaussées*, **277**, 31–41.

Larrarte F., Joannis C., Mignot E., Rivière N. & Lipeme Kouyi G. (2016a). *Guide Technique – Fiabiliser les mesures de vitesse – Représentativité spatiale des mesures en continu de vitesse et incertitudes sur les mesures de débit – Guides techniques du projet MENTOR [Technical guide – Making flow velocity measurements reliable – Spatial representativeness of continuous flow velocity measurements and uncertainties on flow measurements – Technical guides of the MENTOR project]*, 28 p. Available at http://wikhydro. developpement-durable.gouv.fr/index.php/Fichier:MENTOR_GT_Fiabilisation_debits-vfinale.pdf (accessed 21 Nov. 2020). (in French)>.

Larrarte F., Sturycz E., Lebouc L. & Riochet B. (2016b). New technique for continuous monitoring of sediment height. *Flow Measurement and Instrumentation*, **49**, 40–45. doi: 10.1016/j.flowmeasinst.2016.04.005.

Leeungculsatien T. & Lucas G. P. (2013). Measurement of velocity profiles in multiphase flow using a multi-electrode electromagnetic flow meter. *Flow Measurement and Instrumentation*, **31**, 86–95. doi: 10.1016/j.flowmeasinst. 2012.09.002.

Lepot M., Makris K. F. & Clemens F. H. L. R. (2017). Detection and quantification of lateral, illicit connections and infiltration in sewers with infra-red camera: Conclusions after a wide experimental plan. *Water Research*, **122**, 678–691. doi: 10.1016/j.watres.2017.06.030.

Lepot M., Momplot A., Lipeme Kouyi G. & Bertrand-Krajewski J.-L. (2014). Rhodamine WT tracer experiments to check flow measurements in sewers. *Flow Measurement and Instrumentation*, **40**, 28–38. doi: 10.1016/j. flowmeasinst.2014.08.010.

Lipeme Kouyi G. (2004). *Expérimentations et modélisations tridimensionnelles de l'hydrodynamique et de la séparation particulaire dans les déversoirs d'orage [Experimentations and three-dimensional modeling of hydrodynamics and particle separation in storm overflows]*. PhD thesis, Université Louis Pasteur, Strasbourg, France, 274 p. (in French).

Lipeme Kouyi G., Vazquez J. & Poulet J.-B. (2003). 3D free surface measurement and numerical modelling of flows in storm overflows. *Flow Measurement and Instrumentation*, **14**(3), 79–87. doi: 10.1016/S0955-5986(03) 00011-6.

Lipeme Kouyi G., Vazquez J., Rollet D., Gallin Y. & Sadowski A.-G. (2005). Use of 3D modelling and several ultrasound sensors to assess overflow rate. *Water Science and Technology*, **51**(2), 187–194. doi: 10.2166/wst. 2005.0047.

Liu Z. & Kleiner Y. (2013). State of the art review of inspection technologies for condition assessment of water pipes. *Measurement*, **46**(1), 1–15. doi: 10.1016/j.measurement.2012.05.032.

Loke M. H. (2020). *Tutorial: 2-D and 3-D Electrical Imaging Surveys*. Revised version 17 Aug. 2020, 231 p. Available at https://www.geotomosoft.com/downloads.php (accessed 22 Nov. 2020).

Lopez-Higuera J. M. (ed.). (2002). *Handbook of Optical Fibre Sensing Technology*. John Wiley & Sons Ltd., Chichester (UK), 828 p. ISBN 978-0-471-82053-6.

Lubbers C. L. (2007). *On Gas Pockets in Wastewater Pressure Mains and their Effect on Hydraulic Performance*. PhD thesis, TU Delft, The Netherlands, 304 p. ISBN 978-1-58603-789-5.

Macmillan N. A. & Creelman C. D. (2005). *Detection Theory – A User's Guide, 2nd edn*. Lawrence Erlbaum Associates, Mahwah, NJ (USA), 512 p. ISBN 978-0-8058-4230-6.

MENTOR (2016). *MENTOR Project Final Deliverables*. Available at http://wikhydro.developpement-durable.gouv.fr/index.php/Autosurveillance_et_diagnostic_en_r%C3%A9seau_d%27assainissement_-_Projet_MENTOR (accessed 20 Nov. 2020). (in French).

Michalski A., Starzynski J. & Wincenciak S. (2001). Electromagnetic flowmeters for open channels - Two-dimensional approach to design procedures. *IEEE Sensors Journal*, **1**(1), 52–61. doi: 10.1109/JSEN.2001.923587.

Miller G. A. (1956). The magical number seven, plus or minus two: some limits on our capacity for information processing. *Psychological Review*, **63**(2), 81–97. doi: 10.1037/h0043158.

Munser R. & Hartrumpf M. (2003). Detektion verdeckter Anomalien im Bettungsbereich von Abwasserrohren mit einem Mikrowellen-Rückstreusensor [Detection of hidden anomalies around sewer pipes by means of a microwave back-scattering sensor]. *Technisches Messen*, **70**(7–8), 359–369. doi: 10.1524/teme.70.7.359.22643. (in German).

Nguyen L. S., Schaeli B., Sage D., Kayal S., Jeanbourquin D., Barry D. A. & Rossi L. (2009). Vision-based system for the control and measurement of wastewater flow rate in sewer systems. *Water Science and Technology*, **60**(9), 2281–2289. doi: 10.2166/wst.2009.659.

Nikles M., Vogel B. H., Briffod F., Grosswig S., Sauser F., Luebbecke S., Bals A. & Pfeiffer T. (2004). Leakage detection using fiber optics distributed temperature monitoring. *Proceedings SPIE 5384, Smart Structures and Materials 2004: Smart Sensor Technology and Measurement Systems*, 27 July, San Diego, USA, 8 p. doi: 10.1117/12.540270.

Panasiuk O., Hedström A., Langeveld J. G., Liefting E., Schilperoort R. P. S., de Haan C. & Viklander M. (2017). Methods for localization and volume estimation of the infiltration and inflow: Comparative study. *Proceedings of the 14th International Conference on Urban Drainage*, Prague, Czech Republic, 392–395.

Pothof I. W. M. & Clemens F. H. L. R. (2010). On elongated air pockets in downward sloping pipes. *Journal of Hydraulic Research*, **48**(4), 499–503. doi: 10.1080/00221686.2010.491651.

Pothof I. W. M. & Clemens F. H. L. R. (2011). Experimental study of air–water flow in downward sloping pipes. *International Journal of Multiphase Flow*, **37**(3), 278–292. doi: 10.1016/j.ijmultiphaseflow.2010.10.006.

Pothof I. W. M., Kooij C., Clemens F. H. L. R. & Schuit A. D. (2009). Gasbellen in persleidingen: beter voorkomen dan genezen [Gas pockets in pressure mains, prevention is better than recovery]. *Land+Water*, **49**(6/7), 30–31. (in Dutch).

Prigiobbe V. & Giulianelli M. (2011). Quantification of sewer leakage by a continuous tracer method. *Water Science and Technology*, **64**(1), 132–138. doi: 10.2166/wst.2011.639.

Prodanović D. & Ivetić D. (2019). Primeri primene ravnih elektromagnetnih sondi za merenje protoka u Kolektorima [Examples of flat EM sensor application for flow measurements in collectors]. *Vodoprivreda*, **51** (300–302), 197–209. Available at http://www.vodoprivreda.net/wp-content/uploads/2020/01/5-Dusan-Prodanovic-i-Damjan-Ivetic-Redigovano.pdf (accessed 30 Nov. 2020). (in Serbian).

Ramirez A., Daily W., Binley A., LaBrecque D. & Roelant D. (1996). Detection of leaks in underground storage tanks using electrical resistance methods. *Journal of Environmental and Engineering Geophysics*, **1**(3), 189–203. doi: 10.4133/JEEG1.3.189.

Revitt D. M., Ellis J. B. & Paterakis N. (2006). Comparison of tracer techniques for monitoring sewer losses. *Journal of Environmental Monitoring*, **8**(5), 564–571. doi: 10.1039/B600522E.

Reynolds J. M. (2011). *An Introduction to Applied and Environmental Geophysics, 2nd edn*. Wiley-Blackwell, Chichester (UK), 710 p. ISBN 978-0-471-48535-3.

Rieckermann J., Neumann M., Ort C., Huisman J. L. & Gujer W. (2005). Dispersion coefficients of sewers from tracer experiments. *Water Science and Technology*, **52**(5), 123–133. doi: 10.2166/wst.2005.0124.

Rieckermann J., Vojtěch B., Kracht O., Braun D. & Gujer W. (2007). Estimating sewer leakage from continuous tracer experiments. *Water Research*, **41**(9), 1960–1972. doi: 10.1016/j.watres.2007.01.024.

Rizzo P. (2010). Water and wastewater pipe nondestructive evaluation and health monitoring: A review. *Advances in Civil Engineering*, paper ID **818597**, 13 p. doi: 10.1155/2010/818597.

Schilperoort R. P. S. (2004). *Natural Water Isotopes for the Quantification of Infiltration and Inflow in Sewer Systems*. MSc thesis, Delft University of Technology, Delft, The Netherlands, 151 p.

Schilperoort R. P. S., Hoppe H., de Haan C. & Langeveld J. G. (2013). Searching for storm water inflows in foul sewers using fibre-optic distributed temperature sensing. *Water Science and Technology*, **68**(8), 1723–1730. doi: 10.2166/wst.2013.419.

Schilperoort R. P. S., Meijer H. A. J., Flamink C. M. L. & Clemens F. H. L. R. (2007). Changes in isotope ratios during domestic wastewater production. *Water Science and Technology*, **55**(4), 93–101. doi: 10.2166/wst.2007.099.

Selvakumar A., Tuccillo M. E., Martel K. D., Matthews J. C. & Feeney C. (2014). Demonstration and evaluation of state-of-the-art wastewater collection systems condition assessment technologies. *Journal of Pipeline Systems Engineering and Practice*, **5**(2), paper ID 04013018, 11 p. doi: 10.1061/(ASCE)PS.1949-1204.0000161.

Shercliff J. A. (1962). *The Theory of Electromagnetic Flow-Measurement*. Cambridge University Press, Cambridge (UK), 164 p. ISBN 978-0521335546.

Sliwczynski L. & Krehlik P. (2014). Measurement of acoustic noise in field-deployed fiber optic cables. *Proceedings of the Conference European Frequency and Time Forum (EFTF)*, 23–26 June, Neuchatel, Switzerland, 339–342. doi: 10.1109/EFTF.2014.7331504.

Smits J., Moens M. R., Klootwijk M. & van Vliet H. (2008). Testing flow-meters using a field laboratory. *Proceedings of the 11th International Conference on Urban Drainage*, 31 Aug.–5 Sept., Edinburgh, Scotland, UK, 12 p.

Stanic N. (2016). *Assessment Methods for Structural and Hydraulic Properties of Concrete Sewer Pipes*. PhD thesis, Delft University of Technology, The Netherlands, 162 p. ISBN 978-94-6233-2058. doi: 10.4233/uuid:3ea2146b-21cb-49b0-9aca-40ae8338e4d3.

Stanic N., Clemens F. H. L. R. & Langeveld J. G. (2016). Estimation of the hydraulic roughness of concrete sewer pipes by laser scanning. *Journal of Hydraulic Engineering*, **143**(2), paper 04016079. doi: 10.1061/(ASCE)HY.1943-7900.0001223.

Tuccillo M. E., Wilmut C., Feeney C., Martel K. & Selvakumar A. (2011). Field demonstration of electro-scan defect location technology for condition assessment of wastewater collection systems. *Proceedings of the Water Environment Federation*, **5**, 265–281. doi: 10.2175/193864711802837309.

Tukker M., Kooij K. & Pothof I. (2016). *Hydraulic Design and Management of Wastewater Transport Systems – CAPWAT Manual*. IWA Publishing, London (UK), 152 p. ISBN 9781780407821. Available at https://www.iwapublishing.com/books/9781780407821/hydraulic-design-and-management-wastewater-transport-systems (accessed 20 Nov. 2020).

van Daal-Rombouts P. M. M. (2017). *Performance Evaluation of Real Time Control in Urban Wastewater Systems*. PhD thesis, TU Delft, Deft, The Netherlands, 256 p. ISBN 978-94-6233-707-7. doi: 10.4233/uuid:b1d5d733-b271-474f-ad32-b5fdde257161.

van Daal-Rombouts P. M. M., Tralli A., Verhaart F. I. H., Langeveld J. G. & Clemens F. H. L. R. (2017). Validation of computational fluid dynamics for deriving weir discharge relationships with scale model experiments and prototype measurements. *Flow Measurement and Instrumentation*, **58**, 52–61. doi: 10.1016/j.flowmeasinst.2017.09.011.

Vazquez J., Lipeme Kouyi G. & Zug M. (2006). Modelling and instrumentation of the storm overflows of the combined sewer system of sélestat. *Urban Water Journal*, **3**(2), 91–110. doi: 10.1080/15730620600855936.

Vazquez J., Zug M., Buyer M. & Lipeme Kouyi G. (2005). CSOs: Tools for assessing their operation in our systems. *Water Science and Technology*, **51**(2), 179–185. doi: 10.2166/wst.2005.0046.

Verhaart F. I. H., de Fockert A. & Zwanenburg S. A. A. (2016). Velocity profiles in the bell mouth throat of vertically submersible pumps. *Journal of Applied Water Engineering and Research*, **4**(2), 102–111. doi: 10.1080/23249676. 2015.1090350.

Weiß G., Brombach H. & Haller B. (2002). Infiltration and inflow in combined sewer systems: long-term analysis. *Water Science and Technology*, **45**(7), 11–19. doi: 10.2166/wst.2002.0112.

Wilmut C. G., Dsouza B. J. & Guidry B. A. (2005). Electro-scan technology - Is it the 'silver bullet' for rainfall dependent infiltration (RDI) and exfiltration. *Proceedings of the Water Environment Federation*, **2005**(**4**), 697–706. doi: 10.2175/193864705784291529.

Wirahadikusumah H., Abraham D. M., Iseley T. & Prasanth R. K. (1998). Assessment technologies for sewer system rehabilitation. *Automation in Construction*, **7**(4), 259–270. doi: 10.1016/S0926-5805(97)00071-X.

Wolf L. (2006). *Influence of Leaky Sewer Systems on Groundwater Resources Beneath the City of Rastatt, Germany*. PhD thesis, Universität Karlsruhe, Karlsruhe, Germany, 231 p.

Wood W. & Palmer D. (2000). The application of mise-à-la-masse and resistivity surveys to the detection of pollution from leaking sewers. *Exploration Geophysics*, **31**(3), 515–519. doi: 10.1071/EG00515.